WHAT MAKES ENTANGLED PHOTONS ENTANGLED?

AN EXPERIMENTAL COMPARISON BETWEEN ENTANGLED PHOTONS AND WEAK FEMTOSECOND PULSES

BY

ANDREAS PIERRE THÖRN

THESIS PRESENTED TO OBTAIN THE DEGREE OF
PHILOSOPHIAE DOCTOR

UNIVERSITY OF OSLO

September 2015

Series of dissertations submitted to the
Faculty of Mathematics and Natural Sciences, University of Oslo
No. 1662

ISSN 1501-7710

Cover: Hanne Baadsgaard Utigard.
Printed in Norway: AIT Oslo AS.

Produced in co-operation with Akademika Publishing.
The thesis is produced by Akademika Publishing merely in connection with the thesis defence. Kindly direct all inquiries regarding the thesis to the copyright holder or the unit which grants the doctorate.

"Whenever a theory appears to you as the only possible one, take this as a sign that you have neither understood the theory nor the problem which it was intended to solve."

K. Popper[1]

"In theory, theory and practice are the same. In practice, they are not."

A. Einstein[2]

[1] *Objective Knowledge: An Evolutionary Approach*, Oxford University Press, 1972, p. 266

[2] This statement (or variants of it) is said to originate from a variety of different people. While many of these claims do not have a more specified source, for the claim that Einstein said this, the Washington post is quoted as the source. However, any further specification of the exact location could not be found, and one might therefore question whether Einstein actually made this statement at all.

Abstract

Which physical properties are essential for entanglement? In a series of experimental measurements of the relations between registrations at the detectors in a setup similar to the setup described by Kuklewicz et al.[3] this question has been investigated. Real physical changes to the experimental setup cause real changes in the measurement results. Thus, the results seem to depend on real physical effects. Can entanglement be understood in such a context?

Two setups, with different type of sources, but the same analysing and detection setup, were used in the investigation. For measurements involving entangled states, a nonlinear crystal combination with a continuous wave laser source was used. This produced both entangled and non-entangled photon pairs with orthogonal polarizations through spontaneous parametric down-conversion. The second source was an ultrafast Ti:sapphire laser connected to a modified Mach-Zehnder interferometer, which generated highly attenuated pulses with orthogonal polarizations and varying phase relations.

In the analysing setup, the incoming light was split by a non-polarizing beam splitter. In each of its arms a rotating half wave plate, a polarizing beam splitter and two detectors were located. In this way the correlations among the state of polarization could be measured. With these two configurations, an attempt was made to emulate the results obtained when using the entangled photon pair source, but using the pulsed source instead. Specifically, by looking at the theoretical parameters that change when a product state is replaced by an entangled state, due to changes in the optical setup, we tried to emulate and optimize these parameters in the pulsed case and then conduct a series of similar measurements.

The reason for using a pulsed source was first and foremost to be able to control single parameters (such as timing and overlap) without having to rely on an abstract, mathematical formalism. By removing ourselves from concepts like indistinguishability and collapse of wave functions, which can be difficult to interpret, we wished to investigate if we could relate the change in the measured results to more familiar physical processes (such as interference and phase relations). It is important to note the difference between the mathematical formalism and the interpretations or ”mental pictures” used when trying to explain the processes. This relationship has been discussed lively since the birth of quantum mechanics, with the discussion between Bohr and Einstein perhaps being the most famous. While we make no attempt to settle this debate here, one should note that our understanding of a phenomenon is mirrored by the mental pictures we present, and that it would seem unsatisfactory to utilize the formalism without having a consistent picture of what is actually taking place in the experiment.

[3] C. E. Kuklewicz, M. Fiorentino, G. Messin, F. N. C. Wong, and J. H. Shapiro, *Phys. Rev. A* **69**, 013807 (2004)

The results from our measurements showed that under certain conditions the pulsed source can generate outcomes which are similar to the entangled case. This is especially true for the close-to rotational invariant correlation in a so called twin scan (i.e. a scan where the rotating half wave plates of both Alice and Bob are kept at the same angle). Classical physics tell us that we should have no such invariance.

However, although this experimental result would suggest that we have obtained light which can be described as entangled, there are obvious flaws in this interpretation. The necessity of including the complete set of measurements is essential for making a valid statement about the nature of the light. This becomes obvious if we attempt to do a measurement of Bell's inequality.

Nevertheless, the physical interpretations of the quantum mechanical theory describing the spontaneous parametric down-conversion process in these experiments, does introduce a number of questionable assumptions. This includes the question of where the entanglement process is taking place in the optical setup (since we've seen that a change in the setup can cause the entanglement to disappear), how the process of spontaneous parametric down-conversion should be interpreted in terms of photons (are the photon pair created instantaneously at some position inside the non-linear crystal?), what the concept of indistinguishability means (our detectors cannot discriminate between the photon in the entangled and unentangled case based on timing, such as the theory demands) and the role of time and space when regarding photon (can the photon be considered something similar to a wave packet and how does the effect of the so called coincidence time relate to this?). We will try to relate our findings to these questions and the interpretations of them.

Acknowledgement

I would first and foremost like to thank my supervisor associate professor Arnt Inge Vistnes for giving me the opportunity to work in his group on such an exciting and intriguing field of science as the very nature of light.

I would also like to direct a sincere thanks to Dr. Guillaume Adenier, who's been an invaluable source of knowledge, both in the theoretical and experimental work.

A big thanks also goes to professor Joakim Bergli, for his constructive feedbacks and support, and for always asking the correct and difficult questions.

I would also like to acknowledge the Norwegian defence research establishment (FFI), whom generously let us borrow some of their equipment during the setup and testing of the lasers we have used.

A great thanks also goes to Thor Bakke and Jo Gjessing at SINTEF for letting us borrow their newly developed piezoelectric mirror and for helping us making a customized holder for it. We are indebted to them for all their help and support.

In addition, I would like to mention all the people at the electronics group, and especially Johan Ludvig Tresvig, who helped us making the special amplifiers needed for driving the Pockels cell, and who were always willing to help out when needed.

Other people that have been involved in realizing these experiments are Steinar Skaug Nilsen and his group of talented engineers, who has helped us making non-standard metal parts and components.

Lastly, I would like to thank the University of Oslo for their financial support. Without it, none of the experiments that has been done during this project would have been possible.

Contents

Part I

Introduction

Chapter 1

The difficult nature of light

As is well known, the fundamental question about the nature of light has been lively debated since the 17:th century [1]. The main issue in these discussions were whether light should be considered a particle or a wave phenomena, as it sometimes would fit a particle description (mainly through the exchanges of energy and momentum between matter and radiation) and other times a wave description (for example in describing interference effects). Over the next four centuries great minds like Newton, Huygens, Young, Fresnel, Maxwell, Planck and Einstein (among others) all contributed to the progress of interpreting the nature of light, though without being able to satisfactory unify its two seemingly conflicting characteristics.

Today, the most comprehensive theory for light is the quantum theory of light (see for example [2], [3] or [4]). It is a strong mathematical formalism which has helped us predict experimental outcomes where other theories have failed. It has also expanded the characteristics of light, giving us new concepts like entanglement, bunching and anti-bunching, indistinguishability and the concept of photons. The wave-particle conflict has been replaced with a complementary duality – light is now said to have both characteristics. Yet, quantum optics has not improved our understanding of the *physics behind* the conflicting nature of light.

The concept of entanglement is the most central phenomenon discussed in this thesis. This is because entanglement is considered a purely quantum mechanical effect with no classical analog. It can be expressed mathematically by using the concept of quantum states. Let's look at a photon and assume that it can exist in two such precisely defined states

$$|H\rangle \text{ and } |V\rangle,$$

where H and V stands for the horizontal and vertical direction, respectively, of the linear polarization which here defines the state of the photon.

Assume now that we have two photons, both of which has a probability of 50 % of being in either state $|H\rangle$ or $|V\rangle$, but with the condition that if one photon is in state $|H\rangle$ the other one has to be in the state $|V\rangle$, or the other way around. If we cannot tell which state either of the photons are without making a measurement, the complete state for the two photons before any measurement is performed, can be written as

$$|\psi\rangle = \frac{1}{\sqrt{2}} \left(|HV\rangle + |VH\rangle\right) \tag{1.1}$$

This is one of the Bell states, which is an entangled state.[1]

The physical interpretation of these states is that the photons (which themselves have a difficult interpretation as far as mental pictures go) exists in an undefined state of having both horizonal and vertical polarization (or no polarization, depending on your point of view). Einstein, Podolsky and Rosen argued [5] that such a description of nature has to be an incomplete description, and that the photons really must have a defined polarization even though it has not yet been measured.

Although Bell, with his inequality [6], made it possible to experimentally determine whether it could be possible to add some hidden variable, undetectable in the realm of quantum mechanics, to make it a "complete" theory or not, the understanding of the actual physical processes which may lead to light being described as entangled, has no satisfactory description.[2] Instead, the question about what physical processes are responsible for the observations that we make, is in many respects left out of the quantum mechanical theory. While we can always introduce concepts like indistinguishability or bi-photons [7] to explain the processes, it is really nothing more than a rewriting of the initial problem. Does an unlocalized bi-photon entity really tell us more about the physics behind the Hong-Ou-Mandel experiment, for example? In a mathematical sense it may, but much less on a physical level. In that respect, we could resort to the well known expression "Shut up and calculate!", which in this context can be interpreted to mean that quantum mechanics does not give any information about the actual physical processes (and has no intention of doing so), and therefore should not be used for the purpose of explaining what is going on. And in some sense that is a reasonable approach, because quantum mechanics is mainly a set of mathematical rules that can be applied to physical problems in order to calculate the probability of finding a given outcome. However, in order to try to interpret the physics behind the mathematics, new concepts, such as entanglement, indistinguishability, interference of probability amplitudes and collapse of wave functions, to mention a few, has been introduced. Yet, the physical understanding of these new concepts, and above all, attempts to create useful mental pictures of them, does not seldom lead to a behaviour and a language which seems to shroud the nature of light in a cloud of mystery and strangeness rather than explaining it. Thus, it is not uncommon to find phrases like:

> *"[...] the fact that the predictions of quantum mechanics hold for individual particles and not just for ensembles is best illustrated by the finding that each individual photon 'knows' it should never end up in the minimum of an interference fringe."* [8],

> *"This photon now has the choice of either reflecting off B_2 or transmitting through B_2. [...] Assume the photon chooses to transmit through B_2 [...]."* [9]

or

> *"In other words, the photon simply chooses one of the routes and follows it to the end [...]."* [10].

[1] We could also have written $\frac{1}{\sqrt{2}}(|HV\rangle - |VH\rangle)$, which is another Bell state, but we would then have an anti-symmetric (i.e. fermionic) state.

[2] That is, we can describe the process in mathematical terms and we know how to do the experimental setup, but a satisfactory mental image of the complete process is still absent.

Of course, the photon is not an intelligent being and cannot choose to do anything. It is therefore important to lift this cloud of strangeness if we are to satisfactory understand the nature of light. The approach used in this thesis has been to try to obtain results similar to what we obtain with an entangled state, but in an environment where the parameters assumed relevant for the entanglement process can be controlled individually. Under such conditions, by varying single parameters one can study the effects they have on the measured outcome and in that way obtain information about what parameters (and physical processes) are responsible for the differences in the experimental results. In this way we may also test, to some extent, the interpretations made in the quantum theory about the aforementioned concepts.

1.1 Organization of this thesis

The organization and layout of this thesis has been inspired by the thesis of Alain Aspect [11], and is organized in the following manner: After this short introduction to the difficult nature of light, we will in chapter 2 look at how the classical and quantum mechanical theories interprets the concept of light, and where the real difference lies. We will also try to motivate why the use of spontaneous parametric down-conversion can be used as a source for studying quantum effects in light.

We will then discuss Bell's inequality as interpreted by Aspect, who used an experimental setup which has similarities to our own. In this context we will describe the down-conversion process and the calculation of the experimental outcomes using the standard approach. We will talk a little bit about the common interpretation of the so called compensating crystal and the concept of periodic poling.

Chapter 3 is a short summary of the most relevant concepts from the field of ultrafast optics, and a discussion about methods how to characterize a pulse with a very short duration and limitations connected with these measurement results. This is of relevance when we later wish to characterize our own pulsed source.

Chapter 4 describes the optical setup, both with the crystal source for spontaneous parametric down-conversion and the pulsed source. We will go through the components and their effects, and try to motivate why we've chosen a particular setup or component, and relate this to the interpretations discussed in chapter 2.

In chapter 5 we will use the methods described in chapter 3 to characterize the pulses from our ultrafast laser source, as well as investigating what effects the optical components may have on the shape of the pulse. We will also discuss the challenges and possible sources of error when comparing the experimental setups. In addition, the optimization process for making the pulsed source match (as close as possible) the nonlinear crystal source is included here.

Chapter 6 and 7 discloses the measurement process, the results of these measurements and the conclusions we draw from them. The results include measurements made with the crystal source, both entangled and un-entangled, and measurements with different settings on the pulsed source. These results are compared and similarities and differences are discussed, and we will try to put these in context with the interpretation of physical processes.

The final chapter, chapter 8, contains copies of published papers.

A relatively large part of the thesis is devoted to the optical setup and testing of equipment. This is partially because the setup itself is relatively large and has many active components that needs to work together in order to accomplish the tasks that we set. Another reason is that one of our goals was to see if and how physical processes could be connected with theoretical concepts. It would therefore seem crucial to know and understand where we are starting from and how the different components may affect the light and the effects we wish to study. This is especially true for effects that are correlated and in different degrees dependent on each other.

As was mentioned, the experimental setup for the quantum mechanical measurements is in large based on other people's work. The setup used here for the quantum mechanical measurements were in large parts set up by Guillaume Adenier and in operation before I started on this thesis. However, a detailed description of it, including the acquisition program, seemed to be lacking. In addition, from the fact that the same analyzing setup also was used with our pulsed source, it seemed necessary to include a more complete description of it. The pulsed setup have not been used before and it therefore discussed in length.

The measurements and results we have obtained are, naturally, related to our specific settings and components, but they are not limited locally only to this specific setup. The result of the experiments we have conducted can hopefully be used in the continuous search for a better understanding of light.

References

[1] J. Gribbin, *Schrödinger's Kittens and the Search for Reality: Solving the Quantum Mysteries*, Back Bay Books, 1996, pp. 39-51

[2] L. Mandel and E. Wolf, *Optical coherence and quantum optics*, Camebridge University press, 2008

[3] M. Born and E. Wolf, *Principles of Optics*, 7th edition, Camebridge University press, 2011

[4] R. Loudon, *The Quantum Theory of Light*, 3rd edition, Oxford science publications, 2010

[5] A. Einstein, B. Podolsky and N. Rosen, *Phys. Rev.* **47**, 777 (1935)

[6] J. S. Bell, *Physics* **1**, 195 (1964)

[7] Y. Shih, *In introduction to quantum optics Photon and biphoton physics*, CRC Press, 2011

[8] A. Zeilinger, G. Weihs, T. Jennewein and M. Aspelmeyer, *Nature* **433**, 230 (2005)

[9] R. Blumel, *Foundations of Quantum Mechanics*, Jones and Bartlett Publishers, 2009, p. 157

[10] J. Matson, *Quantum Flip-Floppers: Photon Findings Add to Mystery of Wave-Particle Duality*, Scientific American, 2012

[11] A. Aspect, *Three Experimental Tests of Bell Inequalities by Measurement of the Polarization Correlation of Photons*, Springer, not yet published

Part II

Theory

Chapter 2

Theoretical models and their interpretations

Light can be described in many different ways, using different types of mathematics. Under different physical conditions, the validity of the different models changes, leading to each model being valid only under certain conditions. Thus, often one speaks of different types of light, such as thermal light, coherent light or entangled light, for example. But these conditions remain in many cases as abstract mathematical formulations, and it is not always clear cut how these are related to the changes in the real-world physical conditions. In fact, much of the seeming conflict between the photon/wave picture can be found in how mathematical results are interpreted and to what extent these results are used to describe real physical processes.

While there are differences in the mathematics, there are also similarities. These are often hidden in plain sight, that is, the model may put up so strong restrictions on the behaviour of the light that the reader does not immediately recognize the similarity. An example may be the indivisibility of the photon which ”forbids” the photon to be split at a beam splitter. However, the expression for the probability distribution at the output ports is pretty much the same as the intensity distribution of classical light being split by the beam splitter. Thus, in mathematical terms, without interpretations, the calculations are actually quite similar.

It is, however, the difference in the experimental outcomes which really shows the physical difference in the nature of the light. As was mentioned in the introduction, these differences are often explained on an abstract theoretical level, where physical interpretations and mental manifestations become a challenge. Therefore, in order to understand what differentiates the different models for light, and especially what separates so called classical light from quantum light, let’s have a look at how these theories are describing the light phenomena. We will in this process also try to motivate why the use of spontaneous parametric down-conversion has been used as a method for generating non-classical light. This deviation may seem lengthly, but we will make a few comments along the way in order to highlight some of the challenges that arises when tying to interpret the mathematics into physical form.

2.1 Classical theory

In the classical theory, light is described as oscillating electric and magnetic fields which are perpendicular to each other and the direction of propagation. The expression for the propagation of the fields in time and space is given from the wave equation, which is derived from Maxwell's equations. We can write the wave equation as

$$\nabla^2 \mathbf{u} - \frac{1}{c^2}\frac{\partial^2 \mathbf{u}}{\partial t^2} = 0 \tag{2.1}$$

where $\mathbf{u}$ is either the electric or the magnetic field, and the speed of light is defined from $c = 1/\sqrt{\mu_0 \epsilon_0}$. In the simplest case, the solution to the above equation is a plane wave, which for a monochromatic wave propagating in the $\mathbf{k}$ direction is given by

$$\mathbf{u}(\mathbf{r}, t) = A_0 e^{i(\mathbf{k}\cdot\mathbf{r} - \omega t)} \tag{2.2}$$

where A_0 is a constant amplitude, ω is the angular frequency, $\mathbf{k}$ is the wave vector and $\mathbf{r}$ is the position vector. In the more general case, A is a slowly varying function of position called the complex envelope of the field. In the context of pulses, which will be most interesting to us when trying to simulate the results in chapter 6, the complex amplitude becomes a function of finite duration. A simple example can be the Gaussian pulse, where the complex envelope can be written

$$A(t) = e^{-4\ln 2\left(\frac{t}{\tau}\right)^2} \tag{2.3}$$

where τ is the FWHM[1] pulse duration.

In free space, the plane wave, when propagating in the z-direction, extends to infinity in the xy-plane, and thus can only be used as a limiting case when describing real physical situations.

The solution of the wave equation does not uniquely determine the fields however, and this introduces the effect of superposition, i.e. the possibility of generating/decomposing a field from/into a sum of fields. In order to uniquely determine the field from the wave equation, we have to introduce boundary conditions.

The energy of the light is determined from the magnitude of the time average of Poynting's vector

$$I(\mathbf{r}, t) = \langle |\mathbf{S}| \rangle = \langle |\mathbf{E} \times \mathbf{B}| \rangle \tag{2.4}$$

We see from this equation that the intensity will be proportional to the time average of the amplitude of the fields. The amplitudes are continuous quantities, so the intensity can be continuously adjusted to any level.

Interference and diffraction effects are described as real interactions of the electric (and magnetic) fields, and thus the phase relation, the polarization, as well as the coherence of the light, are all viewed as real, fundamental processes responsible for the observed interference effects.

Polarization is governed by the direction and amplitude of the electric field, thus elliptical and circular polarized light can always be decomposed into linear polarized light with different phases and directions. This is a result of the arbitrariness in the solutions of the wave equation.

[1] Full Width Half Maximum

In that respect, it is interesting to look at our understanding of the interaction process when considering two orthogonal, linearly polarized beams of light with a fixed phase relation traveling collinearly. If we send these beams to an opaque screen, we will not observe any interference pattern. However, if we now make a measurement in, say, the diagonal basis (i.e. in the direction diagonal to both polarizations) we will indeed see an interference pattern. So, depending on our measurement we can generate an interference pattern which did not seem to be present when looking at the light from a more general point of view.

In a way, one cannot help to think about the similarity with the Schrödinger's cat paradox, in which our measurement causes the physics to change to a defined state. Or, perhaps even more fitting, a quote from Einstein in a conversation with Pais [3]:

> *I recall that during one walk Einstein suddenly stopped, turned to me and asked whether I really believed that the moon exists only when I look at it,*

which would freely translate into the question: *is the interference really there when no one is measuring it?*

2.2 Quantum theory

The starting point for the quantum theory is, just as for the classical theory, Maxwells equations. By writing the electric and magnetic fields as vector potentials[2], and imposing certain constraints on these (the so called Coulomb or radiation gauge), the wave equation can be derived and will be equal to the classical case.

The difference however, between the classical and quantum theories lies in the possible values of the energy that the field can have. We know from the work of Planck on blackbody radiation that the energy has to be quantized in order to fit the radiation spectrum.

In order to quantize the theory one can introduce canonical conjugate coordinates for each degree of freedom, and apply commutation relations between them. At any given instant of time, the vector potential must be defined at any given point in space. But this implies that the electromagnetic field has continuous infinite degrees of freedom, thus making it difficult to solve. The usual trick to simplify this is to imagine a large cube, of side L and volume $V = L^3$, enclosing the radiation. This imposes boundary conditions on the vector field. At the end of the calculation we let $L \to \infty$, and thereby avoid the unphysical cube.[3] The vector potential can then be expressed as a Fourier series, and by doing so, becomes specified by a discrete number of Fourier expansion coefficients. In this way we have gone from a *continuous* number of infinite degrees of freedom to a description of the field in terms of an infinite set of *discrete* number of degrees of freedom. The Fourier analysis corresponds to finding the normalized modes of the radiation field, where each mode here means a particular single-frequency oscillatory pattern, defined by

[2] A vector potential, $\mathbf{A}$, is a vector field, whose curl also is a vector field; $\mathbf{v} = \nabla \times \mathbf{A}$

[3] It can be shown that in the limit $L \to \infty$ the introduction of the boundary conditions is not strictly necessary [5, 6]. However, even if this way of solving for $\mathbf{A}$ does simplify calculations later on, it does nevertheless remove some of the physical understanding of the phenomena.

the wave vector and the direction of polarization. Each mode is described by a harmonic oscillator equation, which makes it possible to use the familiar results found in quantization of the harmonic oscillator.

We can generalize directly from a single harmonic oscillator to a superposition of independent oscillators, each with a specific mode given by $\mathbf{k}$ and s. The eigenfunctions for a single harmonic oscillator can be written as a creation operator acting on the vacuum state

$$|n\rangle = \frac{\left(\hat{a}^\dagger\right)^n}{\sqrt{n!}}|0\rangle \tag{2.5}$$

with energy eigenvalues

$$E_n = \hbar\omega\left(n + \frac{1}{2}\right), \quad n = 0, 1, 2, 3, \ldots \tag{2.6}$$

The eigenfunctions of the radiation Hamiltonian then becomes a product of the individual states given by equation (2.5)

$$|\ldots n_s(\mathbf{k})\ldots\rangle = \prod_{\mathbf{k}_i}\prod_{s_i}|n_{s_i}(\mathbf{k}_i)\rangle \tag{2.7}$$

with energy

$$\hat{H}_{rad} = \sum_{\mathbf{k}}\sum_{s}\hbar\omega_{\mathbf{k}}\left(n_s(\mathbf{k}) + \frac{1}{2}\right) \tag{2.8}$$

Such a state is known as a *Fock state* of the radiation field, and it specifies the state space for the radiation. Using the lowering operator, $\hat{a}_s(\mathbf{k})$, on the Fock state will reduce the occupation number, $n_s(\mathbf{k})$, of the mode $(\mathbf{k}, s)$ by one, and the energy is reduced by $\hbar\omega_{\mathbf{k}} = \hbar c|\mathbf{k}|$. The discrete excitations of the quanta of the radiation field are known as photons, and thus a state $|\ldots 0, 0, 1_{\mathbf{k},s}, 0, 0, \ldots\rangle$ is described as a state with one photon of wave vector $\mathbf{k}$ and polarization s.

The state with the lowest energy is the vacuum state $|0\rangle$. The energy of this state can be found by using equation (2.6) and putting $n_s(\mathbf{k}) = 0$. This gives

$$\hat{H}_{rad,0} = \frac{1}{2}\sum_{\mathbf{k}}\sum_{s}\hbar\omega_{\mathbf{k}} \tag{2.9}$$

This is a constant infinite energy, and is thus unphysical. The standard way to avoid this is to shift the zero of the energy scale, so that the Hamiltonian of the radiation field becomes[4]

$$\hat{H}_{rad} = \sum_{\mathbf{k}}\sum_{s}\hbar\omega_{\mathbf{k}}\hat{a}_s^\dagger(\mathbf{k})\hat{a}_s(\mathbf{k}) \tag{2.10}$$

When the states of the harmonic oscillators are specified as in equation (2.7) with occupation numbers $n_s(\mathbf{k})$, the representation is called number representation. This representation makes

[4]Although it is necessary to do this shift in the energy scale, it may be considered a weakness that the correct zero point energy does not come naturally form the theory. Especially since the error would appear to be infinitely large.

it possible to calculate the transitions between states containing a definite number of photons with well defined properties. The occupation number for the photon can take any integer value. Thus, photons satisfy Bose-Einstein statistics. In other words, they act like bosons. The energy eigenvalue in the number representation can be interpreted to mean that each of the $n_s(\mathbf{k})$ photons belonging to this mode carries an energy $\hbar\omega$.

Finally, looking at the polarization of the photons from a more general point of view, and not only looking at the two linear polarizations that we have done so far, one finds that a general polarization state can be obtained by forming linear combinations of a real and a complex part of the polarization vector

$$-\frac{1}{\sqrt{2}}[\epsilon_1(\mathbf{k}) + i\epsilon_2(\mathbf{k})], \quad \frac{1}{\sqrt{2}}[\epsilon_1(\mathbf{k}) - i\epsilon_2(\mathbf{k})] \tag{2.11}$$

If we remember that the vectors $\epsilon_1(\mathbf{k})$, $\epsilon_2(\mathbf{k})$ and $\mathbf{k}$ form a right handed Cartesian coordinate system, we can see that the two combinations above corresponds to angular momentum $\pm\hbar$ in the direction $\mathbf{k}$. In other words, they represent right- and left-circular polarization, and the photon behaves like a spin 1 particle.

All of these properties of the photon may suggest that it should be treated as a particle, but we have to remember that there is no position operator for the photon, and the quantization we have done is a quantization of the energy.

However, it is possible [4] to create a state that would give an approximate localized photon at some given time. This would then smear out the value of the wave vector $\mathbf{k}$ into a Gaussian shape around some $\mathbf{k}_0$. This can then be regarded as a photon approximately localized in the form of a wave packet centred at some position $\mathbf{r}_0$ at the given time. This is a description which will be used later when describing the down-conversion process, and is the simplest and most common description of light from a quantum mechanical point of view. The challenge arises when one is trying to picture the photon as a classical particle and give it behavioural characteristics based on this picture. This interpretation is the reason for the seemingly conflict between the wave and particle picture of light. If we remember back, the starting point for the quantum mechanical derivation are fields, and it is primarily the quantization in the energy and characteristics from this that allows of a particle-like interpretation.

We should also note that a state with a definite number of photons cannot be a classical field, even if the number of photons in this state would go to infinity.[5] This is a consequence of the fact that the electric field being linear in the creation and annihilation operators. Thus, the expectation value of the electric field in such a state vanishes. One can, however, recover the classical fields in the limit when the number of photons going to infinity, by introducing a so called coherent state.

2.2.1 Coherent states, mixed states and P-representation

In classical theory we've seen that the complex envelope A_0 (equation (2.2)) can have well defined phase and amplitude. In quantum theory, A_0 gets replaced by the annihilation operator $\hat{a}$,

[5] Is the opposite true as well? That we cannot go to a Fock state by reducing the intensity of the beam to single photon level?

and as such, the expectation value of $\hat{a}$ should be identified with the complex envelope. However, using the Fock states $|n\rangle$ we find that

$$\langle n|\hat{a}|n\rangle = 0 \tag{2.12}$$

Thus, as it turns out, using the Fock states we get no information about the amplitude or phase of the field, and thus they cannot be used to describe classical fields. In order for us to be able to represent a field with a well defined amplitude and phase, we need to introduce a new class of states called *coherent states*. These states were introduced by Glauber [8, 9] and are written as $|\alpha\rangle$. Since Fock states form a complete set, we write the coherent state as a superposition of these

$$|\alpha\rangle = e^{-\frac{1}{2}|\alpha|^2} \sum_{n=0}^{\infty} \frac{\alpha^n}{n!} |n\rangle \tag{2.13}$$

Using this expression, we can find that the coherent states also form a complete set, that they are non-orthogonal, so that any coherent state can be written in terms of other coherent states, and that a coherent state can, just like the Fock state, be generated from the vacuum state. However, unlike Fock states, coherent states are so called minimum uncertainty states, which means, from Heisenberg's uncertainty relation, that the product of two quadratures of the field is equal to its minimum value. We will see in a moment why this is of interest. In addition, coherent states do not spread out with time like a wave packet in free space. As time progresses the coherent state evolves into another coherent state, just with a different phase.

Yet another class of states of the radiation are *mixed states*. A mixed state is, as usual, a state expressed in terms of density matrices. For thermal radiation, which belongs to this class, the density matrix becomes

$$\rho = \frac{e^{-\frac{\hbar\omega\hat{a}^\dagger\hat{a}}{K_B T}}}{\mathrm{Tr}\left(e^{-\frac{\hbar\omega\hat{a}^\dagger\hat{a}}{K_B T}}\right)} \tag{2.14}$$

where K_B is Boltzmann's constant and T the temperature. Using the Fock state we can write this as

$$\rho_T = \sum_n p_n |n\rangle\langle n| \tag{2.15}$$

where p_n is the Bose-Einstein distribution, which is a function of the mean number of photons, which again is dependent on the frequency and temperature.

These three examples of different states of the radiation field (Fock, coherent and mixed) are all examples of different mathematical descriptions of light, with different properties. It is, however, possible to express *any* state, ρ, as a sum over coherent states, $|\alpha\rangle$, even though these are non-orthogonal. This kind of representation is called P-representation:

$$\rho = \int P(\alpha)|\alpha\rangle\langle\alpha|\mathrm{d}^2\alpha \tag{2.16}$$

where

$$\int P(\alpha)\mathrm{d}^2\alpha = 1 \tag{2.17}$$

This representation can be considered valid for all radiation fields, if one removes the restriction that $P(\alpha)$ must represent a probability distribution. The general expressions for P for the Fock state, the coherent state and the thermal state, respectively, are given from

$$\rho = |n\rangle\langle n| \Rightarrow P_n(\alpha) = e^{|\alpha|^2}\frac{1}{n!}\frac{\partial^{2n}}{\partial\alpha^n\partial\alpha^{*n}}\delta^{(2)}(\alpha) \tag{2.18}$$

$$\rho = |\alpha_0\rangle\langle\alpha_0| \Rightarrow P_c(\alpha) = \delta^{(2)}(\alpha - \alpha_0) \tag{2.19}$$

$$\rho = \frac{e^{-\frac{\hbar\omega\hat{a}^\dagger\hat{a}}{K_BT}}}{\mathrm{Tr}\left(e^{-\frac{\hbar\omega\hat{a}^\dagger\hat{a}}{K_BT}}\right)} \Rightarrow P_T(\alpha) = \frac{1}{\pi\langle n\rangle}e^{-|\alpha|^2/\langle n\rangle} \tag{2.20}$$

Interesting to note is that P for the thermal state has a Gaussian distribution, similar to a classical probability distribution, which is what we would expect for thermal light. But one has to remember that $P(\alpha)$ may be singular or non-existent for other states. Yet, the fact that we can represent many different types of light using the same mathematical formalism, while we see clear differences in measurement outcomes when real physical changes are made to the setup, indicates that the differences between the light may originate from real physical processes.

Because the P-function for the coherent field behaves in the same manner as a classical probability distribution, a photon detector will not differentiate between a quantum field described by a coherent state and a classical field. This is because the coherent states have, like classical states, well defined phases and amplitudes.

The Fock states, on the other hand, differ very much from coherent or classical states. This can be seen if one looks at the fluctuation in the number of photons. For a coherent state the fluctuations become smaller and smaller as the average number of photons increases. For the Fock state, the number of photons in the field is very precisely specified. This also means that the the average field is zero and the P-function for a state of n photons becomes singular. Thus, the behaviour of the P-function determines if the field can be considered non-classical: if the P-function does not have the properties of a classical probability distribution, then the field is to be considered non-classical.[6]

Unfortunately, the P-function for non-classical fields cannot be measured directly, since it might be singular or not even exist. We therefore have to use other characteristics to experimentally determine the state of the fields.

2.3 Experimental measurements of the non-classicality of light

Fortunately, there are a few other parameters which can be used besides the P-function to characterize the state of the field. One way is to use the quadratures of the field, X and Y, and measure the fluctuations in these. By introducing the factor

$$X_\theta = \frac{ae^{-i\theta} + a^\dagger e^{i\theta}}{\sqrt{2}} \tag{2.21}$$

[6]Still, a coherent state can be expressed using Fock states (equation (2.13)), so mathematically there is a strong connection between these two representations.

and define a squeezing parameter

$$S_\theta = \langle : (X_\theta)^2 : \rangle - \langle X_\theta \rangle^2 \tag{2.22}$$

where :: stands for normal ordering of the operators, we get $S_\theta = 0$ for coherent states, $S_\theta = \langle n \rangle$ for thermal states and $S_\theta = -n$ for Fock states. The negative value of S_θ can be shown to be an indicator of non-classical fields.

Squeezed states are states which has a larger fluctuation in one of its quadratures than in the other, while the product of these is equal to the lowest value given by the uncertainty relation (in the same way as the coherent states). This is a non-classical state, in the sense that S_θ becomes negative (note that X_θ is a linear combination of X and Y, as $\theta = 0 \rightarrow X_\theta \rightarrow X$ and $\theta = \pi/2 \rightarrow X_\theta \rightarrow Y$).

The importance of squeezed states in connection to the non-classicality of light is that squeezed states have a S_θ which is negative. This is, however, a mathematical constructed entity, while we are mostly interested in the real physical processes and effects. Experimentally, squeezed states can be generated in interactions between light and a non-linear material, and in particulary in processes of spontaneous parametric down-conversion.

2.3.1 Spontaneous parametric down-conversion

Spontaneous parametric down-conversion[7] (SPDC) is a process in which a coherent beam of light of frequency ω_p interacts with a non-linear material to produce light with a frequency $\omega_p/2$. In a photon description we say that a photon with energy $\hbar\omega_p$ is split into two photons with energy $\hbar\omega_p/2$.[8]

The total single-mode Hamiltonian for this interaction process (unperturbed plus interaction) can be written as follows [10]

$$\hat{H}(t) = \hbar\omega_1 \hat{a}_1^\dagger \hat{a}_1 + \hbar g \left(\hat{a}_1^{\dagger 2} v_0 e^{-2i\omega_1 t} + v_0^* \hat{a}_1^2 e^{2i\omega_1 t} \right) \tag{2.23}$$

where ω_1 is the frequency of the down-converted photons, v_0 is the complex amplitude of the pump field and g is a coupling constant which depends on the non-linear susceptibility and the lower index 1 indicates the single mode. One should also note that the creation and annihilation operators in this expression are time dependent. The Heisenberg equation of motion for the annihilation operator $\hat{a}_1(t)$ then becomes

$$\dot{\hat{a}}_1(t) = \frac{1}{i\hbar} \left[\hat{a}_1, \hat{H} \right] = -i\omega_1 \hat{a}_1 - 2ig\hat{a}_1^\dagger v_0 e^{-2i\omega_1 t} \tag{2.24}$$

with the general solution

$$\hat{a}_1(t) = \hat{a}_1(0) \cosh(2g|v_0|t) e^{-i\omega_1 t} - i\frac{v_0}{|v_0|} \hat{a}_1^\dagger(0) \sinh(2g|v_0|t) e^{-i\omega_1 t} \tag{2.25}$$

[7] Sometimes called *parametric fluorescence* or *parametric scattering*

[8] This is a simplified description, because the two photons do not need to have exactly the same frequency as long as the requirement $\omega_p = \omega_s + \omega_i$ (where s and i represents the two down converted photons) is fulfilled.

This will give us, under the assumption that $\hat{a}_1(0)|0\rangle = 0 = \langle 0|\hat{a}_1^\dagger(0)$,

$$\langle \hat{a}_1(t)\rangle = 0 \tag{2.26}$$

$$\langle \hat{a}_1^2(t)\rangle = -\frac{i}{2}\frac{v_0}{|v_0|}\sinh(4g|v_0|t)e^{-2i\omega_1 t} \tag{2.27}$$

$$\langle \hat{n}_1(t)\rangle = \langle \hat{a}_1^\dagger(t)\hat{a}_1(t)\rangle = \sinh^2(2g|v_0|t) \tag{2.28}$$

If we now construct the following Hermitian operator (similar to equation (2.21))

$$\hat{X} = \hat{a}_1 e^{i(\omega_1 t-\beta)} + \hat{a}_1^\dagger e^{-i(\omega_1 t-\beta)} \tag{2.29}$$

and calculates the dispersion of $\hat{X}$

$$\langle\left[\Delta\hat{X}(t)\right]^2\rangle = \langle\hat{a}_1^2(t)\rangle e^{2i(\omega_1 t-\beta)} + \langle\hat{a}_1^{\dagger 2}(t)\rangle e^{-2i(\omega_1 t-\beta)} + 2\langle\hat{a}_1^\dagger(t)\hat{a}_1(t)\rangle + 1 \tag{2.30}$$

we arrive at

$$\langle\left[\Delta\hat{X}(t)\right]^2\rangle = -\sinh(4g|v_0|t)\sin(2\beta - \arg v) + \cosh(4g|v_0|t) \tag{2.31}$$

when using the results above. By choosing the phase angle β such that $2\beta - \arg v = \pi/2$, then $\langle\left[\Delta\hat{X}(t)\right]^2\rangle = e^{4g|v_0|t}$, which is less than unity for all $t > 0$. So the fields that are generated from spontaneous parametric down-conversion are always squeezed states, and hence non-classical.[9] This fact has been used in several experiment for studying the non-classical nature of light, so also in our own.

2.4 Bell's inequality as formulated by Aspect

As was mentioned in the introduction, our own experimental setup resembles very much the setup used by Aspect and his colleagues in their measurements. With this setup, Bell's inequality can be measured and thus reveal information about the nature of the light involved in the measurement process. We will therefore here follow Aspect's theoretical derivation to show how to relate the different measurement results to Bell's inequality.

In the article "On the Einstein Podolsky Rosen paradox" [11] from 1964, Bell discussed the thought experiment given by Einstein, Podolsky and Rosen (EPR) in their famous article "Can Quantum-Mechanical Description of Physical Reality Really Be Considered Complete?" [12], where the authors questions the completeness of the quantum theory. Bells article leads to the derivation of the so called Bell inequality, which gives an experimental way of testing the validity of any local, hidden variable theory, thus makes it possible to test the thought experiment by EPR. Quantum mechanics predicts that the inequality should not be fulfilled. Thus, if we can measure

[9] Under the given assumption about the phase angle. For another value of β than the one given, $\langle\left[\Delta\hat{X}(t)\right]^2\rangle$ does not have to be less than unity.

it with the light we use in our experiments, we can use the result as an indication of the nature of the light involved in the measurements.

Several important works have been based on the Bell inequality and consequences thereof [13–15], mainly in the frame of testing the EPR thought experiment. In 1969 Clauser, Horne, Shimony and Holt (CHSH) published an article [15] that generalized Bell's inequality so that it could be applied to realizable experiments. But although this article allows Bell's inequality to be tested experimentally, it restricts the experiment to a specified experimental setup and introduces large uncertainties through the coincidence rates. In an article from 1982 Aspect, Grangier and Roger [13] derived an expression for the Bell inequality based on probabilities, which in this context makes the end result somewhat clearer. Here we follow the argumentation as given by [16].

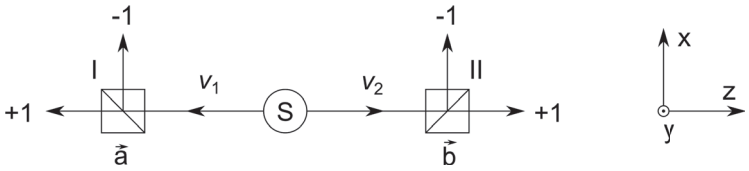

Figure 2.1: Two polarization correlated photons are sent towards two polarizing beam splitters (I and II) and registered. If the direction of polarization of photon 1 is parallel to the direction of the PBS the outcome becomes +1, while a polarization in the direction perpendicular to the direction of the PBS registers as -1 in the detectors.

Our starting point is a source that emits photon pairs with correlated polarizations, see Figure 2.1. The two photons move in either direction from the source towards polarizing beam splitters. The polarization measurement along the direction a (which is perpendicular to the propagation direction of the photon) can give the results $+1$ or -1, indicating a linear polarization either parallel or perpendicular to a. The corresponding eigenstates are

$$\begin{aligned} |+_a\rangle &= \cos\theta_1|x\rangle + \sin\theta_1|y\rangle \\ |-_a\rangle &= -\sin\theta_1|x\rangle + \cos\theta_1|y\rangle \end{aligned} \tag{2.32}$$

where θ_1 is the angle between a and the x-axis, and $\{|x\rangle, |y\rangle\}$ is the basis of linear polarization along x and y.

The observable that correspond to this polarization measurement along a, with eigenvalues ± 1, is

$$\hat{A}(a) = (+1)|+_a\rangle\langle+_a| + (-1)|-_a\rangle\langle-_a| \tag{2.33}$$

In the $\{|x\rangle, |y\rangle\}$ basis it can be written

$$\hat{A}(a) = \begin{bmatrix} \cos 2\theta_1 & \sin 2\theta_1 \\ \sin 2\theta_1 & -\cos 2\theta_1 \end{bmatrix} \tag{2.34}$$

Similarly, polarizer II performs a measurement on photon 2 along b associated with an observable $\hat{B}(b)$.

We assume that the source is producing pairs of photons which can be represented by the state

$$|\phi(1,2)\rangle = \frac{1}{\sqrt{2}}\{|x,x\rangle + |y,y\rangle\} \tag{2.35}$$

where $|x,x\rangle$ is a state with photon ν_1 polarized along x and propagating towards polarizer I, and photon ν_2 polarized along x and propagating towards polarizer II. Quantum mechanics gives that the probability to measure $+1$ in I (oriented along a) and $+1$ in II (oriented along b) is given as

$$P_{++}(a,b) = |\langle +_a, +_b|\nu_1,\nu_2\rangle|^2 = \frac{1}{2}\cos^2(\theta_{II} - \theta_I) = \frac{1}{2}\cos^2\theta \tag{2.36}$$

with $\theta = \theta_{II} - \theta_I$ being the relative angle between the polarizers, and $|\nu_1,\nu_2\rangle$ being the photon state. In a similar manner we get

$$\begin{aligned} P_{--}(a,b) = P_{++}(a,b) = \frac{1}{2}\cos^2\theta \\ P_{+-}(a,b) = P_{-+}(a,b) = \frac{1}{2}\sin^2\theta \end{aligned} \tag{2.37}$$

We can also calculate $P_+(a)$, the probability to obtain $+1$ in I whatever the result in II,

$$P_+(a) = P_{++}(a,b) + P_{+-}(a,b) = \frac{1}{2} \tag{2.38}$$

and similarly

$$P_-(a) = P_+(b) = P_-(b) = \frac{1}{2} \tag{2.39}$$

The results of measurements in I and II appear as random variables $\mathscr{A}(a)$ and $\mathscr{B}(b)$, which can take the values $+1$ and -1, with mean values equal to zero ($\overline{\mathscr{A}(a)} = P_+(a) - P_-(a) = 0$, $\overline{\mathscr{B}(b)} = 0$). We know that two random variables are correlated if the mean value of their product is different from the product of their mean values. In a quantitative way, we define the coefficient of correlation

$$r(\mathscr{A},\mathscr{B}) = \frac{\overline{\mathscr{A}\cdot\mathscr{B}} - \overline{\mathscr{A}}\cdot\overline{\mathscr{B}}}{(\overline{\mathscr{A}^2}\cdot\overline{\mathscr{B}^2})^{1/2}} \tag{2.40}$$

We can simplify this expression since $\overline{\mathscr{A}^2} = \overline{\mathscr{B}^2} = 1$ and $\overline{\mathscr{A}} = \overline{\mathscr{B}} = 0$

$$r(\mathscr{A},\mathscr{B}) = \overline{\mathscr{A}(a)\cdot\mathscr{B}(b)} \tag{2.41}$$

So the correlation coefficient is equal to the mean value of the product $\mathscr{A}(a)\cdot\mathscr{B}(b)$. This product can only take values $+1$ or -1 and its mean value can be written as

$$E(a,b) \equiv \overline{\mathscr{A}(a)\cdot\mathscr{B}(b)} = P_{++}(a,b) + P_{--}(a,b) - P_{+-}(a,b) - P_{-+}(a,b) \tag{2.42}$$

Using the results from equation (2.37) we arrive at

$$E_{QM}(a,b) = \cos 2\theta \tag{2.43}$$

where again $\theta = \theta_{II} - \theta_I$ is the relative angle between the polarizers.

We now assume that the two photons possess a set of common properties, characterized by the parameter λ. The two photons move in either direction from the source towards polarizing beam splitters (I and II). The polarization measurement along the direction a can give the results $+1$ or -1, indicating a linear polarization either parallel or perpendicular to a. We call these results, which now are deterministic, $A(a, \lambda)$. In a similar way we obtain for the orientations b, $B(b, \lambda) = \pm 1$.

We now assume that each pair generated by the source is characterized by different λ, and that the behaviour of the source is described by a probability density ρ, such that

$$\rho \geq 0 \tag{2.44}$$

$$\int_\Omega \mathrm{d}\lambda \rho(\lambda) = 1 \tag{2.45}$$

where Ω is the space of λ.

Any particular theory should be able to specify the functions $\rho(\lambda)$, $A(\lambda, a)$ and $B(\lambda, b)$. One can then calculate the probability associated with the measurement results. In particular, using the quantity

$$\frac{1}{2}\left[A(\lambda, a) + 1\right] = \begin{cases} +1 & \text{when } a = +1 \\ 0 & \text{when } a = -1 \end{cases} \tag{2.46}$$

one can express the probability for getting $+1$ when the beam splitter I is oriented along a as

$$P_+(a) = \frac{1}{2}\int_\Omega \mathrm{d}\lambda \rho(\lambda)\left[A(\lambda, a) + 1\right] \tag{2.47}$$

In the same manner, the coincidence probabilities can be expressed as

$$P_{++}(a, b) = \frac{1}{4}\int_\Omega \mathrm{d}\lambda \rho(\lambda)\left[A(\lambda, a) + 1\right]\left[B(\lambda, b) + 1\right] \tag{2.48}$$

But we saw above (equation (2.42)) that the correlations appear in the expression for the coefficient of correlation, which can be expressed as the mean value of the product of $A(\lambda, a)$ and $B(\lambda, b)$

$$E(a, b) = \overline{A(a, \lambda) \cdot B(b, \lambda)} = \int_\Omega \mathrm{d}\lambda \rho(\lambda) A(a, \lambda) B(b, \lambda) \tag{2.49}$$

We can now use this coefficient of correlation $E(a, b)$ to express Bell's inequality, in terms of the formalism of CHSH. Consider four successive measurements of the polarization correlation coefficient, obtained for two orientations (a and a') of polarizer I, and two orientations (b and b') of polarizer II. If we consider the expression

$$s = A(\lambda, a) \cdot B(\lambda, b) - A(\lambda, a) \cdot B(\lambda, b') + A(\lambda, a') \cdot B(\lambda, b) + A(\lambda, a') \cdot B(\lambda, b') \tag{2.50}$$

where $A(\lambda, a) = A(\lambda, a') = B(\lambda, b) = B(\lambda, b') = \pm 1$, we can see that $s = \pm 2$. The mean value of s, $S(a, a', b, b')$, must then lie between -2 and 2.

$$-2 \leq \int \mathrm{d}\lambda \rho(\lambda) s(\lambda) \leq 2 \tag{2.51}$$

By simply inserting the expression for s we immediately see that S can be expressed as

$$S = E(a,b) - E(a,b') + E(a',b) + E(a',b') \tag{2.52}$$

A thought experiment is given to relate measurable quantities with the inequality by Bell. This experiment consists of the same setup as in Figure 2.1, but the orientations of the beam splitters is random and recordings are done on the outcome from the detectors ($++$, $--$, $+-$ or $-+$) as well as the positioning ($\vec{a}$ and $\vec{b}$) of the beam splitters. After N measurements carried out on N pairs, four numbers, $N_{\pm\pm}(a_i, b_j)$, are recorded for each configuration (a_i, b_j). From this it is possible to determine the correlation coefficient for each configuration.

$$E(a_i,b_j) = \frac{N_{++}(a_i,b_j) + N_{--}(a_i,b_j) - N_{+-}(a_i,b_j) - N_{-+}(a_i,b_j)}{\sum_{\pm\pm} N_{\pm\pm}(a_i,b_j)} \tag{2.53}$$

By relating this expression to the one above, the Bell inequality in the case of varying polarizers becomes

$$S = E(a_i,b_j) - E(a_i,b_{j'}) + E(a_{i'},b_j) + E(a_{i'},b_{j'}) \tag{2.54}$$

where

$$-2 \leq S \leq 2 \tag{2.55}$$

2.5 Simple model for SPDC in our setup

In measurements were we study the differences in the behaviour between classical and quantum light, the concept of entanglement is a key component. This is because entanglement does not have any classical analog. An entangled state is an inseparable state, meaning that it cannot be factorized into states being summations of single entities (so called pure states), and such an entangled state has no classical counterpart.

As was mentioned, light generated from SPDC can be made non-classical and has therefore been used as a source for experiments studying the quantum nature of light. In our experiments, we've used type II SPDC in a periodically poled potassium titanyl phosphate crystal (ppKTP), with the photon pairs exiting the crystal collinearly with the pump beam. The natural birefringence of the ppKTP crystal is said to introduce an arrival time difference of the photons in the pair, which is compensated for by adding an additional KPT crystal rotated 90° in relation to the ppKTP. The photon pair then enters a 50/50 non-polarizing beam splitter (NPBS) and is analysed by having a rotating half wave plate (HWP) and a polarizing beam splitter (PBS) in each arm. In essence; similar to Aspect's setup in Figure 2.1. A more comprehensive discussion about the implementation of this setup will be presented in section 4.1.

As was mentioned earlier, it is possible to approximate the location of the photon at some given time. This gives a very simple interpretation of the different steps of the calculations, since we can imagine photons as they pass through the optical setup. Let us go through this calculation and see how we can interpret this description in terms of physical processes.

2.5.1 Quasi-localized photons

In this model, spontaneous parametric down-conversion can be described as one incoming photon being split into a pair of photons with orthogonal polarizations. In the simplest case, this can be written as an annihilation operator acting on the incoming photon state and two creation operators acting on the vacuum state. The annihilation is often dropped however, so our starting point is the following state

$$|\Psi\rangle = a_H^\dagger a_V^\dagger |0\rangle \otimes |0\rangle = |H\rangle \otimes |V\rangle = |H\rangle|V\rangle = |HV\rangle \tag{2.56}$$

where H and V stands for horizontal and vertical linear polarization, respectively, and the last three terms are just equivalent ways often found in the literature of writing the same state. The photon pair, which according to the standard theory is not yet entangled in polarization, continues to the NPBS, which acts differently depending on whether the photons are being reflected or transmitted

$$\begin{aligned} |H\rangle &\xrightarrow{\text{NPBS}} |H\rangle_a + i|H\rangle_b \\ |V\rangle &\xrightarrow{\text{NPBS}} |V\rangle_a - i|V\rangle_b \end{aligned} \tag{2.57}$$

where a and b indicates the state of the photon with the given polarization (H or V) in the transmitted (Alice) and reflected (Bob) arm. This gives

$$|H,V\rangle \xrightarrow{\text{NPBS}} (|H\rangle_a + i|H\rangle_b)\,(|V\rangle_a - i|V\rangle_b) \tag{2.58}$$

If we use the fact the there is no special meaning to the ordering of the states in the tensor product, so that we can write $|H\rangle_b|V\rangle_a = |V\rangle_a|H\rangle_b$, we can expand this product to obtain

$$|H,V\rangle \xrightarrow{\text{NPBS}} |H\rangle_a|V\rangle_a - i|H\rangle_a|V\rangle_b + i|V\rangle_a|H\rangle_b + |H\rangle_b|V\rangle_b \tag{2.59}$$

By post-selecting on the combinations giving coincidences, i.e. choosing only the terms that has an ab-combination, we get a polarization entangled state

$$|\Psi^-\rangle_{ab} = |H\rangle_a|V\rangle_b - |V\rangle_a|H\rangle_b. \tag{2.60}$$

Or properly normalized

$$|\Psi^-\rangle_{ab} = \frac{1}{\sqrt{2}}\left(|H\rangle_a|V\rangle_b - |V\rangle_a|H\rangle_b\right). \tag{2.61}$$

This is state is an entangled state.

After the the NPBS the photons will pass through the HWP in Alice's and Bob's arm. The effect of these HWPs, when set at angles α and β in real space with respect to the horizontal direction, on a state with one horizontal and one vertical polarized photon, can be written out as

$$|HV\rangle \xrightarrow{\text{HWP at } \alpha,\beta} |H_\alpha V_\beta\rangle = (\cos 2\alpha|H\rangle + \sin 2\alpha|V\rangle)\,(-\sin 2\beta|H\rangle + \cos 2\beta|V\rangle) \tag{2.62}$$

$$|VH\rangle \xrightarrow{\text{HWP at } \alpha,\beta} |V_\alpha H_\beta\rangle = (-\sin 2\beta|H\rangle + \cos 2\beta|V\rangle)\,(\cos 2\alpha|H\rangle + \sin 2\alpha|V\rangle) \tag{2.63}$$

The probabilities for finding the system in each of the four basis states ($|HH\rangle$, $|HV\rangle$, $|VH\rangle$ and $|VV\rangle$) as functions of α and β then becomes

$$p^{++} = |\langle HH|\Psi^-\rangle|^2 = \frac{1}{2}\sin^2 2(\alpha-\beta) \tag{2.64}$$

$$p^{+-} = |\langle HV|\Psi^-\rangle|^2 = \frac{1}{2}\cos^2 2(\alpha-\beta) \tag{2.65}$$

$$p^{-+} = |\langle VH|\Psi^-\rangle|^2 = \frac{1}{2}\cos^2 2(\alpha-\beta) \tag{2.66}$$

$$p^{--} = |\langle VV|\Psi^-\rangle|^2 = \frac{1}{2}\sin^2 2(\alpha-\beta) \tag{2.67}$$

which gives a correlation coefficient that goes as

$$E_{|\Psi^-\rangle} = p^{++} - p^{+-} - p^{-+} + p^{--} = -\cos 4(\alpha-\beta) \tag{2.68}$$

During what we call a twin scan, where the angles α and β are always equal, the correlation becomes -1 for all angles and thus indicates the presence of entanglement between the photons. This result is important, because the same rotational invariance cannot be seen in the classical calculation (as we will show later). Thus, it is an experimental indication of the different nature of the light.

2.5.2 The role of the compensating crystal

The simplistic quantum picture of spontaneous parametric down-conversion used above, we say that a single photon with, in our case, a wavelength of 405 nm, is being split into two photons of 810 nm at some random position inside the crystal. Since we used a crystal cut for type II phase matching, the photons will have orthogonal linear polarizations, and thus travel at different velocities inside the crystal. It is then said that one of the polarized photons will always exit the crystal first, no matter where in the crystal the pair is created, and because of that, the photons can in principle be distinguished by their arrival time. The concept is schematically illustrated in Figure 2.2. Here we have chosen the horizontal polarization (H) to be the one that exit the crystal first.

The role of the compensating KTP crystal is to make sure that no distinction can be made between the photons due to their arrival time, and we say that, due to its orientation, it allows the photon that lags behind to catch up. Now, in this picture, this compensation is only exact (i.e. the two photons exit the compensating crystal at the same time) for a specific location of creation inside the ppKTP, as indicated in Figure 2.2. It has been found, however, that the time compensation is optimal (meaning that we have the greatest violation of Bell's inequality) when the KTP is half of the length of the ppKTP. The idea is that a pair created at the beginning of the ppKTP will be a time shifted version of a pair created at the very end of the ppKTP after the pairs have passed through the compensating crystal. So the pairs created symmetric about the middle of the ppKTP crystal become time shifted versions of each other and we can no longer discriminate between the photons in a pair by looking at their arrival times, according to the standard interpretation.

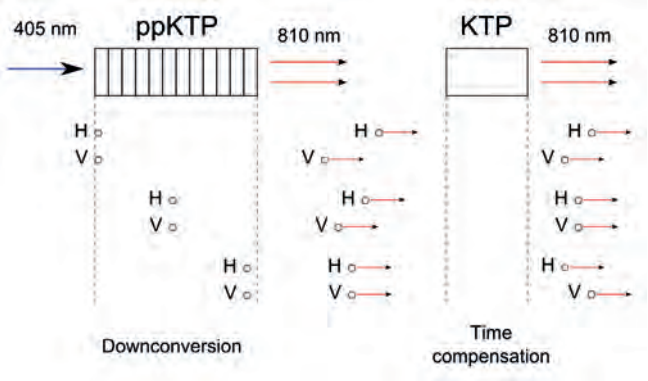

Figure 2.2: A simplistic picture of the SPDC process in a ppKTP crystal with a time compensating KTP making the pair indistinguishable. Depending on where inside the ppKTP crystal the creation of the photon pair takes place, different temporal orderings of the photon pair exiting the compensating crystal will emerge.

It is important to note how this effect really depends on the statistical distribution of many pairs, while the requirement of indistinguishability is very much applied to the behaviour of a single photon pair. In other words, the effect of the indistinguishability in the arrival times of the photons may not be seen for a single pair, yet its effect on a statistical ensemble is used on this single pair.

If we assume that the photon pair is created somewhere inside the ppKTP crystal, there will always be a time difference between the two photons (except for the pairs created exactly in the middle). The extreme value of this time difference (i.e. for a photon pair created at the very beginning or the very end of the crystal) can be calculated from the properties of the KTP material.

KTP is an abbreviation for potassium titanyl phosphate ($KTiOPO_4$), and is a birefringent, biaxial crystal under normal conditions. This means that it has an optics axis (the axis where both the ordinary and extraordinary fields experiences the same index of refraction) which does not follow any of its principle axes (the axes where the index of refraction is constant (n_x,0,0), (0,n_y,0), (0,0,n_z)), and its birefringence does not have any rotational symmetry. From the information given by the crystal supplier (Raicol Crystals Ltd), the ppKTP is cut in such a way that the beam entering the crystal propagate along its x-axis. For this crystal the x-axis corresponds to the two values for the indexes of refraction given by n_y and n_z. These values are given from the Sellmeier equations [17] for the wavelength of interest. We find that

$$\begin{aligned} n_y^2 &= 2.1518 + \frac{0.87862\lambda^2}{\lambda^2 - 0.21801^2} - 0.01327\lambda^2 \\ n_z^2 &= 2.3136 + \frac{1.00012\lambda^2}{\lambda^2 - 0.23831^2} - 0.01679\lambda^2 \end{aligned} \tag{2.69}$$

which for $\lambda = 0.810$ μm[10] gives us

$$\begin{aligned} \mathrm{n_y} &= 1.758 \\ \mathrm{n_z} &= 1.843 \end{aligned} \tag{2.70}$$

Let us look at a photon pair created in the beginning of the ppKTP crystal. The time difference between the two polarizations when they exit the 10 mm long crystal will then be

$$\tau = \frac{L}{c}(\mathrm{n_z} - \mathrm{n_y}) = 2.84 \text{ ps} \tag{2.71}$$

where L is the length of the ppKTP crystal (10 mm). After passing through the compensating crystal, this time difference will be divided by two, so the maximum time difference for a pair of spontaneous parametric down converted photons exiting the KTP is

$$\Delta t = \frac{\tau}{2} = 1.42 \text{ ps} \tag{2.72}$$

This time difference is short enough to include both photons within the 8 ns window of acquisition used in our measurements, but what is interesting is that our event timer can't discriminate between these times. Thus, to the detection process, it is completely indifferent whether we have included a compensating crystal or not. We will discuss this in more detail later, but in terms of interpretations we could just mention that the standard interpretation says that it is the indistinguishability *in principle* which is responsible for the generation of the entangled state. As argued for above, such a indistinguishability is difficult to apply to a single pair, within the present description of the process. In addition, the photons are allowed to have slightly different frequencies, so there is really no indistinguishability in all respects.

2.5.3 Periodic poling

Our nonlinear crystal is periodic poled KTP crystal. This means that the crystal is constructed from alternating sections or layers of KTP, oriented in such a way that the crystal's nonlinearity, $\chi^{(2)}$, switches signs from one layer to the next. Such a construction results in a *continuous* buildup of the intensity of the SPDC light.

In a nonlinear process there is an interaction between the incoming field (the pump field) and the polarization of the material. This material polarization is then generating the new frequencies (signal and idler). In expressing the relationship between the amplitudes of the pump field and the signal and idler, one obtains two expressions which can be interpreted as the spatial wavelength of the nonlinear polarization of the crystal and as the wavelength of the field that it is generating. These two fields are not always in phase, which results in an energy flow alternating between going into the material polarization and going into the generated field.

When these two wavelengths are equal, we say that we have phase matching. The condition for this to be the case is

$$\Delta k = k_p - k_s - k_i = 0 \tag{2.73}$$

[10]The wavelengths in the Sellmeier equations are given in μm, and not in the nowadays more common nm.

where p, s and i stands for pump, signal and idler, respectively. If the orientation of the polarization is not the same in all the fields, phase matching can be achieved in an bi- or uniaxial crystal by using clever orientation of the crystal itself, since k is a function of n and n is depending on the orientation of the crystal's axes and the state of polarization of the light. Thus, the effect of birefringence in the crystal can be used to create a state where $\Delta k = 0$ and is hence named birefringent phase matching.

But phase matching can also be achieved without crystal birefringence by using periodically poling. The length over which the energy flows from the polarization of the material into the generated field is called coherence length.[11] Since the direction of the energy flow is directly dependent of the sign of $\chi^{(2)}$, and this sign can be flipped for special reorientations of the crystal axes, we can achieve a buildup of energy in the field (i.e. create a seemingly long coherence length) similar to phase matching, by using alternating crystal sections, each one coherence length long. Figure 2.3 shows the intensity output in the field in the case of no phase matching (left) and quasi-phase matching through periodically poling (right).

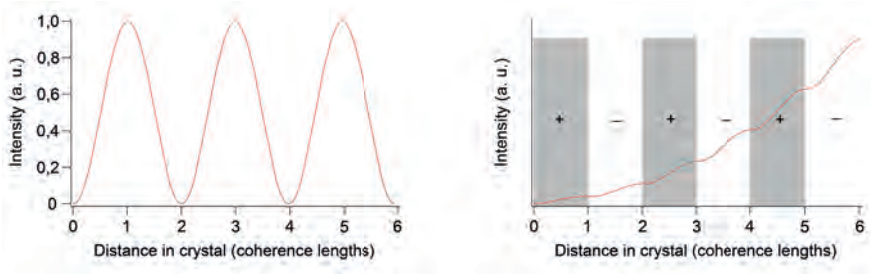

Figure 2.3: The time averaged intensity of the generated field inside the crystal as a function of distance when we have no phase matching (left), and the time averaged intensity inside a periodically poled crystal (right) as a function of distance. Note that the scaling of the amplitude is not the same in these two plots.

Since the orientations of the crystal sections are 0° and 180° there will be no changes to the velocity of the two polarized fields when they go from one section to the next (the fast and slow axis are always parallel to the directions in the preceding segment). So the arrival time difference due to the birefringence can be calculated as if the periodic poling wasn't there, as we have done above.

It should be noted again that in this description of the nonlinear process the intensity of the signal and idler fields is a gradual process, pretty much in direct opposition to the simplified quantum mechanical formalism above, where the photon pair was said to be created at a specific location inside the crystal. We should remember though that the picture of the photon as a localized entity cannot be taken too literally. In the description that we have looked at above, the behaviour was very simplified. In quantum field theory we may use Feynman diagrams to describe the SPDC process, and in such a description we may say that we integrate over all possible locations.

[11] Not to be confused with the coherence length used in coherence theory.

But even if we try to describe the SPDC process in more simple terms, we can only at best use a semi-classical description. This is because the generation of the signal and idler fields requires an input from the zero point vacuum fluctuations. Thus, one usually say that effectively the quantum fluctuations are equivalent to the presence of 1/2 photon in both the signal and idler modes, or one photon in either mode. The total generated power output of the signal and idler is the collective sum of all generated photons. So while the total intensity can be viewed as a gradual process, the generation of the intensity of a single photon cannot. One should note though that, again, we've assumed a process for a single photon based on the statistical behaviour of a large ensemble.

References

[1] Richard A. Beth, *Phys. Rev.* **50**, 115 (1936)

[2] L. Mandel and Emil Wolf, *Optical coherence and quantum optics*, Cambridge university press, 2008, p. 157

[3] A. Pais, *Rev. Mod. Phys.* **51**, 863 (1979)

[4] F. Mandl and G. Shaw, *Quantum field theory*, John Wiley & Sons, 2002, pp. 2-10

[5] W. Ledermann, *Proc. Roy. Soc A* **182**, 362 (1944)

[6] R. Peierls, *Selected Scientific Papers of Sir Rudolf Peierls with Commentary*, World Scientific Publishing, 1996, pp. 121-126

[7] L. Mandel and Emil Wolf, *Optical coherence and quantum optics*, Cambridge university press, 2008, pp. 465480

[8] R. J. Glauber, *Phys. Rev.* **131**, 2766 (1963)

[9] R. J. Glauber, *Phys. Rev. Lett.* **10**, 84 (1963)

[10] A. Yariv, *Quantum electronics*, Wiley, p. 423, (1989)

[11] J. S. Bell, *Physics* **1**, 195 (1964)

[12] A. Einstein, B. Podolsky and N. Rosen, *Phys. Rev.* **47**, 777 (1935)

[13] A. Aspect, P. Grangier, and G. Roger, *Phys. Rev. Lett.* **49**, 91 (1982)

[14] A. Aspect, J. Dalibard and G. Roger, *Phys. Rev. Lett.* **49**, 1804 (1982)

[15] J.F. Clauser, M.A. Horne, A. Shimony, R.A. Holt, *Phys. Rev. Lett.* **23** 880 (1969).

[16] A. Aspect, *Three Experimental Tests of Bell Inequalities by Measurement of the Polarization Correlation of Photons*, Springer, pp. 12-39, not yet published

[17] Dmitriev, V., Gurzadyan, G., Nikogosyan, D., *Handbook of Nonlinear Optical Crystals*, Springer, 2010, p. 113

Chapter 3

Ultrafast optics

Ultrafast optics is the common name for working with pulses that have durations in the picosecond range (10^{-12} s) or below. Today, pulses with durations of the order of a few tens of femtoseconds (10^{-15} s) are routinely generated in many optics labs, and their uses are diverse. Ultrashort pulses have found applications in spectroscopy, metrology, communications, medical applications, studies of filamentation and laser-matter interactions, high-energy physics, and material processing. The pulsed source used in our measurements was an ultrafast Ti:sapphire laser which could generate pulses with durations close to 50 fs.

To put this extremely short pulse duration in some perspective, imagine that we could stretch 1 femtosecond so that it became 1 second long. A single second would then be roughly 30 million years in comparison. At these short durations, effects usually not considered with continuous wave (CW) light or pulses with longer durations, has to be taken into account. Most important in relation to our measurements is the time-bandwidth product and the group velocity dispersion.

3.1 The time-bandwidth product

The time-bandwidth product is a minimum uncertainty expression, similar to Heisenberg's uncertainty relation, and states that the product of the pulse duration and its spectral bandwidth cannot be smaller than some given value. This value is dependent on the temporal shape of the pulse. This means that there is a minimum width of the spectral bandwidth which depends on the duration of the pulse; the shorter the pulse, the wider the bandwidth. Thus, if we picture a photon as a classical wave packet, the photon energy, as given by $E = h\nu$, can only be sharp if the pulse duration tends to infinity.

For a Gaussian pulse the minimum time-bandwidth product is 0.44, and for a sech^2 pulse it is 0.32. Thus, a sech^2 pulse of 50 fs duration can have a minimum bandwidth of

$$\Delta\nu \geq \frac{0.32}{50 \cdot 10^{-15}} \text{ Hz} = 6.4 \cdot 10^{12} \text{ Hz} \tag{3.1}$$

For a central wavelength of $\lambda_c = 800$ nm, this gives us

$$\Delta\lambda = \Delta\nu \frac{\lambda_c^2}{c} = 6.4 \cdot 10^{12} \frac{(800 \cdot 10^{-9})^2}{3 \cdot 10^8} \text{ m} = 1.4 \cdot 10^{-8} \text{ m} = 14 \text{ nm} \tag{3.2}$$

Table 3.1 shows the relation between different pulse lengths and the corresponding minimum spectral bandwidth.

Table 3.1: The minimum bandwidth for Gaussian and sech^2 pulses with different pulse durations and center wavelengths. (Taken from [1].)

Pulse duration	Gaussian bandwidth (nm)					sech^2 bandwidth (nm)				
	450 nm	800 nm	1.3 µm	3 µm	10 µm	450 nm	800 nm	1.3 µm	3 µm	10 µm
25 fs	12	38	99	$5.3{\cdot}10^2$	$5.9{\cdot}10^3$	8.6	27	72	$3.8{\cdot}10^2$	$4.3{\cdot}10^3$
50 fs	5.9	19	50	$2.6{\cdot}10^2$	$2.9{\cdot}10^3$	4.3	14	36	19	$2.1{\cdot}10^3$
70 fs	4.2	13	35	$1.2{\cdot}10^2$	$2.1{\cdot}10^3$	3.1	9.8	26	$1.4{\cdot}10^2$	$1.5{\cdot}10^3$
100 fs	3.0	9.4	25	$1.3{\cdot}10^2$	$1.5{\cdot}10^3$	2.2	6.8	18	96	$1.1{\cdot}10^3$
300 fs	1.0	3.1	8.3	44	$4.9{\cdot}10^2$	0.72	2.3	6.0	32	$3.6{\cdot}10^2$
500 fs	0.59	1.9	5.0	27	$2.9{\cdot}10^2$	0.43	1.4	3.6	19	$2.1{\cdot}10^2$
1 ps	0.30	0.94	2.5	13	$1.5{\cdot}10^2$	0.22	0.68	1.8	9.6	$1.1{\cdot}10^2$
2 ps	0.15	0.47	1.2	6.6	73	0.11	0.34	0.90	4.8	53
5 ps	0.049	0.19	0.50	2.6	29	0.043	0.14	0.36	1.9	21
10 ps	0.030	0.19	0.25	1.3	15	0.021	0.14	0.18	0.96	11
20 ps	0.015	0.047	0.12	0.66	7.3	0.011	0.034	0.090	0.48	5.3

3.2 Group velocity dispersion

Unlike CW laser beams, which can have a fairly small spectral bandwidth (i.e. approximately monochromatic), the bandwidth of an ultrashort pulse has to be considerably larger, due to the time-bandwidth product. For pulses with durations in the range of attoseconds, we talk about a spectral bandwidth consisting of all visible wavelengths – a so called supercontinuum.

Due to the much larger bandwidth for ultrashort pulses, effects such as dispersion in optical components become much more important. As illustrated in Figure 3.1, a short pulse tends to get broadened when passing through an optical transparent material, due to the fact that the index of refraction is different for different frequencies and thus causing lower frequencies (red) to travel faster through the material than higher frequencies (blue). If the material is thick, this can cause the pulse to stretch out and thus become an issue if one wishes to preserve the pulse duration through an optical setup.

The phenomenon that the group velocity depends on the frequency of the light when it passes through a transparent material, is mathematically expressed through the group velocity dispersion (GVD), which is the partial derivative of the inverse group velocity with respect to the angular frequency

$$\mathrm{GVD} = \frac{\partial}{\partial\omega} v_g^{-1} = \frac{\partial}{\partial\omega}\frac{\partial\beta}{\partial\omega} = \frac{\partial^2\beta}{\partial\omega^2} \tag{3.3}$$

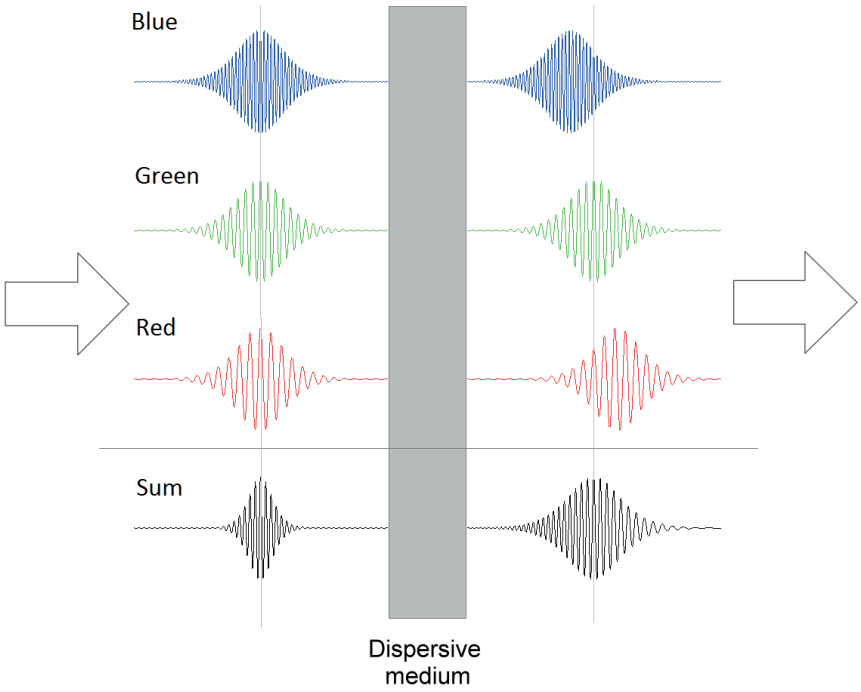

Figure 3.1: An ultrafast pulse (bottom left) can mathematically be described as a linear superposition of (quasi-)monochromatic wave packets (here represented by three different frequencies). Due to dispersion, these wave packets will travel through the dispersive material with different velocities. This results in both a broadening and chirp of the the pulse (bottom right).

where ω is the angular frequency as usual and β is called the propagation constant. This propagation constant can be expressed as a Taylor series

$$\beta(\omega) = \beta(\omega_0) + \frac{\partial\beta}{\partial\omega}(\omega - \omega_0) + \frac{1}{2}\frac{\partial^2\beta}{\partial\omega^2}(\omega - \omega_0)^2 + \dots \tag{3.4}$$

where the derivative is taken at $\omega = \omega_0$. The meaning of the different terms can be written out as

$$\beta(\omega) = \frac{\omega_0}{\text{Phase velocity}} + \frac{\omega - \omega_0}{\text{Group velocity}} + \frac{\text{GVD}}{2}(\omega - \omega_0)^2 \tag{3.5}$$

GVD is measured in units of s^2/m, usually specified in fs^2/mm, which is group delay dispersion (GDD) per length. GDD is the change in group delay with frequency for light passing though a transparent material.

The GDD can be both negative and positive, and is usually referred to as being normal or anomalous, respectively. Normal dispersion is the most common type of dispersion, and means

that higher frequencies travels slower and are thus displaced towards the end of the pulse. For anomalous dispersion higher frequencies are traveling faster and become displaced towards the front of the pulse. Anomalous dispersion is in many cases more favorable, as it can used to compensate for the broadening of a pulse as it passes through other optical components. Also, since GDD is a function of frequency, some materials will pass from normal to anomalous dispersion in the range of the frequencies of interest for the application (that is, for a specific frequency the dispersion will be zero). Thus, cleaver choice of materials can reduce the dispersion to a minimum, if the spectral bandwidth of the pulse that's being used is not too wide and is close to the specified frequency.

GVD can also lead to chirp in an optical pulse. Chirp is the change in the instantaneous frequency as a function of time. In Figure 3.1, normal dispersion leads to a delay in the bluer parts of the pulse spectrum, which means that the pulse becomes chirped, since the instantaneous frequency becomes a function of time.

3.3 Pulse characterization

Most devices for characterizing ultrashort pulses measures, in one way or the other, the electric field as a function of time only. This limits the available information that we can get from the pulse, because possible couplings between space and time (space and frequency) are disregarded. In this way, the effect of these couplings, which may appear as distortions in the pulse, remains undetected.

This, however, is not the only challenge we have to face when wanting to characterize an ultrashort pulse. To directly measure the variation in intensity as a function of time for very short pulses one would need a detector with a very fast response time. For measuring pulses with fs or even ps duration, this would not be possible with present day technology. But there is a way around this problem, and that is by using the pulse itself for the measurement: a so called autocorrelation measurement.

There are two main types of autocorrelators: the intensity autocorrelator and the interferometric autocorrelator, where we have used the last one in our measurements.

3.3.1 Intensity autocorrelation

The intensity autocorrelator, sometimes also known as the background free autocorrelator, works in the following manner (see right hand side of Figure 3.2). A pulse is split in two by a beam splitter (usually a pellicle beam splitter to avoid large group velocity dispersions). One part is delayed with respect to the other, and the two pulses are then recombined and focused onto a nonlinear crystal. If the nonlinear crystal is oriented such that second harmonic generated (SHG) light is generated, the intensity of this light will depend on the amount of overlap between the pulses, i.e. the amount of delay in one of the arms. The intensity will be proportional to the product of the intensity of the two input pulses

$$I^{\text{SHG}} \propto I(t)I(t-\tau) \tag{3.6}$$

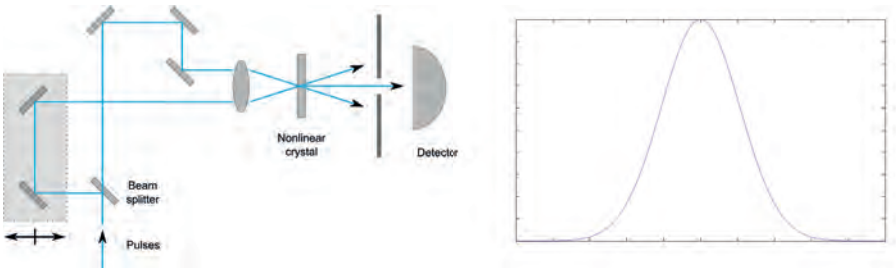

Figure 3.2: A schematic setup of an intensity autocorrelator (right), and the corresponding autocorrelation function (left).

where τ is the delay time. A detector will be too slow to resolve the variations in time, and thus will measure an average given by

$$A(\tau) = \int_{-\infty}^{\infty} I(t)I(t-\tau)\mathrm{d}t \tag{3.7}$$

This is the intensity autocorrelation, and its shape is shown on the left hand side in Figure 3.2.

In the calculations above we have used SHG, but it is also possible to use higher order nonlinearities in the measurement setup. One of the advantages of using higher order nonlinear processes is that the higher power required also results in a better sensitivity in the pulse shape.

The pulse duration cannot be taken directly from the autocorrelation function however, but depends on the shape of the incoming pulse. Unfortunately, its shape cannot be measured with this method, so we have to assume one (usually Gaussian or sech^2). The problem though is that many different intensity distributions can give the same autocorrelation function. In fact, the more complex the intensity distribution is, the more simple does the autocorrelation function become, and approaches the shape of a narrow peak on a pedestal.

3.3.2 Interferometric autocorrelation

We can improve on the above intensity measurement method by making some changes in the measurement setup. In the intensity autocorrelation measurement the two pulses intersected at the nonlinear crystal, but then continued in different directions, as shown in Figure 3.2. In an interferometric autocorrelator the two pulses are collinear, causing interference fringes in the autocorrelation function. Thus, interferometric autocorrelation is sometimes called phase-sensitive autocorrelation or frequency-resolved autocorrelation (FRAC). A schematic view of the setup is shown in Figure 3.3.
In this case, the intensity can be expressed as

$$I^{\mathrm{FRAC}}(\tau) = \int_{-\infty}^{\infty} \left|[E(t) + E(t-\tau)]^2\right|^2 \mathrm{d}t \tag{3.8}$$

If we did not have the squared terms in the above expression, we would again get the expression for the intensity autocorrelation. These new terms are the result of the SHG of each individual

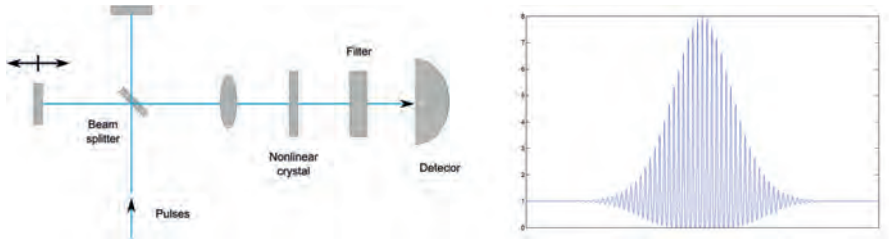

Figure 3.3: The schematic setup of an interferometric autocorrelator (right), and the corresponding autocorrelation function (left). The filter after the non-linear crystal is removing the pump radiation from the beam, so that only the frequency doubled light is involved in the measurement.

pulse, and the interference with each other and the cross term will result in additional information not revealed in the intensity case.

We may also note that the autocorrelation function in this case shows a rapid oscillation with a period of half the optical wavelength. We get a maximum signal when the two pulses exhibit perfect constructive interference. Looking at the signal *before* the nonlinear crystal, the intensity is then twice that of a single pulse, or four times the amplitude. *After* the crystal the amplitude of the signal is 16 times as high as the single pulse amplitude, or eight times the background signal. Hence the peak-to-background ratio is always eight, provided that the interferometer is properly aligned. Thus, by observing this ratio we can get a measure of how well our system is aligned.

Unlike the intensity autocorrelation function, the interferometric autocorrelation function is sensitive to changes in the intensity distribution. Thus, chirped pulses and satellite pulses does affect the shape of the autocorrelation function. Though it is not possible to determine the true shape of the pulse, because different distortions can generate the same autocorrelation function, as shown in Figure 3.4, it is possible to observe changes in the pulse shape due to external influences.

3.3.3 Other pulse characterization methods

There are several other methods, and different variants of these, for obtaining more information about the pulse. Three of the more common ones are listed below.

Modified-spectrum autointerferometric correlation (MOSAIC)

In 2002 Hirayama and Sheik-Bahae presented a new technique to measure the chirp in ultrashort pulses [2]. They called this technique modified-spectrum autointerferometric correlation, or MOSAIC for short.

The technique is based on either post or direct analyzing of interferometric autocorrelation data, by removing the terms involving the fundamental wavelength and enhancing the terms involving the second harmonic wavelength by a factor 2. This can be done using Fourier transform algorithms.

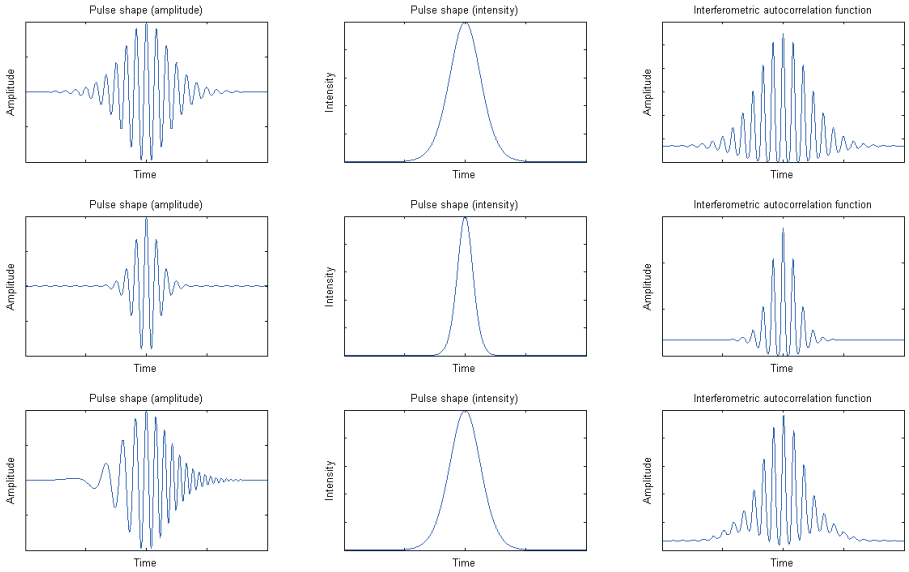

Figure 3.4: The intensity shape and interferometric autocorrelation function for three different sech^2 pulses. From top to bottom: a pulse with 50 fs FWHM duration, a pulse with 25 fs duration, and a chirped 50 fs pulse. Using the interferometric autocorrelation function alone to determine the pulse duration, it would appear that the chirped pulse is much shorter than it really is.

Assume that the electric field of the pulse can be written as $E(t) = f(t)^{1/2}\cos(\omega t + \phi(t))$, where $\int f(t)\mathrm{d}t = 1$, $f(t) \propto \mathrm{sech}^2(t/t_p)$, t_p is the pulse length and $\phi(t) = a(t/t_p)^2$ is a linear chirp. We can then write the intensity in an interferometric autocorrelation plot as a function of delay between the pulses (τ) as

$$\begin{aligned} I_{\mathrm{IAC}}(\tau) = 1 &+ 2\int f(t)f(t+\tau)\mathrm{d}t \\ &+ \int f(t)f(t+\tau)\cos(2\omega\tau + 2\Delta\phi)\mathrm{d}t \\ &+ 2\int f(t)^{1/2}f(t+\tau)^{3/2}\cos(\omega\tau + \Delta\phi)\mathrm{d}t \\ &+ \int f(t)^{3/2}f(t+\tau)^{1/}\cos(\omega\tau + \Delta\phi)\mathrm{d}t \end{aligned} \tag{3.9}$$

where $\Delta\phi(t,\tau) = \phi(t+\tau) - \phi(t)$. Using the MOSAIC algorithm on this expression gives us

$$I_{\text{MOSAIC}}(\tau) = 1 + 2\int f(t)f(t+\tau)\mathrm{d}t + 2\int f(t)f(t+\tau)\cos(2\omega\tau + 2\Delta\phi)\mathrm{d}t \tag{3.10}$$

Figure 3.5 shows the MOSAIC traces of three different interferometric autocorrelation plots. The one on the top is with no chirp in the pulse ($a = 0$), and the ones below are from pulses with different strengths of the temporal chirp ($a = 0,15$ and $a = 0,25$, respectively). From these plots the presence of a chirp in the pulse becomes much easier to observe, as the lower amplitude values of the graphs in these cases deviates from the constant value.

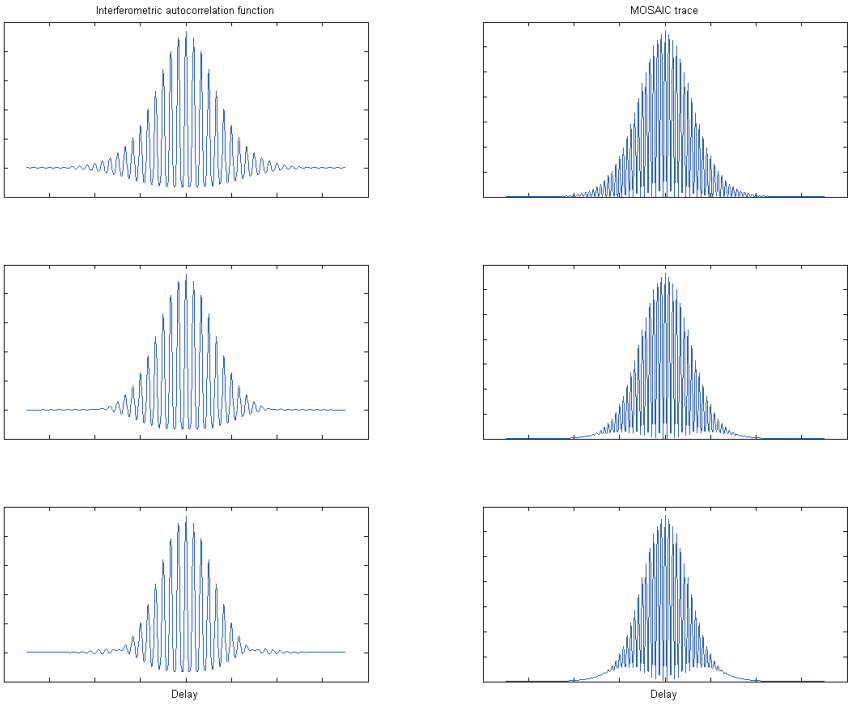

Figure 3.5: Interferometric autocorrelations and their corresponding MOSAIC traces for an unchirped pulse (top) and two chirped pulses with different strengths of the temporal chirp.

Frequency resolved optical gating (FROG)

Another method for getting information about the characteristics of very short pulses is a method called *frequency resolved optical gating*, or FROG. In its simplest form FROG is similar to an

autocorrelation measurement, but with the difference that the detector is not only measuring the intensity as a function of time delay, but also the frequency as a function of time. Thus, the autocorrelation function can now be recorded both in the time and frequency domains, similar to a wavelet analysis. Using the same setup as the intensity autocorrelator, the nonlinear material will only let radiation hit the spectrometer if the pulses are overlapping (hence the name *optical gating*). It is then possible to obtain a spectrogram of the pulse, which in turn can be used to find the electric field as a function of time or frequency. Thus, more information about the pulse can be obtained with this method. This is because a FROG measurement allows for the possibility to compare the measured spectral trace with a mathematical deduced one, which is obtained from an estimated signal field and an algorithm which involves Fourier and inverse Fourier transforms, and an error calculation between the deduced mathematical FROG trace and the measured one. The algorithm is repeated until the error is sufficiently small. This then gives us a much more characterized pulse.

Spectral phase interferometry for direct electric field reconstruction (SPIDER)

Spectral phase interferometry for direct electric field reconstruction or SPIDER, was developed by Iaconis and Walmsley in 1999 [3]. The method uses nonlinear frequency mixing to generate a pair of identical, but frequency differentiated replicas of the original pulse. These pulses are allowed to interfere and the output is recorded using a spectrometer and an integrating (slow) detector.

To find the spectral phase of the pulse, a Fourier transform is applied to the interferometric pattern. This results in three terms of the electric field: one DC term which contains information about the spectral intensity, and two AC terms which contains information about both the spectral intensity and the phase of the pulse. The two AC terms are Hermitian conjugates of each other and thus contain the same information.

Now, one of these terms is removed and the resulting field is inversely Fourier transformed to the frequency domain, where the spectral phase and spectral intensity can be extracted through various means.

It should be noted that we did not have access to these improved methods for measuring pulse characteristics in our laboratory.

References

[1] http://www.cmxr.com/Education/TBproduct.html (01.06.2015)

[2] T. Hirayama and M. Sheik-Bahae, *Opt. Lett.* **27**, 860 (2002)

[3] C. Iaconis and I. A. Walmsley, *IEEE J. Quant. Elec.* **35**, 501 (1999)

Part III

Experimental setup and testing

Chapter 4

Experimental setup

4.1 Setup for SPDC light

In section 2.5 the theory for the Bell/CHSH inequality measurements done by this group was briefly discussed. The experimental setup in these experiments was largely based on the setup described by Kuklewicz et al. [1], while the acquisition method was inspired by the experiments performed by Weihs et al. [2]. In these experiments, spontaneous parametric down-conversion was used to generate a pair of photons with orthogonal polarization. In our case we used, as in [1], a ppKTP crystal for the down-conversion process. By using a continuous-wave diode laser at 405 nm as a pump, we could down-convert one photon to a pair of photons with a wavelength of 810 nm. Due to the fact that the ppKTP crystal was of type II, these photons had orthogonal polarization, and because of this they would not exit the birefringent ppKTP crystal simultaneously. A so called compensating crystal (KTP) was therefore inserted just after the ppKTP, to allow the polarization the lagged behind to catch-up [3], as was discussed earlier.

The experimental setup is shown in Figure 4.1. One may note that this setup is resembling that used by Aspect, as was discussed in section 2.4. We have already discussed some of the theory for the ppKTP and KTP crystals, but not talked so much about the setup of these. The linear polarized light from the CW laser was first ”cleaned up” using a single mode fiber so that the intensity profile became mainly dominated by the TEM_{00} mode. The intensity of the output light from the fiber was reduced to around 1 mW. This turned out to be optimal for getting enough single and coincidence counts (average around 6000 counts/s and 200 counts/s, respectively) to both have good statistics (i.e. clear angle dependence) and the acquisition program run smoothly without being slowed down due to too much data. The polarization was then rotated using a half wave plate to match the spatial directional settings of the ppKTP crystal. The crystal itself was mounted in a custom built thermoelectric heated holder, which was attached to a five axis translational stage (MT3/M + GNL20/M, Thorlabs) for optimum positioning of the crystal in relation to the beam. From the phase matching conditions, optimum results were obtained at a crystal temperature of 35.1°C.[1] The compensating KTP crystal was located in another translational stage

[1] An unexpected and very interesting variational behaviour between an antisymmetric and a symmetric state can be observed as the temperature of the crystal was changed, see Paper A, chapter 8.

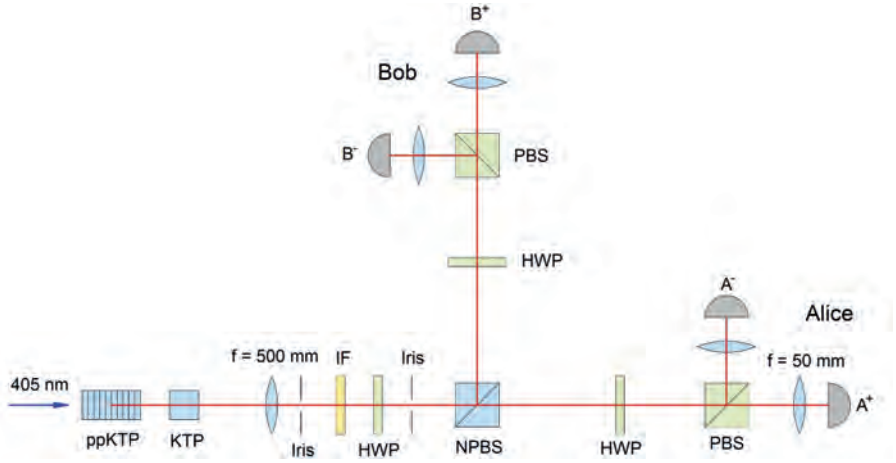

Figure 4.1: Experimental setup for generation and analysis of an entangled photon pair. The pairs of orthogonally polarized photons are down converted from the 405nm pump in the ppKTP crystal. They are time compensated (in a KTP crystal), frequency filtered (IF), and spatially filtered (iris) before being dispatched to Alice and Bob by a non-polarizing beam splitter (NPBS). At each measuring station, a half-wave plate (HWP) rotates the polarization of the photons, and a PBS projects them to a fixed basis. The output of the PBS feed four detectors, A^+ and A^- for Alice, B^+ and B^- for Bob.

in close proximity to the ppKTP crystal. This crystal, however, was kept at room temperature.

The pump beam and the down-converted light were exiting the crystal combination collinearly, so a series of long-pass edge filters had to be applied to filter out the pump wavelength. A 1 nm interference filter (at 810 nm) was also applied to the down-converted photon pair at this point. After this filtering, the photon pair was sent through a 50/50 non-polarizing beam splitter (NPBS) to two polarizing analyzers, as shown in Figure 4.1. The analyzing setup in the transmitted arm is conventionally labeled ”Alice” and the setup in the reflected beam is referred to as ”Bob”. Each of these analyzers consisted of a half wave plate (HWP) mounted in a rotational stage, a polarizing beam splitter (PBS) and two single photon counters, located in each of the arms of the PBS. The output from the detectors was labeled A^+ and A^- for Alice and B^+ and B^- for Bob.

4.1.1 Components

The setup after the compensating crystal started out with a biconvex lens with a focal length of 500 mm. This value was chosen in order to reduce the angular divergence of the light through the analyzing setup.

This was followed by an iris, a number of filters and a HWP (WPH05M-808, Thorlabs). The role of the iris was to spatially confine the beam and to ensure the collinearity of the two photons. Of the filters, the interference filter (a custom filter with a center wavelength of 810 nm and 1 nm bandwidth from Knight Optical) had the most effect on the down-converted light. In general,

the narrower the bandwidth of this filter was, the clearer became the effects and outcomes of the measurements [4]. The HWP was introduced in the setup in order to make sure that the directions of the orthogonal polarizations of the light from the crystal source corresponded correctly to the horizontal and vertical directions of the PBS's in the analyzing setup.

Both the non-polarizing (TWK 1.10, Bernhard Halle Nachfl. GmbH) and the polarizing beam splitters (PTW 1.10, Bernhard Halle Nachfl. GmbH) in the analyzing setup were ordinary cube beam splitters, with moderate extinction ratios.

Detectors

The detectors both used in the measurements with the SPDC source and the pulsed source were so called actively quenched single photon counters (SPCM-AQRH-16, from the company PerkinElmer Optoelectronics[2]). This type of detector consists of a silicon avalanche photodiode, an amplifier, a discriminator and a TTL output driver. The photodiode is temperature controlled by a two stage thermoelectric cooler (a two stage Peltier element) to ensure a stable performance. A picture of the unit and a removed and disassembled capsule containing the photodiode and the cooler is shown in Figure 4.2.

Figure 4.2: The disassembled capsule from a SPCM-AQR-13-FC detector (similar to the SPCM-AQRH-16) shows the avalanche photodiode mounted on a two-stage thermoelectric cooler, with the capsule serving as a heat sink. The black spot in the middle of the photodiode is the photosensitive area, which is only 180 μm in diameter. On the right hand side the assembled unit is shown. (Left: taken from [5]. Right: taken from [6].)

Some of the typical characteristics of these detectors are given in Table 4.1. We see that the dark counts, that is, registrations in the detector which are the result of "false" triggering, are fairly low in these detectors. This is of course an essential characteristic when studying the relative behaviour between photon pairs. Another characteristic of importance is the dead time, which is dependent on the recharge time of the bias voltage after a registration as well as the speed of the electronics. During this time, the detector is more or less blind to any incoming radiation.

[2]Today these detectors are sold by Excelitas Technologies.

Table 4.1: Specifications for the single photon counter SPCM-AQRH-16

Manufacturer	PerkinElmer Optoelectronics
Model	SPCM-AQRH-16
Active area (diameter)	180 μm
Photon detection efficiency at 810 nm	60% (extrapolated from Figure 4.3)
Photon detection variation at constant	
case temperature (2 h at 25 °C)	± 1 %
Photon detection variation from 5 °C to 40 °C	± 4 %
Dark counts	$\leq$ 25 counts/s
Average dark count variation at constant	
case temperature (6 h at 25 °C)	± 1 %
Dead time (count rate below 5M/c)	32 ns
Output count rate before saturation	$29 \cdot 10^6$ counts/s
Afterpulsing probability	0.5 %
Output pulse width	15 ns
Peak light intensity	10^4 photons per pulse and pulse width $<$ 1 ns

The active detection area is only 180 µm in diameter in these detectors, and thus requires a precise alignment for getting reliable results. This is also because the probability for detection is not a linear function of spot diameter, which preferably should be less than 150 µm. The relationship between wavelength and photon detection efficiency is shown in Figure 4.3. At around 810 nm the efficiency is around 60 %, as indicated by the figure.

Half wave plates

The HWP's used in the analyzing setup were standard zero-order half wave plates specified for 808 nm (WPH05M-808, Thorlabs). The rotational control was established by using motorized rotation mounts (PRM1/MZ8E, Thorlabs), which were controlled by the data acquisition program. In order to be able to precisely set the axes of the HWP, they were mounted in a precision rotation mount (CRM1P/M, Thorlabs) which then was mounted onto the motorized rotation mounts.

Due to the rotation of the HWP's, their perpendicularity to the beam was more critical than for other components, as the beam exiting the HWP otherwise could wobble abound the sensitive area of the detector when the HWP was rotating, as illustrated in Figure 4.4. The figure also shows the complete rotational mount as well as a close-up view of the sensitive area of the detectors.

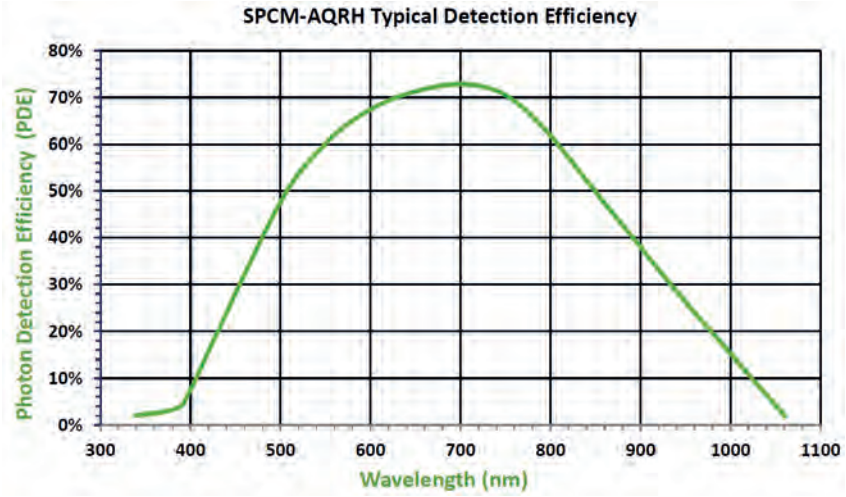

Figure 4.3: Typical photon detection efficiency as a function of wavelength for the SPCM-AQRH detector. (Taken from [6].)

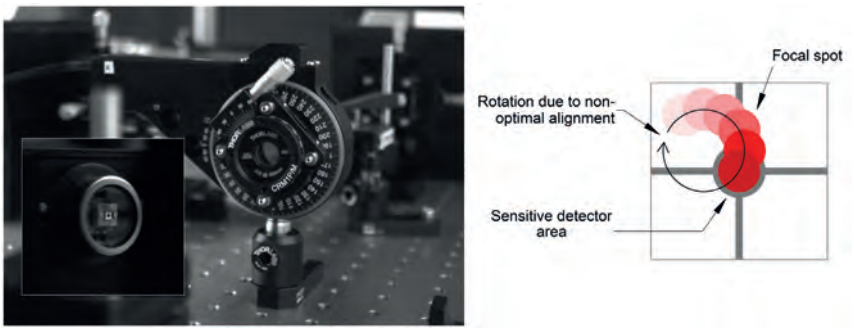

Figure 4.4: Left: The complete and assembled rotational mount and (insert) a close-up of the sensitive area of the detector. Right: An illustration showing the wobbling effect due to a non-normal alignment of the HWP.

4.1.2 Data acquisition

The data acquisition and presentation was generated from an extensive LabView program developed by this group[3]. As was briefly mentioned in section 2.5 the data collected from the single photon detectors was registered and time tagged using a multichannel event timer (Hy-

[3]This is mostly a result of the work conducted by Guillaume Adenier.

draharp 400, Picoquant). This instrument time tagged every single click from each detector with picosecond timing accuracy. We do not, of course, have such a great accuracy in determining the real arrival times of the photons, since there is a delay between photon arrival event and the registration of the photoelectric pulse which is different from detection to detection and from one detector to the other. The reason for this arises from the way the detector is constructed, and is due to both the timing jitter from the electronic noise in the active quenching circuit, and from the statistical fluctuations originating from the uncertainty of the exact location of absorption the photon inside the material [7].

The time tagged single detection events were collected over a time period of 1 s, and for each second calculations of the number of doubles (two detections in the same arm) and coincidence (two detections in different arms) events are made, based on the specified duration of the coincidence window. The correlation was also calculated and all the data was plotted as the measurements were made. The advantage of this was of course that we could directly observe the results, as well as being able to see the effect of immediate external influences. All the data was also saved and could be reanalyzed and exported to other programs. In addition, the number of triple counts (i.e. the number of registrations at three detectors within the same coincidence window) were monitored.

The coincidences as well as the doubles were obtained by comparing the registration times at two detectors. Specifically, by tagging these registration times, say, by 0 for one detector and 1 for the other, we sorted the registration times in increasing order. We could now compare neighbouring times, and register a double or coincidence count if two requirement were fulfilled: 1. the registration times belonged to different detectors (that is, tagged with 0 and 1, and not 0 and 0 or 1 and 1) and 2. the time difference was equal or less than the specified coincidence time.

Controls, such as the coincidence window size, the setting and speed of the rotating HWP's or other components (such as a retroreflector in the pulsed case, see section 4.2) could all be set through the program. It was also possible to change the plotting variable to time, angle of the HWP or position of the retroreflector.

Different types of measuring sequences required different settings and movements of the components. Such sequences were preprogrammed and could be started with the push of a single button. So these measurements could be performed in a routinely manner. Figure 4.5 shows a screenshot of the main tab used when running the program. The other tabs are for setting of the HWP's, the retroreflector, post-analyzing, post-processing, optimization control when aligning the detectors, efficiency measurements, etc. The different control buttons for the preset settings can be seen in the middle of the screen.

4.2 Setup for pulsed light

We have seen from the calculations with the SPDC source in section 2.5 that we can correctly predict all the measured results if we use a quantum mechanical formalism, and it follows from this that entanglement is crucial for arriving at the correct mathematical predictions of the outcomes in the experiments.

The purpose of these new experiments was to investigate if it would be possible to emulate

Figure 4.5: A screenshot of the acquisition program's main tab.

the SPDC processes (and thus the measured results), by using a combination of attenuated pulses from an ultrafast laser attached to a modified Mach-Zehnder interferometer, where we have control over the parameters which we believe governs the SPDC processes. That is, we wished to investigate the physical processes responsible for differentiating an entangled state from a mixed, coherent or classical state. That is, we can observe real changes in the measurements when going from non-entangled to entangled light; what real, physical processes are responsible for this difference in the measured results? Can we find these processes, and if so, can we use the knowledge about them to bring a more intuitive understanding into this type of quantum mechanical process? To be even more precise: can we describe the measured results in, for example a so called twin scan (both HWPs are rotating simultaneously with the same speed and direction), using more familiar physical processes such as interference, timing and phase relations rather than using the concept of indistinguishability and indivisibility, for example?

In the quantum mechanical description of the SPDC process a number of assumptions about the behaviour and state of the photons was given. Most importantly, it was assumed that a single photon was able to create two new photons at a specific location inside the ppKTP crystal. This position is different and randomly located from one pair to the next. Due to the effect of the compensating crystal however, the time difference becomes ordered so that for every pair with, say, the vertical polarized photon arriving before the horizontally polarized there is a equally high probability of detecting the horizontally polarized photon arriving before the vertical polarized. And the arrival time difference is equal in these two cases.

In order to be able to simulate these conditions we had to add some kind of time ordering to the light we were going to use, since the time of arrival of the photons in an ordinary CW laser beam is completely random. This could most easily be accomplished using an ultrafast laser, and split each pulse in two parts. The short duration of the pulses would make sure that the detections would be registered only once at the detectors, as longer pulses would increase the number of triple counts and thus diminish the relations connected with pairs of pulses. This was indeed investigated and confirmed to be the case with a another pulsed laser with ns pulses. In addition, the relatively long, fixed time between the pulses would make sure that only contributions from a single pair entered the analyzing setup at a time. As long as the two parts of the split pulse could be kept similar in all respects except polarization (which we could make orthogonal to each other with the help of HWP set at appropriate angles) and attenuate the pulses to a high degree, a situation similar to the theoretically described SPDC could be created.

A schematic illustration of the optical setup of the source is given in Figure 4.6. The pulsed source was an ultrafast mode-locked Ti:sapphire laser, consisting of an oscillator (TiF-50F, Avesta) and an external pump laser (Millennia Vs 5, Spectra-Physics).

Just after the output coupler of the Ti:sapphire oscillator (but still inside its walls), an angled, slightly reflective coated mirror was located. Its purpose was to send two beams with reduced intensity back, at slightly deviating angles, into the oscillator. One of these beams was then redirected towards a photo diode for surveillance of the power level and the automatic mode-lock trigger, and the other one could be used for an integrated spectrometer (not included in this model). But this angled mirror also caused two deviating beams in the opposite direction, that is, out from the oscillator. These were unwanted and became a source of stray light, so they were blocked out by an iris located just after the exit of the oscillator.

The mode-locked train of pulses then passed through a two-folded mirror configuration, which purpose, together with two irises, was to simplify the alignment of the beam into the Pockels cell and the following optical setup.

After this, a longpass dichroic mirror with 1180 nm cutoff wavelength (DMLP1180, Thorlabs) was positioned. In normal operation a dichroic mirror separates light by having a reflection and a transmission which are functions of the incoming wavelength. Thus, for a longpass dichroic mirror, light above some cutoff wavelength (in our case 1180 nm) is mainly transmitted and below it, most of it is reflected. How much of the light that's being reflected or transmitted is also dependent on the direction of polarization of the light.

In the optical setup in Figure 4.6 however, the dichroic mirror was used as an attenuator, by using the fact that only about 5 % of the wavelengths from the Ti:sapphire oscillator was allowed to pass. Unfortunately, this resulted in multiple reflections inside the mirror (even though it was anti-reflective coated), so an iris had to be placed close to the mirror to avoid ending up with more than one beam in the setup.

This configuration was followed by a pulse picker, consisting of two polarizing filters (LPVIS050-MP2, Thorlabs) acting as polarizer and analyzer, and a Pockels cell (5100ERW-100, Lasermetrics). The polarizer and analyzer were rotated so that they were perpendicular to each other, while the Pockels cell acted as an electrically controlled HWP. Without the Pockels cell the extinction ratio was very high (up to $>$1:100 000), but with the Pockels cell in place only an extinction ratio of roughly 1:200 could be achieved. A quarter wave plate was inserted between the Pockels cell

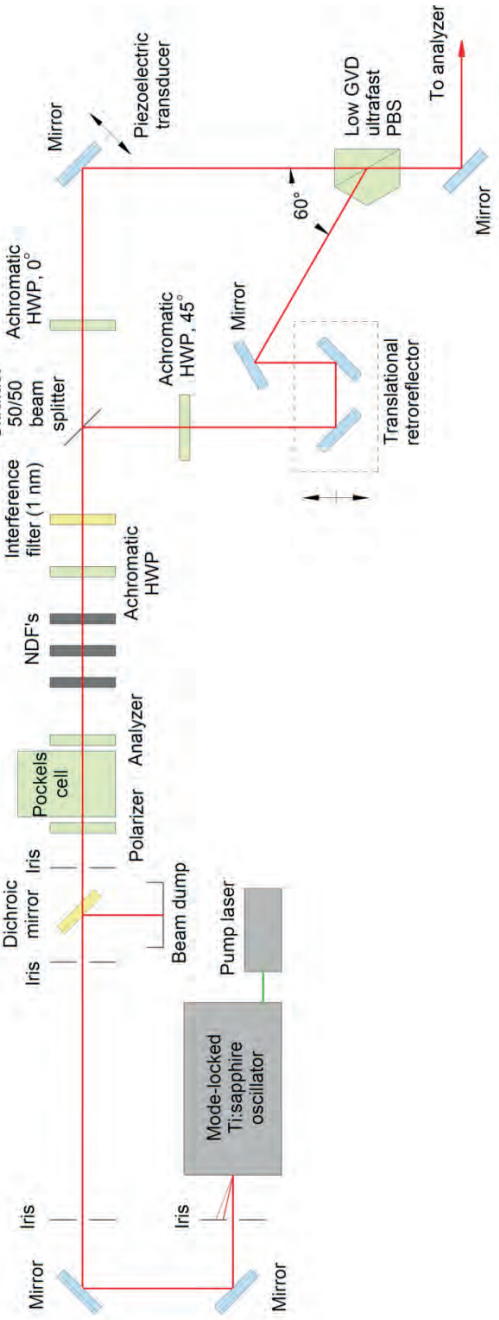

Figure 4.6: The pulses from the Ti:sapphire laser are redirected using a pair of mirrors. The irises that follow are used for aligning purposes. After these, a dichroic mirror is located, which here works as a first stage attenuator. The train of pulses then enters a pulse picker, consisting of a polarizer, a Pockels cell and an analyzer. The pulses are then attenuated using neutral density filters, and continues through an achromatic half wave plate (AHWP) followed by a 1 nm interference filter. After this, a modified Mach-Zehnder interferometer is positioned. It consists of an ultrafast 50/50 beam splitter with one AHWP in each arm. The purpose of these AHWP's is to change the polarizations in the arms so that they become orthogonal to each other. After this the pulses are combined again using an ultrafast polarizing beam splitter. A translational retroreflector is located in the reflected arm to adjust the path lengths so they become equal, and a piezoelectric transducer in the transmitted arm is used for phase control. The combined two-pulse state is then sent to the analyzer (see Figure 4.16).

and the analyzer to compensate, but could only give a marginal improvement. The on/off time of the Pockels cell was controlled by an external clock (NI 6602, National Instruments), which gave us direct control of the number of pulses per second.

This was followed by a second stage of attenuation, here by using a number of NDF's. Their values were determined from the number of observed registrations at the single photon detectors. The theoretical transmission through these was of the order of 10^{-7} (an additional factor of 10^{-2} came from the dichroic mirror).

An achromatic half wave plate (AHWP) was inserted after this. The role of this AHWP was to rotate the polarization of the pulses by 90°. This was a necessary procedure because the beam splitter in the following Mach-Zehnder acted only as a 50/50 beam splitter for light linearly polarized in a specific direction. For any other direction of polarization the splitting ratio was different. Naturally we wanted the two split parts of the pulse to be as equal as possible in all respects, except polarization.

The 1 nm interference filter, which in the measurements using SPDC was located in the analyzer setup, was here moved to a position just after the AHWP. The reason for placing it here was partially to use it as attenuator, partially to reduce the amount of possible chirp from the pulses before they entered the interferometer and partially to simplify the process of finding the position of overlap of the two parts of the split pulse.

Next was the modified Mach-Zehnder interferometer setup. It consisted of beam splitters, half wave plates and a retroreflector mounted on a translational stage, for varying the path length. The first beam splitter was a 50/50 ultrafast beam splitter (UFBS) (UFBS5050, Thorlabs). "Ultrafast" here refers to the fact that it is useable for very short pulse durations without introducing a considerable amount of chirp. Each arm of the Mach-Zehnder contained another AHWP set to 0° in the transmitted arm and 45° in the reflected arm, respectively, making the polarizations orthogonal to each other. In the reflected arm a retroreflector mounted on a stepper motor-controlled translational stage was located. Its primary task was to adjust the path length so that it became equal in the reflected and transmitted arm. During the very short pulse duration of 50 fs, light travels a distance of only 15 μm. This means that if we want the two pulses to overlap, the difference in length should be no less than 15 μm. The smallest step size that our stage could have, however, was 200 nm.[4] In the transmitted arm a piezoelectric transducer was attached to the mirror, thus making even finer adjustments possible. It's main purpose, however, was to control the phase relation between the pulses. The two parts of the split pulse were combined in an ultrafast polarizing beam splitter (UFPBS) (PBS1005-GVD, Semrock) operated in reverse, which, when the path lengths in the two arms were equal, generated a pair of two attenuated pulses with orthogonal polarizations.

4.2.1 The Ti:sapphire laser

The reason for using an ultrafast laser in these experiments was mainly related to the process of maintaining a two-photon-like detection process. Initial attempts was made with a nanosecond

[4]Primarily due to the 1 nm interference filter however the pulse duration is stretched to 1 ps, or 300 μm. We will discuss the effect of the interference filter in more detail later in this chapter.

pulsed laser. This turned out not to work because of an increased number of registrations at three detectors within the same coincidence window (a so called triple count). The triples affect the correlation because the coincidences are no longer occurring between two detectors at a time, but three, and this is of course leading to less visibility in the plots which displays relations between only two detectors, which is what we were interested in.

A possible way around this could be to lower the coincidence window, but then the number of useful data for the doubles and coincidences would go down as well, because the probability for two detections within the coincidence window becomes lower. Thus, with short pulses the detection events would become more time correlated.

As was mentioned, the Ti:sapphire laser consisted of two parts: a pump source and an oscillator. The pump source was a diode pumped, frequency doubled Nd:YVO_4 laser, capable for generating as much as 5 W with a longitudinal spatial mode of TEM_{00}. It also had a very low noise level (below 0.04% rms [8]), so it was well suited for pumping our Ti:Sapphire oscillator.

The oscillator was a CW mode-locked Ti:sapphire oscillator from the company Avesta, capable of generating pulses with $<$50 fs duration. Table 4.2 below summarizes some of its characteristics.

Table 4.2: Measurements made on the TiF-50F

	Measurements by Avesta	Measurements by this group
Tuning range	725-910 nm	Not measured
Pulse duration at 800 nm	46 fs	44 fs
Output power	555 mW	740 mW[5]
Spatial mode	TEM_{00}	TEM_{00}[6]
Polarization	Linear, horizontal	Mostly linear, horizontal
Pulse repetition rate	80.5 MHz	$\sim$80 MHz
RMS stability	0.6 %	2.1 %

The data given by Avesta have been obtained from testing this particular unit [9], using a Lighthouse Photonics Sprout-G 4 W laser as the pump source. In this case the pump laser was mounted inside the oscillator. In our setup, however, the pump laser was too large to fit inside the oscillator, and had to be coupled externally to it. The measured pulse duration, output power and repetition rate were, however, of the same order, as seen in Table 4.2. One should note that the stability is highly dependent on the environmental surroundings, as a simple walk across the lab would result in noticeable fluctuations in the power output (and sometimes even loss of the mode-lock). This could be due to a non-optimal alignment of the oscillator, which is a time consuming and somewhat difficult task to perform.

[5]Maximum CW power. At stable mode-lock the power output is of the order of 200 mW.

[6]But its intensity profile is not Gaussian

Ti:sapphire laser theory

The first successful operation of a Ti:sapphire ($Ti:Al_2O_3$) laser was first reported by P. F. Moulton at the Twelfth International Quantum Electronics Conference in Munich in June 1982 [10] (see also [11]). The Ti:sapphire laser is a solid state laser with a peak emission wavelength around 800 nm, but has a very broad spectral bandwidth. Depending on the optics used, it can be tuned from the visible range (670 nm) all the way up to IR (1070 nm). This broad bandwidth means that it is capable of producing very short pulses, which is one of the reasons for its popularity, in addition to the broad tuning range. The absorption and emission spectra for Ti:sapphire are shown in Figure 4.7.

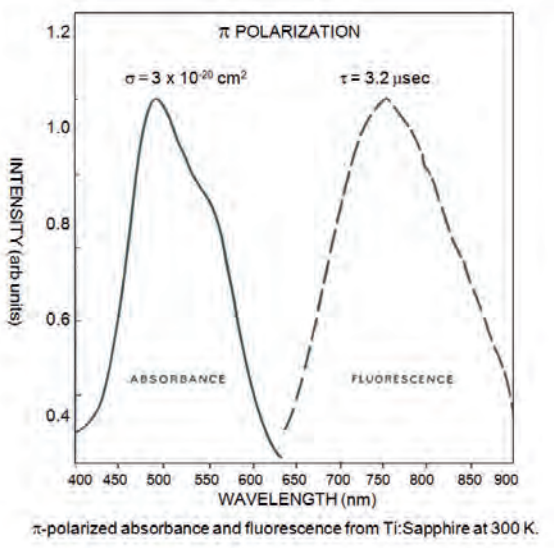

Figure 4.7: The absorbtion and emission spectra for $Ti:Al_2O_3$. The peak absorbtion wavelength is around 490 nm, and its emission peak is close to 800 nm. (Taken from reference [14].)

As can be seen from this graph, the absorption spectrum is also broad, and has a peak close to 490 nm. Earlier, Ar-ion lasers, with emission wavelengths at 514 and 488 nm, were used for pumping, but these have now mostly been replaced by more energy efficient and compact high-power, frequency doubled Nd:YAG and $Nd:YVO_4$ lasers with peak emission wavelengths around 532 nm.

The host sapphire crystal, Al_2O_3, is also very favorable due its very high thermal conductivity, chemical inertness, mechanical rigidity and good optical quality, which makes it superior to dye lasers, which before the invention of the Ti:sapphire laser were the preferable type of laser to use for producing pulses with very short durations. The titanium is introduced into the host crystal by substituting an Al^{3+} ion in Al_2O_3 with a Ti3+ ion, and the doping concentration is usually

around 0.1 % Ti^{3+} by weight.

One disadvantage with the Ti:sapphire laser is its short fluorescence lifetime, which determines the available time for the pump to create and store a population inversion. For Ti:sapphire at room temperature this quantity is only 3.2 µs. Compared to 230 µs for Nd:YAG or 3 ms for ruby, this is a very short lifetime. The population inversion is related to the fluorescence lifetime and what is called the stimulated emission cross section (or gain cross section), which determines how many transitions from the upper to the lower level are caused by a particular flux of photons. Thus, because of the small value of the fluorescence lifetime, the population inversion will be small as well, and the only way to increase it is to increase the photon flux, which we can do by increasing the pump power. This is the reason why Ti:sapphire laser needs to be pumped by high power pump lasers. Fortunately, the saturation power level in Ti:sapphire is very high as well (0.9 J/cm^2), which then makes it possible to actually use such high pump powers.

Figure 4.8 shows the Ti:sapphire crystal in our laser oscillator being pumped by a high power, frequency doubled Nd:YVO_4 pump laser with a wavelength of 532 nm. The input power of 4 W is focused into the 5 mm long, Brewster angle cut Ti:sapphire crystal. The red emission wavelengths from the crystal can be seen in the figure. The crystal, as well as the base plate of the oscillator, needs to be water cooled for stable operation.

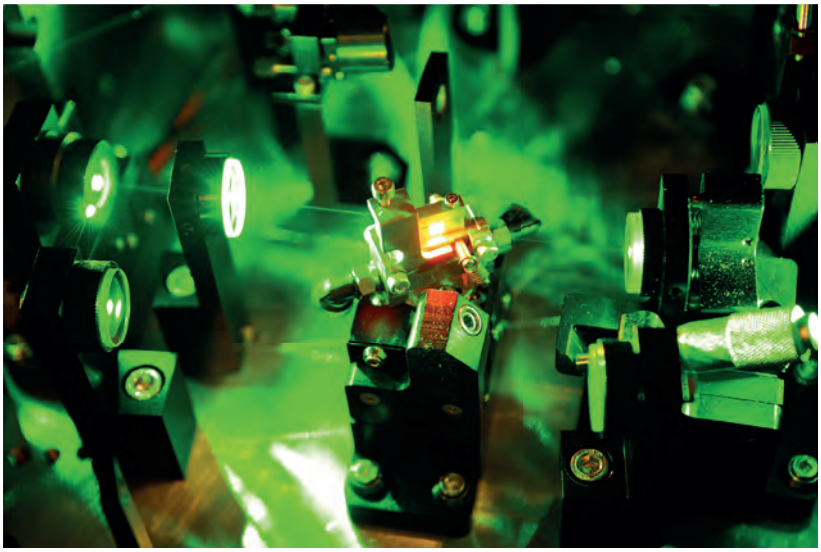

Figure 4.8: The Ti:sapphire crystal during operation of the oscillator. A high power pump laser is focused into the small, water cooled crystal. The red emission spectrum from the crystal is apparent.

Ti:sapphire lasers can be operated in both continuous wave and pulsed mode, but are mainly used for generation and amplification of femtosecond mode-locked pulses. This is also how the Ti:sapphire laser was used here.

Mode-locking

A laser that has a broad spectral bandwidth also necessarily oscillates with a large number of longitudinal modes. Due to the physical constrains that make out the cavity, a close to constant number of longitudinal modes will exist inside the cavity at any time. The different modes will, however, have random phases[7], which, due to interference, results in an output intensity which fluctuates randomly in time. Thus, the the instantaneous output may be viewed as consisting of a random sequence of light pulses with different amplitudes, as shown in Figure 4.9. An

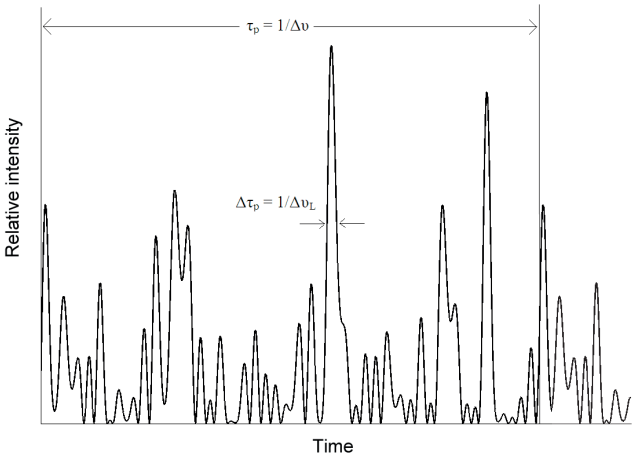

Figure 4.9: A snap shoot of the random intensity from a multi-mode laser.

ordinary photodetector cannot detect these rapid variations in the intensity, so the output from a random-phase, multi-mode laser will therefore be an average, near-constant intensity.

However, because the pulses arise from a finite sum of frequency components which are evenly spaced in frequency, the waveform will be repetitive with a period equal to $\tau_p = 1/\Delta\nu$, where $\Delta\nu$ is the frequency difference between the longitudinal modes. In addition, each light pulse will have a duration which is roughly equal to this period divided by the number of modes, $\Delta\tau_p = 1/(N\Delta\nu)$, where the quantity $N\Delta\nu$ is the total oscillating bandwidth. So lasers with relatively large bandwidths, such as dye, semiconductor and solid state lasers, may produce pulses with very short duration.

Still, the problem of the random phases remains. But if we were able to make the oscillating modes have a fixed relation between their phases, instead of the random variation we just

[7]This might sound odd, since we expect to have standing waves inside the resonator and therefore a fixed phase relationship between all the longitudinal modes. However, fluctuations in the geometry of the cavity from f. ex. mechanical vibrations or thermal expansions results in the randomness which affects each mode individually.

discussed, then we would be able to see a repeating pattern of pulses with a constant repetition rate. The process of creating such a state is called mode-locking, and the laser is then said to be mode-locked.

Mode-locking can be divided into two main categories: active and passive mode-locking. In active mode-locking the element responsible for locking the phase relation of the longitudinal modes is an external source of some kind. This includes devices such as amplitude or phase modulators, or synchronous pumping (i.e. periodic modulation of the laser gain).

Passive mode-locking, as the name suggests, do not require external triggered modulator to create the mode-locked state. Instead, the light itself from the laser is used in some intracavity element, such as a saturable absorber, to generate the phase-locking of the longitudinal modes.

The saturable absorber works by changing its transmission depending on the intensity of the light going through it. Ideally, this device should absorb light when the intensity is low, and transmit it when the intensity is high. By placing such a saturable absorber in the laser cavity, it can then pick out the intensity peaks. With this constraint, the peaks will be amplified as they pass back and forth between the mirrors in the resonator that make up the laser. And since the peaks are repeating with a somewhat constant repetition rate, a pulse train of mode-locked pulses will emerge.

There are several ways to achieve passive mode-locking, but one of the most common in connection with Ti:sapphire lasers is so called Kerr-Lens Mode-locking (KLM). This technique uses the optical Kerr-effect, which is a non-linear process where the refractive index in a material is changed due to the strength of the intensity of the incoming light, to achieve the desired selection of intensity peaks. One advantage using KLM is that it can be very fast in solid materials; the response time can be of the order of a rotation period of the outermost electrons of the atom (a few femtoseconds).

Let's assume that a beam passing though a material exhibiting the optical Kerr effect, has a Gaussian intensity profile. The intensity will then be larger in the center than in the wings, so the change in the refractive index will naturally be largest in the beam center and go to zero in the wings of the beam. The effect is then equivalent to that of a spherical lens.[8] If we now introduce a loss element, such as an aperture, we can then provide the loss needed to generate the passive mode-locking, as is shown in Figure 4.10.

An important point regarding a KLM laser, especially in connection to our measurements, is the fact that although the intensity in the pulses is high, there is always some energy in between the pulses. This background intensity is seldom mentioned and usually disregarded. It has, however, in our case turned out to be a real challenge and has to be taken into account when dealing with single photon detectors. These detectors can in classical terms be thought of as detectors without any minimum detection level. Thus, any light (with an appropriate wavelength) can cause a trigger, no matter how low the intensity is. Neutral density filters, which are linear filters, will not be able to improve the situation, because the ratio between the pulse and background energy remains the same. And if the time between the pulses is long compared to the duration of the pulses themselves (such as can be the case for an ultrafast laser), then there is a

[8] This induced focusing of the beam when the beam power exceeds a critical value can lead to a non-linear optical phenomenon known as self-focusing, which has been actively studied in resent years [12].

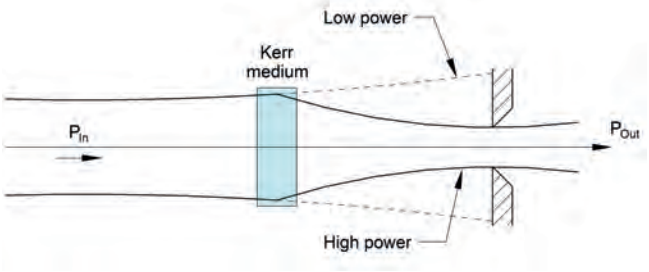

Figure 4.10: Passive Kerr-lens mode-locking using an aperture to generate the loss. When the intensity is high the Kerr effect will focus the beam through the opening in the aperture. When it is low, most of the intensity will be blocked.

non-negligible probability for detection outside the duration time of the pulse.

We considered several different approaches to handle the difficulties connected with this unwanted energy between the pulses, and one possible solution was a post-processing algorithm of the data, where only data coming from the pulses were taken into account. A Matlab program for doing this process is included in the appendix. While this method proved to work, it was not without difficulties. The method relates the data set of registration times to a theoretical square pulse train which corresponds to a pulse train which does not have any energy between the pulses. By choosing the width of the pulses in this theoretical pulse train to correspond to the total width of the pulse from the Pockels cell and assume an appropriate repetition rate, the algorithm will search for the temporal location in the raw data set where the highest number of counts are overlapping with the theoretical. This sounds like a straight forward process, but if the frequency of the of the theoretical pulse train does not correspond to the frequency of the raw data, no matching can be made. As it turns out, the frequency has to be very precisely defined (at least four digits of precision) in order to work. The process of finding the overlap has to be repeated for every second, since the registrations of the event times made by the Hydraharp are sorted into 1 s blocks with little correspondence between them. Thus, the first registration in one block does not have to occur at the same time as the first registration in another block. Thus, the algorithm becomes very time consuming and requires many trials before finding the correct frequency. Even with the right frequency, one measurement series can easily take several hours to complete.

Nor was the real gain of using this method as high as was hoped for. Figure 4.11 shows the comparison between the number of single counts in each detector in a twin scan, with and without post processing. Large fluctuations can be seen and the angular dependence becomes much less visible after the post processing. This results in a number of double counts and coincidences that becomes too low and too much fluctuating to be able to give any conclusive results about the measurements. The correlation does seem to be unaffected by the variations, but on the other hand, no improvement can be seen either, which was the real point of this method.

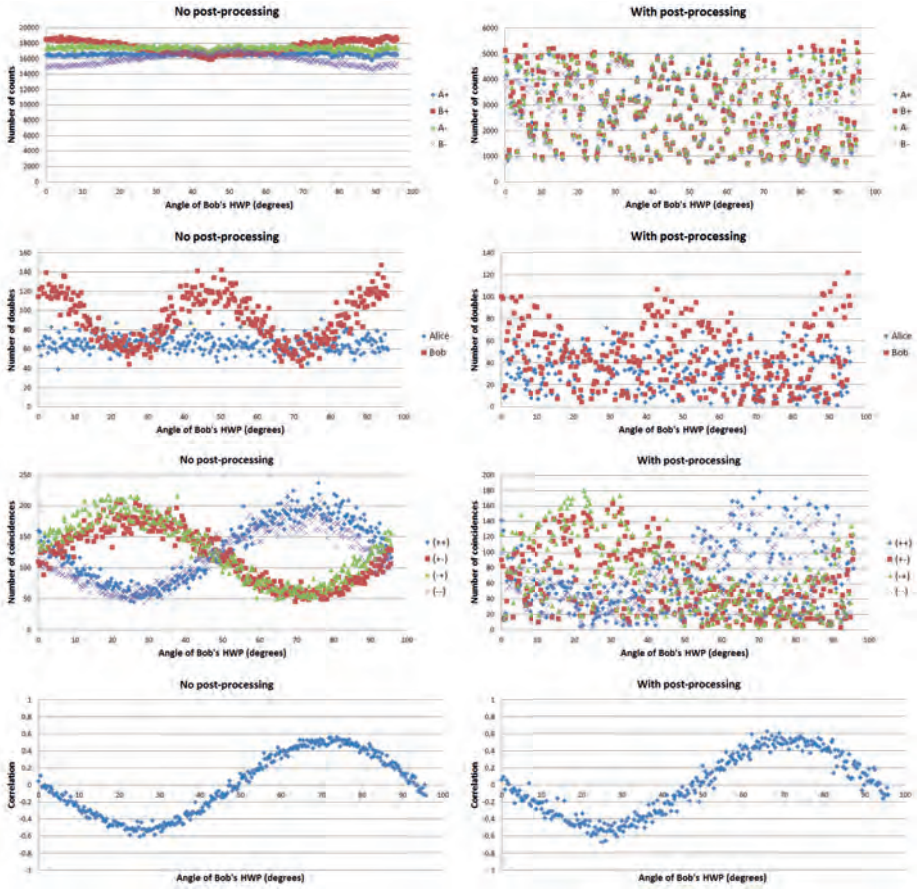

Figure 4.11: The difference between a raw (left) and post processed (right) data set when Alice's HWP is fixed at 22.5° and Bob's HWP is rotating from 0 to 90°. As can be seen, large variations appear in the post-processed plot, leading to a washout of any patterns. Also note that while the correlation seem unaffected, it hasn't improved.

4.2.2 The pulse picker

To be able to control the number of pulses from the Ti:sapphire laser that entered the optical setup, a pulse picker was introduced. The number of pulses per second was an important parameter, partially because our detectors could become saturated at rates which were too high, partially because we wanted the measured number of pulses to correspond to the SPDC case and partially because of the time it took for our analyzing program to process the data. At a too high detection rate the plotted output will not be a truthful representation of the data.

In general, a pulse picker is a device which allows us to pick out one or several pulses from a pulse train or a Q-switched pulse. This is usually accomplished in one of two ways: either through electro-optic modulation or acousto-optic modulation.

An acousto-optic modulator is build around an optical transparent crystal or piece of glass, which the light we wish to modulate pass through. Connected to this crystal material is a piezoelectric transducer, which is driven by oscillating electrical signals causing it to generate pressure waves inside the material. These can be in the range of hundreds of MHz and causes the material to expand and compress, which results in a periodic change in the refractive index. The light that passes though the material then experiences diffraction due to the grating generated by the sound wave. Thus the beam becomes scattered, and the device can then work as a controllable gate for the light that enters it. The frequency and direction of the scattered beam is controlled by the frequency of the sound wave, and the power that is allowed to pass is dependent on the level of acoustic power.

Electro-optic modulation is based on the linear electro-optic effect (or Pockels effect). This effect induces birefringence in a non-centrosymmetric material (many crystals falls within this category) as a result of applying an electric field, and is proportional to the strength of the applied electric field (unlike the Kerr effect, which is proportional to the square of the field). If the field is strong enough, the induced birefringence may cause the material to act like a voltage controlled wave plate. At a specific voltage the crystal will act like a half wave plate. If the incoming light is linearly polarized and we insert a polarizer rotated 90° to the incoming polarization, we have a gate for the light which we can control by turning the voltage on and off.

The pulse picker used in these experiments was a Pockels cell of this type (model 5100ERW-100, Lasermetrics). This device was triggered by an external, computer generated pulse (DAQ NI6602, National Instruments) with a repetition rate that we could adjust somewhat freely[9]. This gave us good control over the number of pulses that could enter the analysing setup per second.

As was mentioned previously, the pulse train from the Ti:sapphire oscillator was monitored by an internal circuit inside the oscillator, where a very small part of the output beam was directed towards a fast photodiode and this signal was amplified and retrievable. The signal was then used by the driving electronics to time the pulse being sent to the Pockels cell. The length and time delay of this outgoing pulse could be adjusted freely. A schematic representation of the pulses involved in the described process is shown in Figure 4.12.

The Pockels cell needed to be correctly optically aligned in order to work, both with the

[9]Although the NI computer interface gives the impression that any frequency is freely selectable, this is not the case, as the NI card uses three different base clocks at 100 kHz, 20 MHz and 80 MHz, and generates other frequencies by integer division of these.

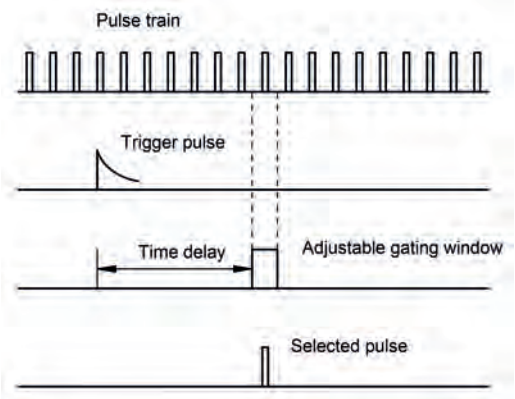

Figure 4.12: Two signals are input to the driving electronics for the Pockels cell: a pulse train from the oscillator and a trigger signal from the computer. The delay and duration of the outgoing pulse can be adjusted.

beam itself and the external polarizers used to block the beam when the Pockels cell was off. The procedure for how this can be done, can be found in [13] (though, one should be aware that the isogyre patterns presented in [13] may not apply to all Pockels cells, specifically not to the type used in these experiments.).

In addition, the driving signals, both from the NI card and from the laser oscillator, had to be amplified in order to work. Since these pulses were of the order of a few ns in duration and the amplification had to be rather substantial, the amplifiers had to be custom built by our electronics lab.

The screen shot of the signal from a detector (DET10A, Thorlabs) measured on an oscilloscope (WavePro 7100A, LeCroy), shown in Figure 4.13, displays the pulses gained when the repetition rate on the Pockels cell is set at 10 kHz and only a single pulse is let through every time the pulse picker is open. Although much lower in amplitude than that of the pulse, the energy between the pulses can be observed in this plot. This signal is slightly larger than when the laser is off, indicating that the Pockels cell does not have an extinction ratio which is 100 %.

4.2.3 Beam splitters

There were two beam splitters in the setup before the analyzer, and both of them were optimized for very short pulses. This means that they would not introduce any large chip into the pulses.

The first beam splitter was a 1.5 mm thick, low group delay dispersion (GDD) plate beam splitter, made from a material called Infrasil. This material is a type of optical quartz with similar mechanical and optical properties as fused silica. More importantly in respect to our ultrashort pulses was that this beam splitter had almost equal GDD in the reflected and transmitted arm, and close to zero GDD at around 800 nm, which was close to our center wavelength.

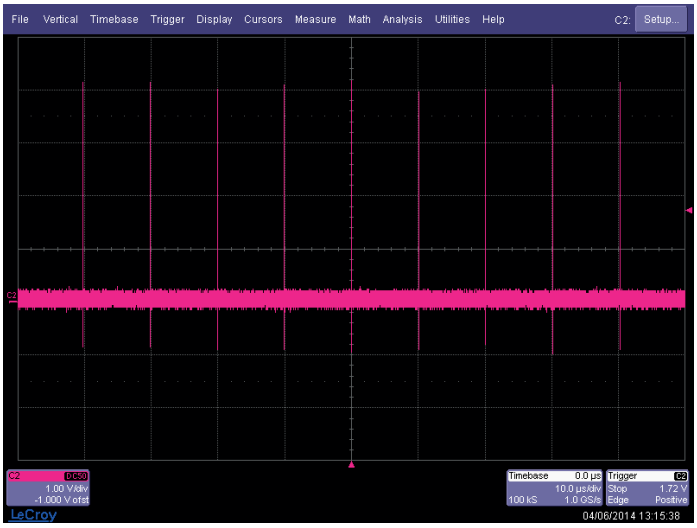

Figure 4.13: A pulse train (thin, narrow vertical lines) after the Pockels cell together with the background energy, where repetition rate has been set to 10 kHz (i.e. one pulse every 10 µs is picked out from the 80 MHz pulse train coming from the Ti:sapphire laser.)

In its function, it is similar to an ordinary 50/50 non-polarizing beam splitter, in the sense that the outgoing beams will have the same polarization as the incoming. However, the beam splitter is dependent on the direction of polarization for the incoming beam, so this had to be taken into account when setting up the optical system.

The other beam splitter in the setup was an ultrafast polarizing beam splitter made from fused silica. It had very low GDD in both the reflected and transmitted arm ($<$10 fs^2 (transmission), $<$20 fs^2 (reflection)) and a very good contrast ratio (typical 1:10 000). In the setup it was used in reverse, meaning that it had two incoming pulses with orthogonal polarizations and, if the pulses exited the beam splitter simultaneously, one single outgoing pulse consisting of a sum of these two. For incoming pulses which would not exit simultaneously, they would simply exit as individual pulses, still with their polarizations preserved.

4.2.4 Half wave plates and mirrors

The half wave plates used in the optical setup were achromatic half wave plates. This means that they are not dependent on the wavelength to the same degree as ordinary half wave plates are, thus, we should expect to have less distortion of the pulses using achromatic half wave plates.

All the mirrors in the setup were silver coated fused silica mirrors, with a SiO_2 layer on top for protection. Whereas pure silver coating has almost no GDD, the dielectric coating on top of the silver may contribute to GDD. No attempt has been made however to measure this dispersion

in our mirrors, due to lack of appropriate measuring equipment.

Retroreflector

The retroreflector was built on a translational stage (PT1/M, Thorlabs) with the micrometer screw replaced by a stepper motor actuator (DRV001, Thorlabs). On top of it, two mirrors were positioned orthogonal to each other and 45° to the incoming beam. A change of a length l on the motor then translated into a change of $2l$ in the path length of the reflected arm, due to the light going both back and forth.

In order to find the position of equal path lengths a method of interference was used. However, due to fact that the pulses from the Ti:sapphire oscillator were so short, that the overall path length of the beam in the reflected arm was complex and difficult to measure precise, and the short range of the stepper motor (only 8 mm), it turned out to be very difficult to use the pulses directly to find the overlap position. In addition, a relatively long coherence length was measured when the Ti:sapphire laser was operating in CW mode, so we could not use the CW light from the laser directly to locate the overlap either. Or in other words: the pulses resulted in an interaction length that was too short, while the CW light resulted in an interaction length that was too long.

Instead, we used a direct emitting semiconductor laser with a center wavelength close to 700 nm, which we had measured before to have a very short coherence length (less than 1 mm). Aligning this laser with beam from the Ti:sapphire by reflecting it off the 45° dichroic mirror (see Figure 4.6) and positioning a polarizer at 45° and a camera after the UFPBS, we could use the variation in the intensity pattern as an indicator for finding the overlap. We can understand this by recognizing that the output from the UFPBS consisted of two pulses with orthogonal polarizations. Because of this orthogonality, they would not display any interference. In order to achieve interference we had to project them into a common basis (here the diagonal), which we could do using a polarizer at 45°. As we approached the equal path lengths, by changing the position of the retroreflector, the intensity observed with the camera started to display an interference pattern. Since the coherence length was short, this pattern was only visible for a short movement of the retroreflector. From this it was possible to estimate an overlap position.

In order to specify the overlap position more precisely, we removed the semiconductor laser and used the analyzer setup by setting Alice's and Bob's HWP's to 22.5°. Since these HWP's were followed by polarizing beam splitters they would give the same effect as using a polarizer set at 45°. The variation in the registrations at the single photon detectors, as we now changed the position of the retroreflector in small steps in the vicinity of the overlap position, would then work as our indicator. Thus, as the retroreflector moved, we could observe an interference pattern in the single counts. Figure 4.14 shows the plot of such a scan.

The lower part of Figure 4.14 shows the interference pattern zoomed in around the position of the maximum overlap. We notice that there appears to be repeating sections of little change in the phase relation between the two interfering parts. It is assumed (but has not been confirmed) that this pattern is a result of a wobbling of the tip of the stepper motor, causing a variation in the path length which is not smooth and steady.

The total length of the interference pattern gave us an estimate of the length/duration of the

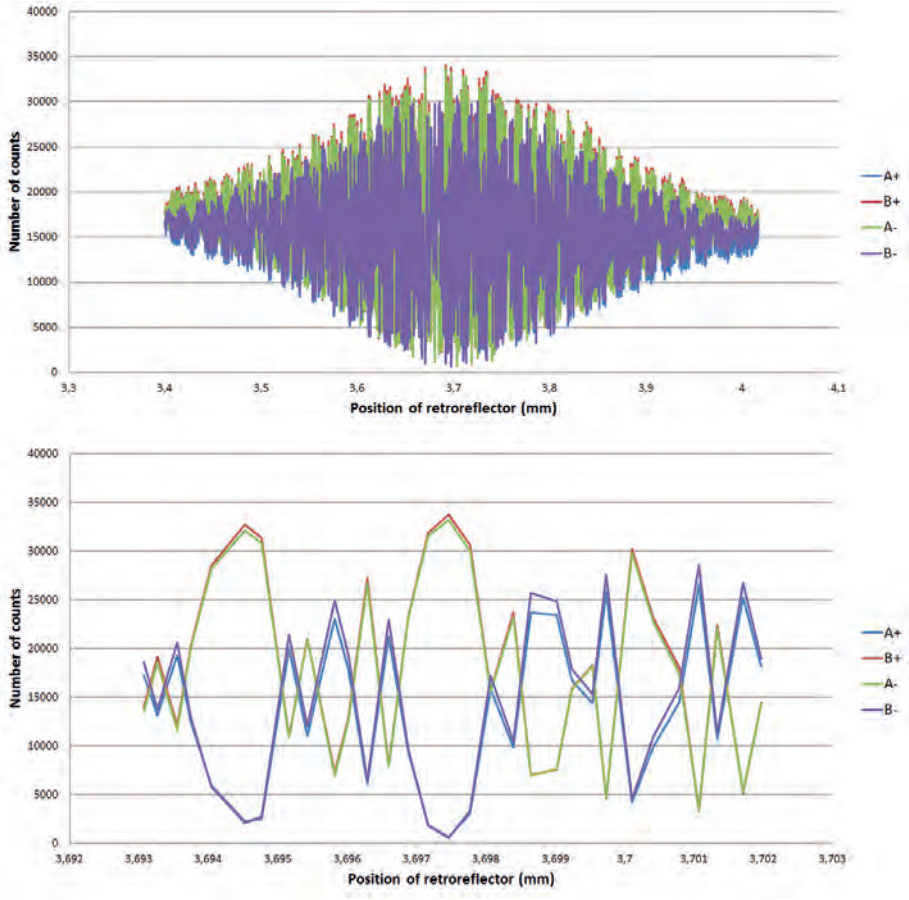

Figure 4.14: The number of singles as a function of retroreflector position. The interference pattern is a result of the two orthogonally polarized pulses being measured in a diagonal basis. The interference pattern is only visible when we have overlap of the two pulses. The lower graph shows a finer scan of the interference pattern. Here one can clearly see the huge variations in the number of counts as the retroreflector is moved.

pulses. If we say that the interference pattern spans 300 μm (FWHM), this would translate into a pulse duration of 1 ps[10]. That was a 20 times increase in the 50 fs long pulses we measured from the oscillator. At first, that seemed to be surprisingly high, but one has to remember that

[10]The 0.3 mm is the movement of the retroreflector, but for the light going back and forth this means a path length of 0.6 mm. However, we have two overlapping pulses, and the width of a single pulse is only half of the interference length, thus the pulse duration becomes $\frac{6 \cdot 10^{-6}}{2 \cdot 3 \cdot 10^{8}}$ s $= 1 \cdot 10^{-12}$ s

the interference filter which was located before the UFBS had a width of only 1 nm. This would naturally affect the duration of the pulse, due to the time-bandwidth product. We can actually see this directly from Table 3.1, which shows that a pulse with a bandwidth of 1 nm and a center wavelength of 800 nm can have a minimum pulse duration close to 1 ps. In addition, the pulses had to pass through thick optical components such as the Pockels cell crystal and the cube beam splitters in the analyzing setup, which were not optimized for ultrashort pulses, and therefor could have affected the pulse duration as well.

4.2.5 Piezoelectric actuator and its role

Looking at the interference patterns in Figure 4.14, we may realise that we would get a large variation in the number of detected singles if we were to change the angle of Alice's and Bob's HWPs. At perfect overlap and with the HWPs set at 22.5°, two of the detectors will be registering a minimum number of pulses while the other two registers a maximum. But when the HWP's are set at 0°, all detectors will register the same number of counts. So there will be a variation as the angle of the HWP's are changed. From the SPDC experiments however, we always observed (both with and without the compensating crystal) that the number of singles in a twin scan were roughly equal and angle independent.

In order to get a constant, angle independent number of singles we can think of two possibilities: either the phase relationship is fluctuating in such a way that on average, all the contributions sums to a constant level, or it is alternating between two orthogonal linear polarizations. This could for example be diagonal and off-diagonal polarizations, that is, the phase difference between the two parts is either 0 or π (and only these two).

In the photon picture we've discussed earlier, the phase relation was not considered. This was because it is assumed to have no affect on the results, since the polarization characteristics of each photon is retained throughout the setup. However, if we do think about the photons in terms of wave packets, the two cases above would mean that either each photon pair has an extremely precisely defined phase relation, or that the phase relation is varying randomly from pair to pair, averaging to a constant level. Although the theory of SPDC does not talk about the phase relation, it is assumed that photon pairs are created at a random location inside the ppKTP crystal. Due to the birefringence of the crystal material, the orthogonally polarized photons travel at different speeds, thus changing the phase relation from pair to pair, within the limits given by the phase matching condition. It would therefore seem likely, from this theory, that the phase relationship is averaging to a constant level.

With a pulsed source however, we will quickly run into troubles with such a setting, because it is only the superposed polarization that's important when the pulses are overlapping. If we would have had a truly random phase relation for all the pulse pairs (that is, a phase relation from one pair to the next which was completely random), the polarization of the superposed pulse would be a random mixture of linear, elliptical and circular polarizations. Thus on average the light would be perceived as unpolarized. Obviously this would give us a constant number of singles, but a true random phase relation would also result in rotational invariant doubles and coincidences.[11]

[11] When the variation is not truly random, the behaviour of the doubles and coincidences will depend on the width

Now, since we were measuring the behaviour of the state of the polarization under different circumstances, a random polarization would not show us anything of interest. Thus, we needed to maintain the polarization characteristics and at the same time have a rotational invariance in the singles. One way to do this was to alternate between two orthogonal directions of linear polarization, such as diagonal and off-diagonal.

The difference between the photon case and classical case is that in the photon case, the photons retain their polarization characteristics if the photon pair should part ways in the beam splitter. For the classical case, this situation does not arise in general because the superposed light will always exit both ports.

In order to still try to simulate the behaviour in the quantum case, by varying the phase relation between two orthogonal, linear polarization states, a small, oscillatory variation in the path length from the overlap position was introduced by changing the position of the mirror located in the transmitted arm of the Mach-Zehnder interferometer. This was accomplished by using a mirror mounted on a piezoelectric actuator (Model P-016.00H, Physik Instrumente (PI)). The movement of the actuator was achieved by introducing a periodic variation in the supply voltage. The offset voltage and amplitude were optimized to a level were the singles became close to being rotational invariant.

4.2.6 Neutral density filters

The neutral density filters (NDF's) were absorptive NDF, since in general any back reflections could cause unwanted distortions in the pulses. As was mentioned before, the value of the attenuation was mainly determined from the number of registered singles at the detectors. With $8 \cdot 10^6$ pulses per second from the Pockels cell, an attenuation with the NDF's of the order of 10^{-7} resulted in a count of 10 000-20 000 singles/s.

The number of singles were not constant however, but did fluctuate over time. The origin of these fluctuations seemed to arise both in the laser oscillator and the Mach-Zehnder interferometer. This could be due to temperature variations (the mirrors were not cooled directly, but only through conduction through the holders down to the base plate) which together with the interference effects involved in the mode-locking process in the oscillator, could cause variations in the energy output.

4.2.7 Interference filter

During the experiments with the SPDC source, the interference filter was located in the analyzing setup. With the pulsed source, it was now moved to before the Mach-Zehnder interferometer. This was done primely to have a longer pulse length in the interferometer, as it turned out to be a bit of a challenge to find the overlap position between the two parts of the pulse when the pulse length was of the order of only a few μm. With the interference filter placed before the

of the coincidence window, the number of pulses within this window and the how well the total polarization remains the same from one window section to the next.

Mach-Zehnder interferometer the pulse length entering it was increased to a few hundreds of μm, as was explained.

An interference (or bandpass) filter is created by placing layers of alternating low and high index materials on a substrate surface. Each layer is $\lambda/4$ thick, where λ is the center wavelength of the filter. By placing spacers between the stacks of layers a Fabry-Perot cavity is formed which effectively prevents light with other wavelengths than close to the center wavelength to pass, through destructive interference. The center wavelength of the filter can be slightly tuned, by changing the angle of incidence, which in effect changes the length of the Fabry-Perot cavity.

The interference filter was an important piece in our setup. In the earlier measurements done with the SPDC source, the clearest results were gained with a 1 nm filter with a center wavelength of 810 nm. Since we wished to emulate this condition, it was important that our center wavelength from the Ti:sapphire oscillator did not deviate far from this. It should be noted, however, that the adjustment of the center wavelength was done by changing the position of a slit inside the oscillator. This procedure also affected the bandwidth, the output power and the stability of the pulses, and was therefore a delicate and time consuming procedure with many variables.

Besides picking out the correct center wavelength, the width of the interference filter also had another effect: it directly affected the pulse duration. Figure 4.15 shows the difference between a 1 nm and a 10 nm interference filter during a mirror scan. Clearly, the pulse duration is highly dependent on the width of the filter. In addition, we may note that the ratio of the widths of the interference patterns is roughly equal to the ratio of the bandwidths of the interference filters.

In addition, one should note from the theory of SPDC that the frequencies of the signal and idler are related to the pump frequency through

$$\omega_p = \omega_s + \omega_i \tag{4.1}$$

From this equation we see that the frequencies of the signal and idler does not have to be the same, but if they are different they have to be symmetrically placed around $\omega_p/2$. This possibility is a variable that is not part of our setup with the pulsed source. It is assumed that the narrow spectral width of the IF would reduce the importance of this effect, but one should nevertheless be aware of this point.

Finally, all measurements were done with the 1 nm filter, and in the theoretical derivations we have assumed that the frequency difference between the down-converted photons is negligible. However, with a wider bandwidth of the interference filter, the photons shows less entangled characteristics.

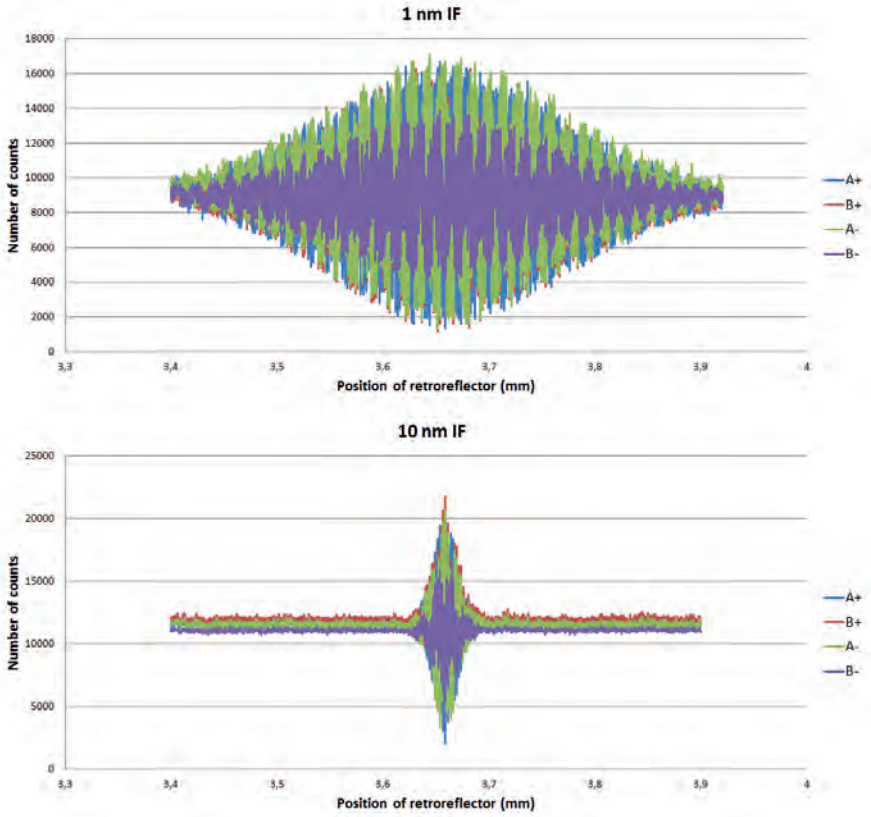

Figure 4.15: The interference pattern obtained with the HWP's at Alice and Bob set at 22,5°, when using a 1 nm filter (top) and a 10 nm filter (bottom). The pulse duration is clearly affected by the width of the filter.

4.2.8 Analyzing setup

As was explained in the introduction, one of our prime objectives was to investigate whether or not it was possible to get results similar to the ones obtained with the SPDC source, but using a source based on ultrafast pulses instead. Thus, the analyzer setup necessarily had to be very similar in both cases. A schematic view of the slightly modified setup for the pulsed source is shown in Figure 4.16.

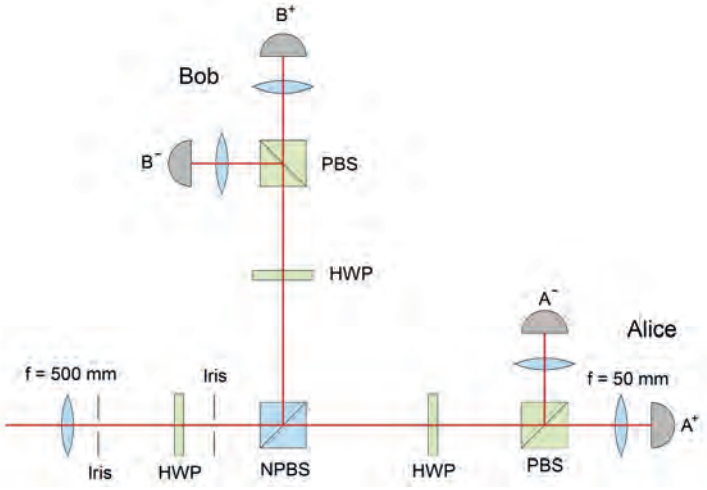

Figure 4.16: The analyzing setup consists of a biconvex lens followed by an iris and a HWP. The light is then split by a 50/50 non-polarising beam splitter, and analyzed in the two arms using rotating HWP and polarizing beam splitters. Another biconvex lens is placed in front of each detector for maximum collection of light.

If we compare with the setup when using the crystal source (Figure 4.1), we see that the only difference is the removal of the dichroic and interference filters. We've used the same lenses in both setups (i.e we kept the first biconvex lens with a focal length of 500 mm and the 50 mm lenses in front of the detectors). In order to check that these where still appropriate for obtaining the very small focus spot needed at the detectors, a measurement of the beam width was conducted in the pulsed case. This was then used in a simple ABCD matrix calculation to plot the theoretical beam waist as a function of distance. The result is plotted in Figure 4.17. From this calculation we found that the spot size (diameter) at the position of the detector (position C in Figure 4.17) would be of the order of 30 μm. Naturally, this is a theoretical calculation, so we do not expect the spot size to be that small, but it showed at least that the same lenses could be used also with the pulsed source.

For optimum alignment of the lenses in front of the detectors, so that the very small focal spot could be correctly positioned on the detector, the lenses were mounted in holders (ST1XY-S, Thorlabs) which could be moved in two dimensions perpendicular to the direction of the beam

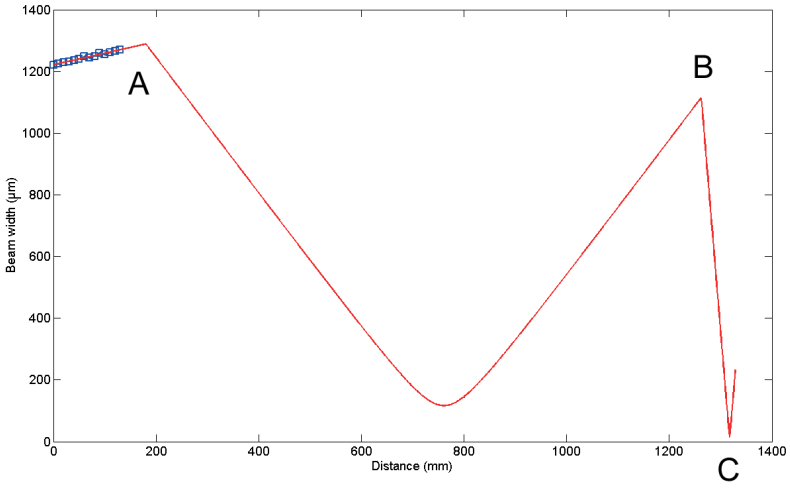

Figure 4.17: The red line is the theoretical calculated beam width through the optical system, while the blue squares in the upper left corner of the graph are measurement data points. A is the location of the first lens (focal length 500 mm), B is the location of the lens before the detector (focal length 50 mm) and C is the position of the detector.

(x and y). The holder itself was mounted on a manual linear stage (MT1/M, Thorlabs) so that also the z direction could be optimized. This was a time consuming procedure since an optimum spot size of 150 µm had to be positioned on a 180 µm large detector, and it had to be conducted in almost complete darkness since the light sensitive single photon detectors had to be on during the alignment procedure.

References

[1] C. E. Kuklewicz, M. Fiorentino, G. Messin, F. N. C. Wong, and J. H. Shapiro, *Phys. Rev. A* **69**, 013807 (2004)

[2] G. Weihs, T. Jennewein, C. Simon, H. Weinfurter, and A. Zeilinger, *Phys. Rev. Lett.* **81**, 5039 (1998)

[3] Shih, Y., *IEEE J. Sel. Top. Quant. Elec.* **9**, 1455 (2003)

[4] G. Adenier, J. Bergli, A. P. Thörn and A. I. Vistnes, "Observation of bosonic coalescence and fermionic anti-coalescence with indistnguishable photons", *Proc. SPIE*, **8832**, 88321K-1 (2013)

[5] S. Sauge, L. Lydersen, A. Anisimov, J. Skaar and V. Makarov, *Opt. Exp.* **19**, 23590 (2011)

[6] SPCM-AQRH Single Photon Counting Module, data sheet, Excelitas (2013)

[7] S. Cova, M. Ghioni, A. Lotito, I. Rech and F. Zappa, *J. Mod. Opt.* **51**, 1267 (2004)

[8] *Millennia eV Data Sheet*, Spectra-Physics (2013)

[9] *Acceptance testing data, Model: TiF_50F, Serial number S/N 0T00143*, Avesta (2013.12.16)

[10] P. F. Moulton, *J. Opt. Soc. Am. B* **3**, 125 (1986)

[11] P. F. Moulton, *Opt. News* **8**, 9 (1982)

[12] R. W. Boyd, S. G. Lukishova and Y. R. Shen, *Self-focusing Past and Present Fundamentals and Prospects*, Springer, 2009

[13] R. L. Goldstein, User's guide for BBO, KDP, RTP and Lithium Niobate Q-switches and modulators for Q-switching, chopping and pulse extraction, http://www.lasermetrics.com/pdf/eomgenl.pdf (01.06.2015)

[14] http://www.hanamuraoptics.com/lasercrystal/csi/csi.htm (01.06.2015)

Chapter 5

Testing

The Ti:sapphire oscillator was a delicate system. It consists of around 20 optical components which had to be aligned correctly in order for the oscillator to work. This was especially true when operating in the mode-locked regime. The Ti:sapphire oscillator had been put together, aligned and tested at Laser Support Service[1] before purchase, so we could be somewhat confident that the internal alignment of the optical components probably were not off by very much (though we did expect some deviation due to vibrations during transport). However, Laser Support Service had used an internal pump laser (the Sprout-G from Lighthouse Photonics) in their alignment process, whereas we had an external pump laser. This proved to be slightly challenging because the alignment apertures to be used in the alignment of an external beam, wasn't aligned with the optics inside the oscillator. Thus, we needed far better control over the pump beam than we initially had.

The solution to this problem was to install a two-mirror configuration (with modified mirror holders due to the space limitation) in the space where the pump laser should have been located if we have had an internal one, as shown in Figure 5.1. This made the actual steering of the pump beam somewhat easier to control. An external mirror configuration, which actually would have made the alignment process even simpler, was rejected due to scattering considerations of the high power beam.

Once the pump laser was in place and aligned, the actual alignment of the oscillator had to be done. The procedure was explained in the manual for the oscillator, which worked out rather well once some familiarity with the setup and functionality was gained. A schematic layout optical setup of the oscillator taken from the manual is shown in Figure 5.2.

The alignment procedure consisted of two parts: the first one was to get the oscillator to work in continuous wave mode, and the second was to make it work in the mode-locked regime. After setting up the CW mode, the measured power output was as high as 740 mW for an input power of 4 W, resulting in 18.5 % optical conversion efficiency.

Making the oscillator work in the mode-locked regime required a bit more work. There were mainly two reasons for this: there was no earlier experience with mode-locking techniques within our group, and the wavelength of the laser, which is outside the range of the human visual

[1]The oscillator is produced by Avesta, but purchased from Laser Support Service.

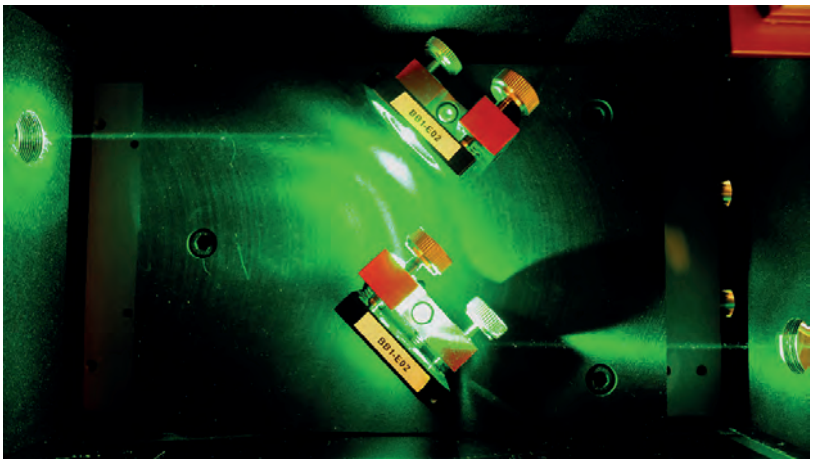

Figure 5.1: Internal mirror configuration for better control of the position and steering of the pump laser beam. The beam is entering from the right.

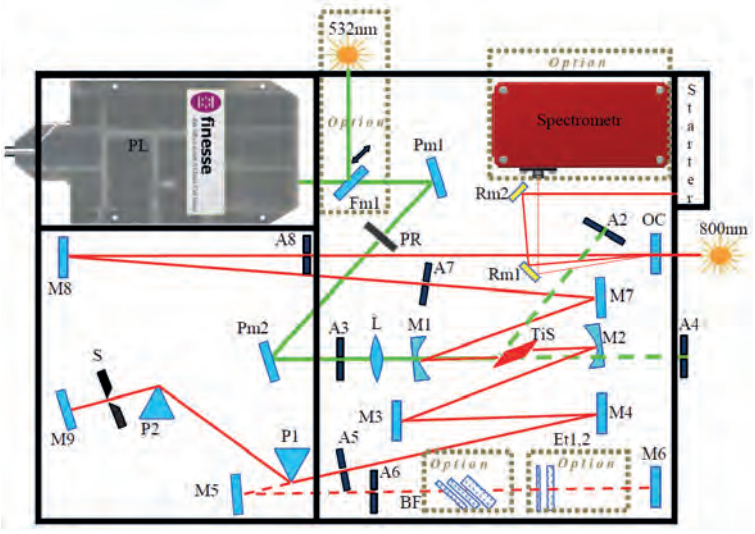

Figure 5.2: The optical setup of the Ti:sapphire oscillator. Taken from [1]. Note that we do not have the internal pump laser Finesse. Nor do we have the birefringence filters (BF) or etalons (Etl.2), which are used for CW wavelength tuning, or the optional spectrometer.

perception, thus making alignment a bit more tedious.

In order to start the mode-locking, prism P2 (see Figure 5.2) had to be moved slightly away from its initial position. This introduction of a small perturbation moved the laser from the CW to mode-locked operation. The oscillator was equipped with an automatic starter circuit and a stepper motor that provided this movement, but this was not always enough from the mode-locking to engage. Sometimes a gentle tap on the platform for prism P2 had to be made in order to make it start. Considering how sensitive the setup was to vibrations, this was not an optimal solution.

In addition to the electronic started circuit, the oscillator was equipped with a number of surveillance indicators, such as a power indicator for checking if the power level was within operational parameters, and a visual/audio indicator for surveillance of the mode-locked pulse train. It was also equipped with a photo diode and a BNC output port for direct observation of the pulse train on an oscilloscope. Such a pulse train, at 2.9 W pump power, is displayed in Figure 5.3.

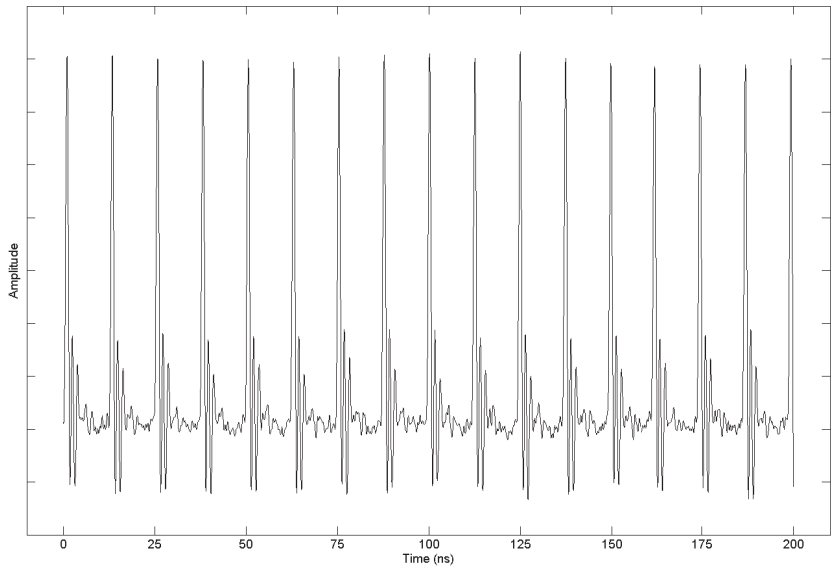

Figure 5.3: A pulse train from the Ti:sapphire oscillator at 2.9 W pump power indicating that the laser is mode-locked (measured with a WavePro 7100A oscilloscope (LeCroy) at a sampling frequency of 1 GHz). The observed repetition rate is 80 MHz. Note that the duration time of each pulse does not correspond to the actual pulse duration.

From this graph we can see that we have one pulse roughly every 12.5 ns, giving us a repetition rate of 80 MHz, as expected. The repetition rate could be adjusted to some extent by changing the position of the prism P2, but the location of the prims also affected the output

power. In general, the location of the prisms determined the width and shape of the output spectrum, which in turn affected the pulse duration. A shorter pulse necessarily needs to have a broader spectrum, due to the time-bandwidth product. The center location of the spectrum was determined by the position of the slit S. These characteristics were possible to measure to some extent with the use of an autocorrelator.

5.1 The autocorrelator

After aligning the pump laser and getting the oscillator to operate in the mode-locked regime, the pulses were sent to an autocorrelator in order to optimize the pulses (duration and center wavelength).

The autocorrelator (which the Norwegian defence research establishment generously let us borrow from them) was a model FR-103MN from Femtochrome Research Inc. It could operate both as an interferometric and intensity autocorrelator. It was specified to have a temporal resolution of the order of 5 fs, and its operating wavelength range is 410-1800 nm, thus well suited for measuring the pulses from the Ti:sapphire laser. The scanning is achieved by a rotating pair of parallel mirrors, where the frequency of rotation could be set by the user (10, 5 or 2.5 Hz). A view of its internal setup is shown in Figure 5.4.

The autocorrelator works as follows: the pulses we wish to analyze first enters a pellicle 50/50 beam splitter, which is only a few μm thick. The transmitted part of the pulse hits two mirrors which reflect the beam back the same way to the beam splitter. The reflected part from the beam splitter hits a rotating mirror pair. If the mirror pair is in an appropriate position the pulse will be sent to a mirror and reflected back. The distance travelled by the pulse is dependent on the location of the mirror pair, thus resulting in a scanning behavior (see also [3]). The two parts of the pulse then combines again at the beam splitter and travels collinearly to a curved mirror, which redirects the pules through a thin nonlinear crystal (here BBO) which frequency doubles the radiation. The reason why the nonlinear crystal has to be thin is that we need to generate second harmonic light for all wavelengths in the pulse. The different wavelengths of this frequency doubled light does, however, exit in different angles, and the total angular width is inversely proportional to the crystal thickness, as illustrated in Figure 5.5. A thick crystal creates a too narrow SHG spectrum in any given direction, and cannot efficiently be used for autocorrelations measurements. A very thin crystal creates a broader spectrum in the forward direction, and is therefore more suitable. The thinner the crystal, the broader the spectrum and the shorter the measurable pulses can be (but a thin crystal also requires higher pulse energy to be able to generate a SHG signal that's strong enough).

A broad band filter located after the crystal blocks the fundamental wavelength, thus, in theory, only the frequency doubled radiation should hit the detector. The intensity of the light hitting the detector is dependent on the intensity of the fundamental wave length. This intensity is highly dependent on the relative phase of the light in the two pulses. When the two pulses are overlapping they may be in or out of phase, causing constructive or destructive interference. As the pulses move further apart, the interference becomes less distinct. Thus, a scan of the overlap gives a measurement of the pulse duration. This results in the interferometric plot of a pulse

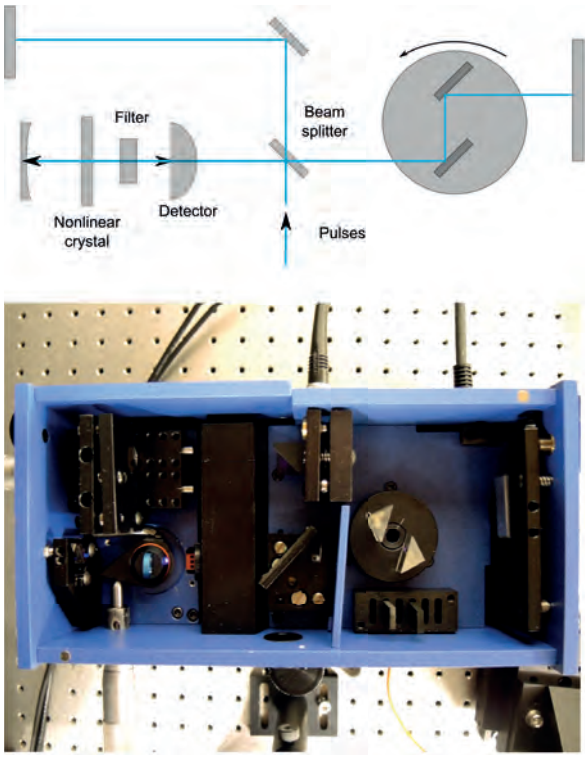

Figure 5.4: The internal optical setup for the FR-103MN autocorrelator. Note that the nonlinear crystal, the filter and the detector in mounted below the optical path from the beam splitter to the curved mirror. This makes the unit very compact, but difficult to align.

duration (the interferometric autocorrelation function), as was discussed in chapter 3.

Naturally, the time scale given by the autocorrelation function is not the same as the real pulse length, due to the graph being made up of several pulses. Thus, a conversion factor has to be included, as well as assumptions about the shape of the pulse, in order to get a realistic value for the pulse duration. This conversion factor was given in the manual for the autocorrelator, and could also be measured by a method given in the manual.

Unfortunately, these two values were not the same (in fact, they differed by a factor 10, suggesting that there is a typing error somewhere). To avoid this problem, we used an alternative method. It based itself on the fact that the shape of the autocorrelation function is determined by the interference, which is given from the wavelength of the light in the pulses. By assuming a center wavelength (which may be criticized as an oversimplified assumption since the pulses have more than a single wavelength and their center wavelength may not be 800 nm) and counting the number of peaks over some finite range in the interference pattern, we got the actual time. The

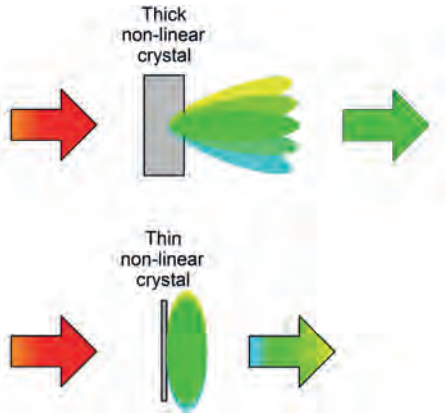

Figure 5.5: The difference in SHG spectrum when using a thick and a thin crystal. The thick crystal shows a stronger angle dependence for the different wavelengths generated than a thin crystal.

factor, ΔT, that we needed to multiply with to get the real time in the autocorrelation function became

$$\Delta T = \frac{N\lambda}{c\Delta t} \tag{5.1}$$

where N is the number of peaks in the chosen range, λ is the wavelength and Δt is the time range we have chosen in units as given on the oscilloscope.

The autocorrelation itself accepts only vertical polarization, so we had to use an achromatic half wave plate just before the autocorrelator. The mirrors used for redirecting the mirror into the autocorrelator were protected silver coated mirrors. As been mentioned, the group velocity dispersion is very low on these mirrors, and thus would have only a minor, if any, effect on the measurement results. Any distortions on the pulse shape due to the achromatic half wave plate could not be observed.

Since we were observing an interference phenomena, it was important that we had a good overlap between the two pulses. Due to the compact size of the autocorrelator, this was somewhat difficult to achieve. The solution was to remove one of the back walls of the autocorrelator and using a prism to reflect the beams out. With a much larger distance it became somewhat easier to make the beams overlap collinearly.

Another challenge for getting the right interference pattern was the number of parameters that could affect it. This included the input power (more power saturates the detector and affects the pulse duration), the gain adjustment on the autocorrelator, the trigger adjustment settings on the oscilloscope (had to be triggered externally by the autocorrelator) and the rotation speed of the mirror pair (faster speed caused the pattern to average out, 2.5 Hz was maximum). All these parameters had to be adjusted and optimized before any measurements could be made.

5.1.1 Autocorrelation measurements

The adjustment controls on the FR-103MN autocorrelator are crude at best, and not really suited for making changes comparable to the wavelength. This made the setup of an interferometric autocorrelation measurement difficult. However, the FR-103MN has an adjustment screw for adjusting the arm length in the stationary arm. Its purpose is really to position the autocorrelation function at any location along the overlapping range. But because the mirror in this arm were not absolute perpendicular to the beam that hit it, or that the axis of the adjustment screw was not exactly parallel to the beam, a change in the lengthwise adjustment acted like a precise sideways adjustment. Using this, it was possible to find a location where the peak-to-background ratio was close to eight. This ratio is important, because if we had a lower peak-to-background ratio our theoretical calculations would not be correct, and we could not in any way claim that the measured pulse duration was close to the actual one. The measured autocorrelation function is shown in Figure 5.6.

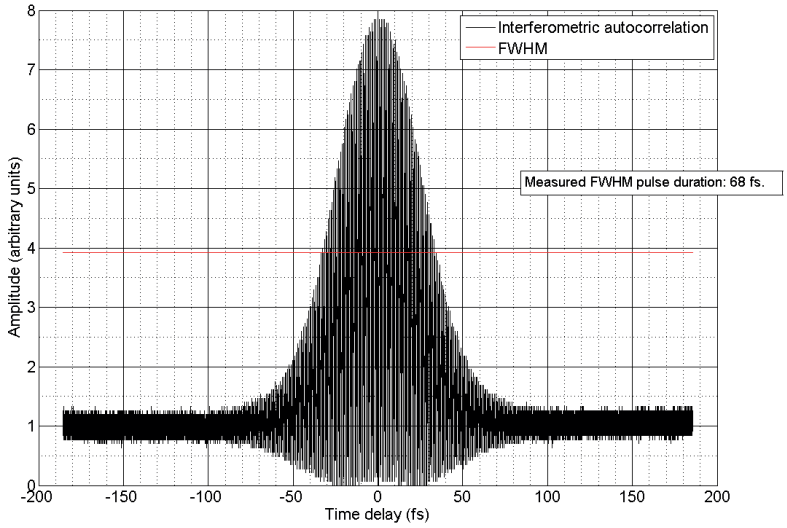

Figure 5.6: The autocorrelation function with a measured peak-to-background ratio that is close to the theoretical value of eight.

Also measured in this plot is the pulse duration. One should note however that in general it is not correct to deduce the pulse duration directly from the measured autocorrelation function, because many different pulse shapes and durations can give the same autocorrelation function, as was mentioned. To get the pulse duration for a measured autocorrelation plot, we need to make some assumptions about the shape and behaviour of the pulse. If we assume that the pulse is purely Gaussian, then the real pulse duration can be calculated from the measured one using the

following expression

$$\text{Pulse duration}_{\text{Gaussian}} = \frac{68 \text{ fs}}{\sqrt{2}} \approx 48 \text{ fs} \tag{5.2}$$

However, if we now plot the theoretical autocorrelation function of a Gaussian pulse, where we've scaled the value of the width so that the theoretical curve matches the measured one, we get the plots shown on the top of Figure 5.7. The theoretical value for the pulse duration has to be 77 fs in order to match the two shapes.

Now, 48 fs and 77 fs are obviously not the same, so let's instead assume a sech^2 shaped pulse. In this case, the real pulse duration can be calculated from the measured one as follows

$$\text{Pulse duration}_{\text{sech}^2} = 68 \text{ fs} \cdot 0,648 \approx 44 \text{ fs} \tag{5.3}$$

If we do the same as above and try to fit a theoretical plot of the pulse with the measured one, we arrive at the plot shown at the bottom of Figure 5.7. The theoretical value for the pulse duration we have to use in the calculations in order to fit the theoretical plot with the measured one is 44 fs. But this is exactly the same value as we got from the measurement if we assumed a well-behaved sech^2 shape of the pulses. Thus, it would seem likely that the pulses are closer to being sech^2 than Gaussian, even though the shape of the theoretical plots fit rather well to the measured one in both cases (except possibly at the wings).

The spectrometer

How does the presumed pulse duration of 44 fs fit with the spectral bandwidth? Using a spectrometer[2] a measurement of the spectral width was undertaken. This particular spectrometer (model CCS175, Thorlabs) was a fiber coupled, CCD based Czerny-Turner spectrometer, with an operating range between 500 and 1100 nm, an optical grating with 830 lines/mm, 800 nm blaze and a spectral resolution of 0.6 nm FWHM at 633 nm [4].

The working principles of a Czerny-Turner spectrometer are rather simple: the beam enters a slit (in our case by first passing though a multimode fiber) and is being reflected towards a grating, which separates out the different wavelengths. The light from the grating is directed and focused on to the CCD camera, which registers the intensity of the particular wavelength that is calibrated to hit that specific pixel. Figure 5.8 shows an illustration of such a Czerny-Turner spectrometer.

The data measured by the CCD camera is displayed by a program, where changes and adjustments to the spectrometer also can be made.

Due to the fact that the spectrometer was fiber coupled, and the oscillator was not, there were some initial concerns about how to actually do the measurements. However, by mounting the input fiber end on a three-axis translational stage it was possible to position the fiber so that it could collect most of the light properly.

The first tests were done by measuring the light directly from the laser. However, the intensity turned out to be too strong for any useful measurements to be made, thus, the solution was to use the weakest of the three beams coming out of the oscillator (which actually was the beam that is

[2] Again, the Norwegian defence research establishment generously let us borrow this equipment from them.

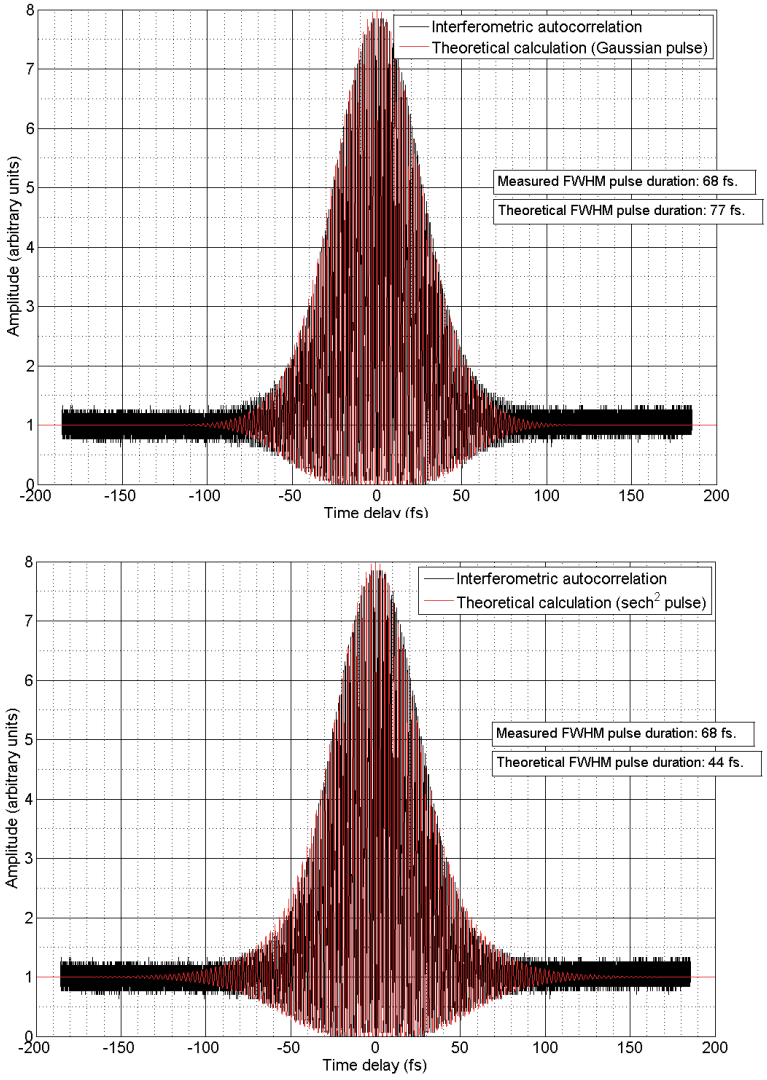

Figure 5.7: The measured and theoretical autocorrelation functions, when the pulses are assumed to be Gaussian (top) and sech^2 (bottom). There is a slight difference between the measured and calculated pulse duration, indicated that perhaps our scaling of the time axis is not entirely correct.

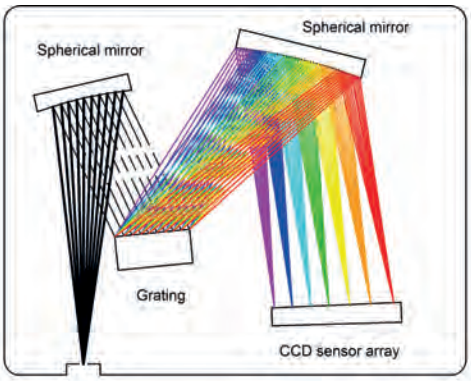

Figure 5.8: The working principles of a Czerny-Turner spectrometer.

supposed to go to the internal spectrometer, had we had one, in the oscillator itself (see Figure 5.2)) and to adjust the integration time in the analyzing program.

Initial measurements on the spectral bandwidth indicated that it was only about 10 nm FWHM. This number is slightly lower that the 14 nm given by the time-bandwidth product (Table 3.1), which, together with an observation that the bandwidth increased when the pump power was increased, suggested that there was a lower limit on the intensity for the spectrometer to respond. This would mean that light with low intensity would seem to have a narrower spectral bandwidth than the same light at higher intensity. To check this, the input power to the oscillator was kept steady at 3 W, but a number of different NDF were placed in front of the tip of the measuring fiber. The combined plot of these measurements is shown in Figure 5.9.

As can be clearly seen from this graph, the spectral bandwidth is indeed reduced when the intensity of the incoming light is reduced. Thus, the measurements from this spectrometer could not be used to correctly determine the bandwidth, it could only be used for locating the central wavelength. In fact, increasing the integration time caused the spectrometer to quickly saturate, while lowering the intensity reduces the apparent bandwidth. Its operating dynamic range was in other words too small to be useful in this analysis.

One may also notice that there are three distinct peaks in the spectrum, at around 807, 809 and 810 nm. In fact, if we look carefully, it does appear that we have peaks at 805, 803, 812 and 814 nm as well. Thus, it would appear that we have distinct wavelengths with a somewhat similar distance between them. From the nature of mode-locking, where the relation among the phases becomes locked, this is perhaps not so surprising.

5.1.2 Effects of optical components

To investigate the effect that different optical components had on the pulse shape and duration, the autocorrelator was set up a distance of roughly 0.5 m away from the Ti:sapphire laser. By

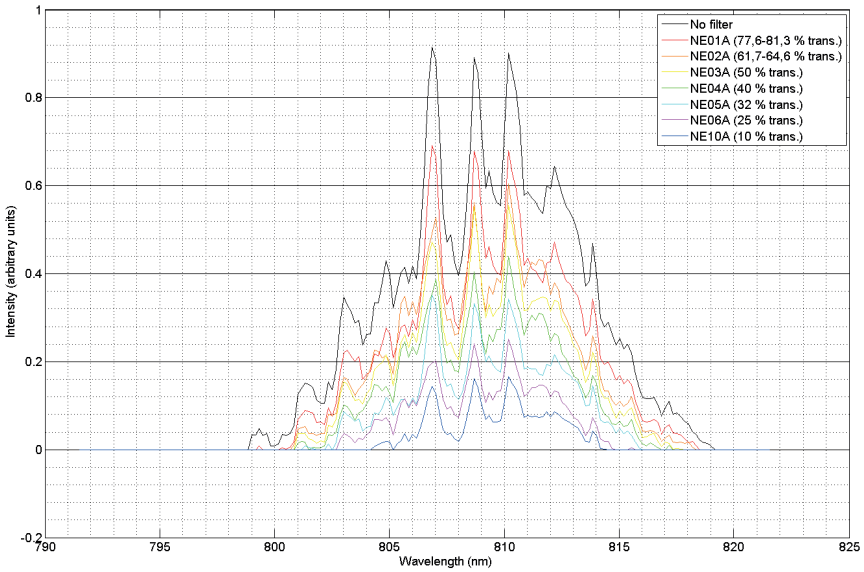

Figure 5.9: The spectral bandwidth is reduced when the intensity of the incoming light is reduced. The zero level in this plot is the cutoff level of the spectrometer.

comparing the autocorrelations with and without different optical components placed in the optical path before the autocorrelator, we could get an indication of any strong distortions, such as chirp.

This method clearly has its weaknesses, because, as has been mentioned earlier, many different pulse shapes can result in the same autocorrelation function. But based on the assumptions that the pulses that exited the Ti:sapphire laser were somewhat well behaved (which we saw some hints of in the matching of the measured and theoretical autocorrelations in Figure 5.7) and that larger distortions in the pulse shape would result in a detectable change in the autocorrelation, some information could still be obtained from this kind of measurement.

The measurements were made primarily on the components in the pulsed setup which were not specifically designed for use with ultrafast pulses. Thus, we specifically focused on a number of different absorbing neutral density filters (NDF) and the Pockels cell.

Neutral density filters

The effect of NDF's on the pulse was of great importance since these were used to reduce the intensity before the pulses entered the Mach-Zehnder interferometer. A series of measurements where done on NDF's ranging from roughly 80 % transmission to 10 %, and the result is plotted in Figure 5.10.

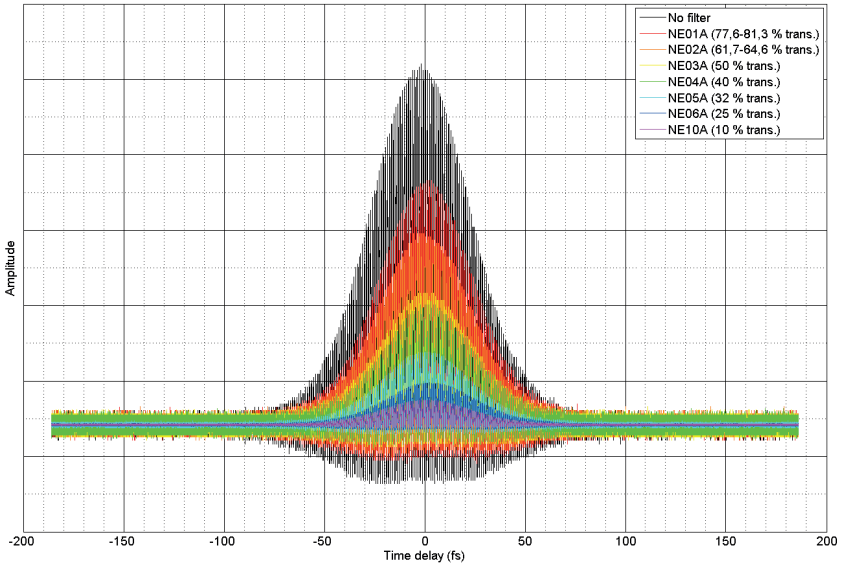

Figure 5.10: Autocorrelation function measurements done with different NDF's.

Here we can see that the overall shape appears to be the similar, but it is hard to make any comparisons when the amplitudes are not the same. Thus, it is difficult to draw any definitive conclusion about the effect on the pulse shape that the filters may have. But if we remember that chirp, which may arise from group velocity dispersion, is very much dependent on the thickness of the material that the light has to pass through, and we also note that the thickness of the NDF's range from roughly 0.5 to 2.5 mm, we may say that it would appear that the effect on the pulses is small, since the actual autocorrelator trace only seems to be attenuated and not distorted. If the thickness would have had an influence on the autocorrelation function we would not have seen just a reduction in the amplitude, which is what we see in Figure 5.10. That being said though, only a more thorough analysis, such as using FROG or SPIDER, would be able to give us a more definite answer.

Pockels cell

The Pockels cell was an important part of the optical setup in the experiments. The repetition rate from the mode-locked oscillator was around 80 MHz, while the maximum repetition rate on the single photon detectors is 40 MHz, but could be as low as 12 MHz, before the detector saturates. Also, in the measurements done with the SPDC source, the single counting rate was of the order of 10 kHz, and since we wished to emulate the measurement results as much as possible, we had to be able to control the repetition rate as well.

Of all the components tested, the Pockels cell had the most effect on the autocorrelation function. This should not come as a surprise, really, since a Pockels cell consists of a relatively long nonlinear crystal with electrodes attached to it. As was mentioned, by changing the voltage over the electrodes the index of refraction is changed (the electro-optic effect), thus the phase delay in the crystal can be modulated and the Pockels cell can be made into a voltage controlled HWP. However, the electro-optic effect is a weak effect and therefore high voltage and somewhat long crystals are used.

Our Pockels cell is made up of two 10 mm long rubidium titanyl phosphate (RTP) crystals and two 4 mm thick fused silica windows [5]. Using this and theoretical values for the group velocity dispersion[3] for the center wavelength, we could calculate the expected group delay dispersion (GDD)

$$\text{GDD} = 2 \cdot 10.0 \text{ mm} \cdot 285.69 \text{ fs}^2/\text{mm} - 2 \cdot 4.0 \text{ mm} \cdot 165 \text{ fs}^2/\text{mm} = 1.06 \cdot 10^4 \text{ fs}^2 \qquad (5.4)$$

With the use of this value, we could then calculate the theoretical shape of the autocorrelation function. In Figure 5.11 both the measured and theoretical autocorrelation functions are displayed.

From this plot we see clearly that there is a distortion of the shape of the pulse, and that it to some extent fit the theoretical calculated plot. It is therefore reasonable to assume that some chirp has been introduced by the Pockels cell.

A chirped pulse would mean that the frequency of the pulse changes over the duration of the pulse. Whether this really would have any effect on the measurements is hard to tell, but with the interference filter being so narrow it is unlikely that the effect of the chirp would be visible. The filter would only pick out a narrow part of the pulse with a bandwidth which corresponded to the bandwidth of the filter itself. Thus, the difference in the frequencies in the pulse would be small, and therefore the dispersion effects would be quite similar as well among the frequencies.

A measurement to confirm this was not made, however, due to lack of appropriate measuring equipment. An important point though, was whether the two split parts of the pulse in the Mach-Zehnder interferometer would be affected differently before they were combined. A possible scenario could be that the pulse would become mirrored in one arm but not the other. For an unchirped, symmetric pulse this would make no difference, but for a chirped pulse it would become important, since the combined pulses no longer are equal which would affect any possible interference. However, no such effects could be observed in the measurements.

Furthermore, we do not know anything about how to understand the ”shape” of the photon in the simplified picture of the SPDC process, if they can be modelled as wave packets similar to the some descriptions of the HOM effect. Based on this fact, it would be preferable to have as a simple shape of the pulses from the Ti:sapphire laser as possible.

5.2 Optimizing the number of pulses

In order to find the optimum voltage over the Pockels cell, the linearly polarized pulse train was sent through the Pockels cell and a HWP on the other side, set to be parallel to the polarized

[3] Most of the values for the GVD have been obtained from either reference [6] or from Thorlabs.

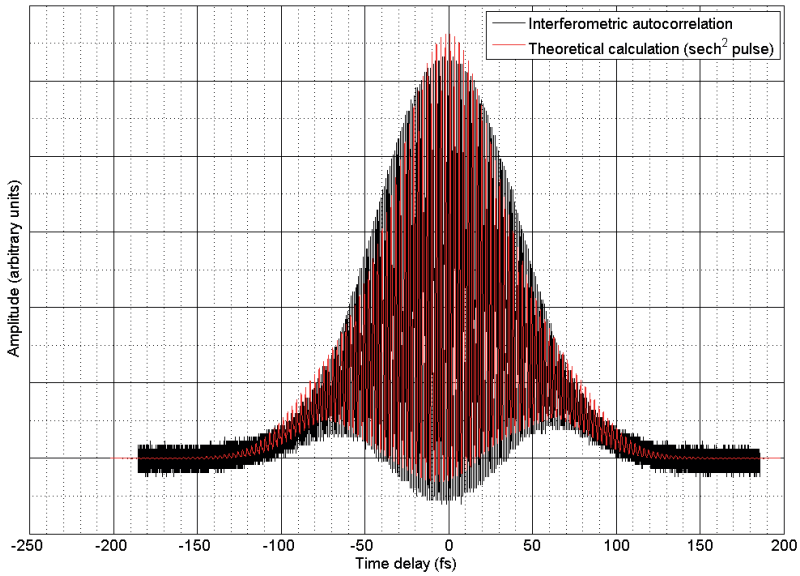

Figure 5.11: The measured and theoretical calculated autocorrelation functions for the Pockels cell. The pulse is assumed to be a sech^2 pulse with a pulse duration of 44 fs, and the Pockel cell is assumed to have a GDD of $1.06 \cdot 10^4$ fs^2. The difference in maximum and minimum values may be due to slight change in the overlap of the two pulses in the autocorrelator as a result of the Pockels cell being inserted to the optical path.

light. Behind this HWP, a detector connected to an oscilloscope was located. As the voltage was changed the amplitude of the pulse train as seen on the oscilloscope was reduced. At minimum amplitude, we would have the optimum voltage. This voltage was around 1.4 kV.

There were several other settings on the power supply control unit for the Pockels cell besides the voltage, such as internal or external triggering, the possibility for delaying the triggering of the Pockels cell and the width of the trigger pulse. The width of the trigger pulse determined how long the gate should be open for the pulse train (see Figure 4.12), thus determined how may pulses from the pulse train the pulse picker should let through for each trigger pulse.

During the initial measurements it became clear that the number of registered doubles and coincidences was far too low to get any reliable statistics. At the time the Pockels cell was only letting a single pulse through per trigger pulse, meaning that the number of pulses were, in theory, the same as the inverse of the frequency of the external clock coupled to the Pockels cell. The reason for doing it like this (only let a single pulse through) was that the dead time of the detectors is much longer than the time between two pulses. It was therefore assumed that more than one pulse per trigger pulse would result in a proportionally higher singles count than doubles and coincidences, which would lead to much longer processing times and eventually

saturation of the detectors. However, it turned out that the relationship between singles, doubles and coincidences was not following this rule, and that the increase in the number of singles could be compensated for by the use of NDF's, which did not affect the doubles and coincidences in the same manner. It therefore seemed preferable to have a larger number of pulses per trigger pulse at the Pockels cell. The maximum number of pulses per trigger pulse for the Pockels cell is 80 and the maximum repetition rate is 100 kHz, which was also the setting used in the measurements.

It should be noted however, that the ratio of singles to doubles and coincidences was much lower for the pulsed source than for the SPDC source. This could be a consequence of the fact that the energy between the pulses also is contributing to the number of singles, but less to the doubles and coincidences due to the intrinsic random nature of the time of registrations in the detectors. As was mentioned earlier, the method of post-processing could not help to improve the situation.

5.3 Instabilities in the Mach-Zehnder interferometer

Getting mechanical and thermal stability in the Mach-Zehnder interferometer turned out to be rather difficult to achieve, even with mechanically stable mirror holders. In particulary, the temperature had a much larger effect than first anticipated, so the whole interferometer setup had to be temperature stabilized using a water heated breadboard with thermally isolating feet and encapsulated in blackout material. Furthermore, the complete system had to be left alone for a couple of hours to reach an equilibrium temperature.

Naturally, the instabilities were greatest when the interference of the two parts was most pronounced, which was the case when the HWP's at Alice and Bob were set at 22.5° (as was explained in the last chapter). Figure 5.12 shows the variation in the number of registrations in each detector as a function of time, when everything is suppose to be fixed and stable. We can see that over time the roles of A+ and B- have switched with A- and B+. Thus, there appears to be a drift or an ever so slight change in the path lengths of the Mach-Zehnder interferometer. This change was highly dependent on changes in the temperature, but as we can see from Figure 5.12 even with temperature stabilization the effect is present.

One may ask why the stability of the interferometer should be of any importance, but this question cannot really be answered until we have looked at the measurements in the next chapter. So we will have to come back to this question in chapter 6.

Another issue which presented itself during the initial testing was the fact that the stepper motor controlling the retroreflector, for some reason moved ever so slightly during the startup of a measurement series. This was probably due to some communication between the program and the stepper motor, since the position of the motor was registered as a parameter when the program was starting to run. In any case, this meant that the stepper motor had to be disconnected from the computer during the measurement. But this also put a restriction on the Mach-Zehnder interferometer, because the exact position had to be maintained and could not be adjusted between different measurement series without having to restart the program. This, in addition to a non-stationary overlap position, made adjustments and setups a non-trivial, and above all time consuming, task.

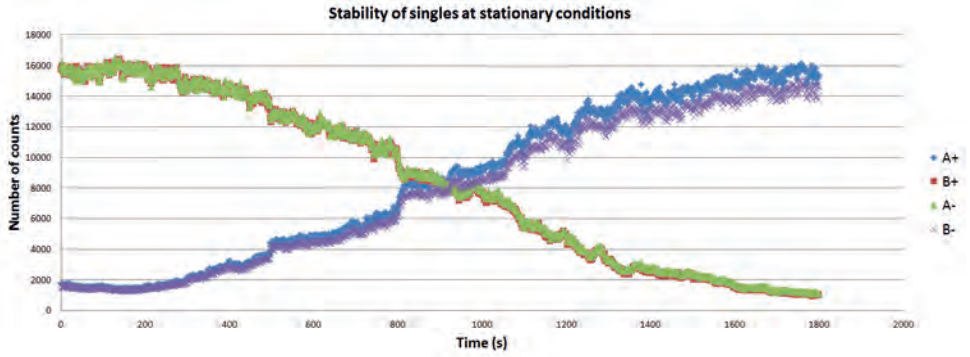

Figure 5.12: The variation in the number of registered singles as a function of time when Alice's and Bob's HWPs are set at 22.5°. The deviation from a constant value is assumed to be due to temperature changes.

5.4 Summary

In this chapter we have investigated several different characteristics concerning both the components in the setup and the pulses. In the introduction we talked about how real physical changes in a setup can result in real changes in the measurements, and if it was possible to relate these to the changes in the nature of the light being measured (such as going from a product state to an entangled state by adding the compensating crystal, for example). Under these premisses it is crucial to look at all aspects of the physical effects that the different components in the setup may have on the light we wish to analyse.

If interference effects are important, then chirp in the pulses will be too, since this can affect the light's ability to interfere. Likewise, the pulse duration will dictate how we can/should set up movement of the piezoelectric mirror, and the spectral distribution (or at least the central wavelength) should comply with the SPDC case, if we want to emulate that as close as possible.

The stability of the setup will of course affect our ability to precisely control for example the phase relation, which in the pulsed case can be identified with the important characteristic of time relations in the SPDC case.

5.5 Dependence chart

Setting up the experiment and all the optical components was one thing, making them work together as intended and doing so over time, something entirely different. Or as was quoted in the very beginning of this work

"In theory, theory and practice are the same. In practice, they are not."

One challenge that was particularly time consuming was a slow drift of the oscillator out of alignment. Possibly, this could be a result of the slight mechanical vibrations coming from the chiller as the water was pumped around the system, or perhaps uneven thermal expansion and contraction in the optical components. In any case, it often happened that the oscillator came out of alignment after a few days of running, resulting in low amplitudes of the pulses, instabilities in the pulse train or even complete loss of the mode lock. This meant that a time consuming realignment of the complete optical system, including optimization of the detectors, had to be conducted quite frequently.

During the setup and alignment process it was observed that all kinds of dependencies among the different components existed, which naturally affected the performance, and some of these were correlated as well. The chart in Figure 5.13 shows some of the interconnected dependencies and how the were affecting the outcomes. The chart is not meant as a complete description, but was developed as a result of challenges that appeared during the buildup process and summarizes some of the difficulties connected to the measurement process.

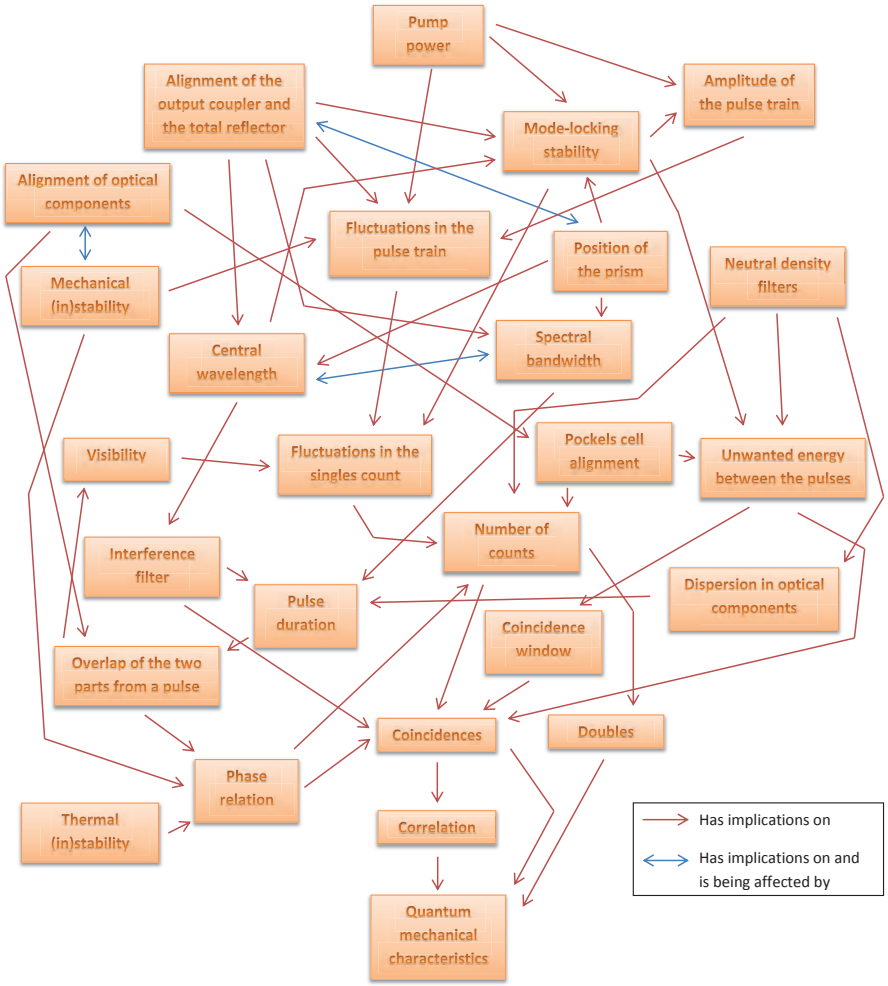

Figure 5.13: This box-pointer chart shows some of the characteristics of the source, their interconnected dependencies and how they are affecting the measurement outcomes.

References

[1] *Mode-Locked Femtosecond Titanium:Sapphire Laser Model TiF-50F*, Rev 143, Avesta (2013)

[2] R. Loudon, *The Quantum Theory of Light*, 3rd edition, Oxford science publications, 2010, p. 118

[3] Zafer A. Yasa and Nabil M. Amer, *Opt. Comm.* **36**, 406 (1981)

[4] *Thorlabs Spectrometer CCS Series Operation Manual*, Thorlabs (2013)

[5] Email correspondence with Mark Percevault, GM & Optical Engineer at FastPulse Technology, April 22, 2014

[6] http://refractiveindex.info/?shelf=main&book=RbTiOPO4&page=Carvajal-%CE%B3 (01.06.2015)

Part IV

Measurements, results and conclusions

Chapter 6

Measurements and results

6.1 Terminology

Every measurement sequence (which for example may be the rotation of a HWP from 0° to 90°) is named "*a scan*". These scans can be "*fixed*", meaning that only one HWP (either Alice's or Bob's) is rotating during the scan. The HWP that is not rotating (i.e. the one that's fixed) can be set in any angle, but two settings are of particular importance: 0° and 22.5°, because these allows us to measure a maximum violation of Bell's inequality. We call these the "*zero basis*" and the "*diagonal basis*", respectively, so that when, for example, Alice's HWP is set at 22.5° while Bob's HWP is rotating, we say that we do "a fixed scan with Alice in the diagonal basis". When both HWP's are rotating simultaneously with the same speed and in the same direction, we call the scan a "*twin scan*".

Five different measurement scans were done with our setup:

- A fixed scan with Alice in the zero basis (Alice's HWP set at 0 while Bob's HWP is rotating)
- A fixed scan with Bob in the zero basis (Bob's HWP set at 0 while Alice's HWP is rotating)
- A fixed scan with Alice in the diagonal basis (Alice's HWP set at 22.5° ($\pi/8$) and Bob's HWP rotating)
- A fixed scan with Bob in the diagonal basis (Bob's HWP set at 22.5° ($\pi/8$) and Alice's HWP rotating)
- A twin scan (both Alice's and Bob's HWP rotating simultaneously at the same speed)

And in each of these cases we measured:

- the number of clicks per second at each detector (which we name "*singles*")
- the number of simultaneous (i.e. within the coincidence window) clicks at the two detectors at Alice or the two detectors at Bob ("*doubles*")

- the number of simultaneous clicks at one detector at Alice and one detector at Bob ("*coincidences*")
- the *correlation* (as specified in equation (2.53))

From these measurements, Bell's inequality, in terms of the CHSH inequality, could be tested as well.

When presenting the measurements we often use a short hand notation and write $(++)$, $(+-)$, $(-+)$ and $(--)$ for the coincidences. The plus and minus signs represents the detector in the transmitted and reflected arms, respectively, of the PBS at Alice or Bob (see Figure 4.1). The labeling is such that we always state the location of Alice's detector first, so that $(+-)$ means the coincidence between a detection in Alice's detector in the transmitted arm of the PBS (A^+) and a detection in Bob's detector in the reflected arm (B^-).

6.2 Spontaneous parametric down-conversion

6.2.1 Theoretical predictions with and without the compensating crystal

The theoretically derivation for predicting measurement results was rather superficially described in section 2.5 using the standard theory. In this derivation the entanglement was introduced after the NPBS. From the argumentation about the distinction of the photons due to their arrival times, it is clear that the entanglement process must be highly dependent on the effects of the compensating crystal (CC), since without the CC in place no entanglement can be seen. Based on the stepwise calculation we made in section 2.5 it may suggest that the entangled state is generated before the NPBS.[1] Thus, let's therefore take another look at the calculations, but this time assume that the photons become entangled after the CC.[2]

As before, we start with the creation of the photon pair from the vacuum state in the ppKTP crystal.

$$|\Psi\rangle_0 = a_H^\dagger a_V^\dagger |0\rangle \otimes |0\rangle = |HV\rangle \tag{6.1}$$

After the ppKTP crystal the photons are in a state where we can distinguish them by measuring their arrival times. The effect of the CC is to remove this possibility, so we get

$$|\Psi\rangle_{\text{CC}} = \frac{1}{\sqrt{2}}(|HV\rangle + |VH\rangle) \tag{6.2}$$

This state is now entangled in polarization. As the photons pass through the NPBS, the state will be affected in accordance with equation (2.57). This gives us

$$\begin{aligned} |HV\rangle \xrightarrow{\text{NPBS}} &(|H\rangle_a + i|H\rangle_b)\,(|V\rangle_a - i|V\rangle_b) \\ =&|H\rangle_a|V\rangle_a - i|H\rangle_a|V\rangle_b + i|H\rangle_b|V\rangle_a + |H\rangle_b|V\rangle_b \end{aligned} \tag{6.3}$$

[1] Provided we have a narrow interference filter.

[2] Although we may arrive at the some of same results in the end using the theory from section 2.5, it does include steps and assumptions which sometimes seem unnecessarily limiting. With the following calculation, some of these steps can be avoided.

$$\begin{aligned}|VH\rangle \xrightarrow{\text{NPBS}} &(|V\rangle_a - i|V\rangle_b)\,(|H\rangle_a + i|H\rangle_b) \\ =&|V\rangle_a|H\rangle_a + i|V\rangle_a|H\rangle_b - i|V\rangle_b|H\rangle_a + |V\rangle_b|H\rangle_b\end{aligned} \tag{6.4}$$

where a and b indicates which arm (Alice or Bob) the specified photon belongs to.

Using these relations on our entangled state after the CC, we get the following state after the NPBS (disregarding the normalization constant)

$$\begin{aligned}|\Psi\rangle_{\text{NPBS}} =&|H\rangle_a|V\rangle_a - i|H\rangle_a|V\rangle_b + i|H\rangle_b|V\rangle_a + |H\rangle_b|V\rangle_b \\ &+ |V\rangle_a|H\rangle_a + i|V\rangle_a|H\rangle_b - i|V\rangle_b|H\rangle_a + |V\rangle_b|H\rangle_b\end{aligned} \tag{6.5}$$

After passing through the NPBS, the photons will go through the HWP's in Alice's and Bob's arm set at angles α and β in real space with respect to the horizontal plane. In general, a HWP set at an angle θ in real space will have the following effect on the states $|H\rangle$ and $|V\rangle$

$$|H\rangle \xrightarrow{\text{HWP at } \theta} \cos 2\theta|H\rangle + \sin 2\theta|V\rangle \tag{6.6}$$

$$|V\rangle \xrightarrow{\text{HWP at } \theta} -\sin 2\theta|H\rangle + \cos 2\theta|V\rangle \tag{6.7}$$

Using these expressions we arrive at the following state after the HWPs

$$\begin{aligned}|\Psi\rangle_{\text{HWP}} =&(\cos 2\alpha|H\rangle_a + \sin 2\alpha|V\rangle_a)(-\sin 2\alpha|H\rangle_a + \cos 2\alpha|V\rangle_a) \\ &- i(\cos 2\alpha|H\rangle_a + \sin 2\alpha|V\rangle_a)(-\sin 2\beta|H\rangle_b + \cos 2\beta|V\rangle_b) \\ &+ i(\cos 2\beta|H\rangle_b + \sin 2\beta|V\rangle_b)(-\sin 2\alpha|H\rangle_a + \cos 2\alpha|V\rangle_a) \\ &+ (\cos 2\beta|H\rangle_b + \sin 2\beta|V\rangle_b)(-\sin 2\beta|H\rangle_b + \cos 2\beta|V\rangle_b) \\ &+ (-\sin 2\alpha|H\rangle_a + \cos 2\alpha|V\rangle_a)(\cos 2\alpha|H\rangle_a + \sin 2\alpha|V\rangle_a) \\ &+ i(-\sin 2\alpha|H\rangle_a + \cos 2\alpha|V\rangle_a)(\cos 2\beta|H\rangle_b + \sin 2\beta|V\rangle_b) \\ &- i(-\sin 2\beta|H\rangle_b + \cos 2\beta|V\rangle_b)(\cos 2\alpha|H\rangle_a + \sin 2\alpha|V\rangle_a) \\ &+ (-\sin 2\beta|H\rangle_b + \cos 2\beta|V\rangle_b)(\cos 2\beta|H\rangle_b + \sin 2\beta|V\rangle_b)\end{aligned} \tag{6.8}$$

This expression can be simplified by using a few trigonometric identities and assume that the ordering of the states in Hilbert space has no importance, so that $|H\rangle_b|V\rangle_a = |V\rangle_a|H\rangle_b$. This gives us

$$\begin{aligned}|\Psi\rangle_{\text{HWP}} =&\sin 4\alpha\,(|V\rangle_a|V\rangle_a - |H\rangle_a|H\rangle_a) \\ &+ \sin 4\beta\,(|V\rangle_b|V\rangle_b - |H\rangle_b|H\rangle_b) \\ &+ 2\cos 4\alpha|H\rangle_a|V\rangle_a + 2\cos 4\beta|H\rangle_b|V\rangle_b \\ &- 2i\sin(2\alpha - 2\beta)\,(|H\rangle_a|H\rangle_b + |V\rangle_a|V\rangle_b) \\ &- 2i\cos(2\alpha - 2\beta)\,(|H\rangle_a|V\rangle_b - |V\rangle_a|H\rangle_b)\end{aligned} \tag{6.9}$$

We can now use this result to calculate the probabilities for any kind of combination at the detectors. For example, the probability for measuring doubles ($|H\rangle_a|V\rangle_a$) at Alice becomes proportional to

$$P_{\text{QM}}(\text{Doubles at Alice}) \propto \cos^2 4\alpha \tag{6.10}$$

If we plot this function (properly scaled) together with the measured doubles at Alice, as is done in Figure 6.1, we can see that there is a good agreement between measurement and theory.

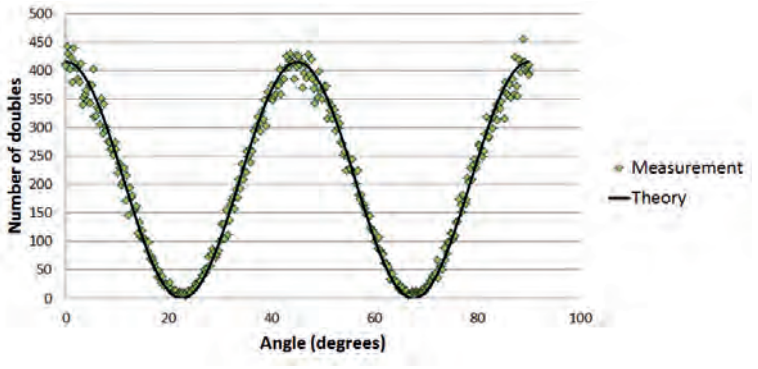

Figure 6.1: The measured and theoretical values of the number of doubles at Alice as a function of angle of Alice's HWP, with the compensating crystal in place.

Another example is the behaviour of the coincidences, say between the transmitted channel at Alice $(+)$ and the reflected channel at Bob $(-)$. Here we have to look for combinations of the form $|H\rangle_a|V\rangle_b$ in equation (6.9). We find that

$$P_{\text{QM}}(+-) \propto \cos^2(2\alpha - 2\beta) \tag{6.11}$$

Plotting this when $\alpha = \pi/8$ together with the measured coincidences displays again a good agreement, as shown in Figure 6.2.

We may also calculate, for example, the coincidences between the transmitted channels both at Alice and Bob $(++)$ in a fixed scan with Bob in the diagonal basis. In this case we only look at states with the combination $|H\rangle_a|H\rangle_b$, which gives us

$$P_{\text{QM}}(++) \propto \sin^2(2\alpha - 2\beta) \tag{6.12}$$

Setting $\beta = \pi/8$, scaling and plotting this together with the measured values gives again a good agreement, as can be seen in Figure 6.3.

From these few examples it would appear that the theoretical expression in equation (6.9) gives the correct behaviour and can be used to calculate the probability for any kind of relation between the detector counts (doubles, coincidences and correlations).[3]

Let us specifically look at the correlation. It is given by equation (2.68). We've just calculated the coincidences between the transmitted channel at Alice and the reflected channel at Bob $(+-)$ and the coincidences between the transmitted channels both at Alice and Bob $(++)$, so we need only to calculate the coincidences between the reflected channels both at Alice and Bob $(--)$ and between the reflected channel at Alice and the transmitted channel at Bob $(-+)$. They simply become

$$P_{\text{QM}}(-+) \propto \cos^2(2\alpha - 2\beta) \tag{6.13}$$

[3]This is in contrast to the standard calculation, where the expression for the doubles usually isn't calculated.

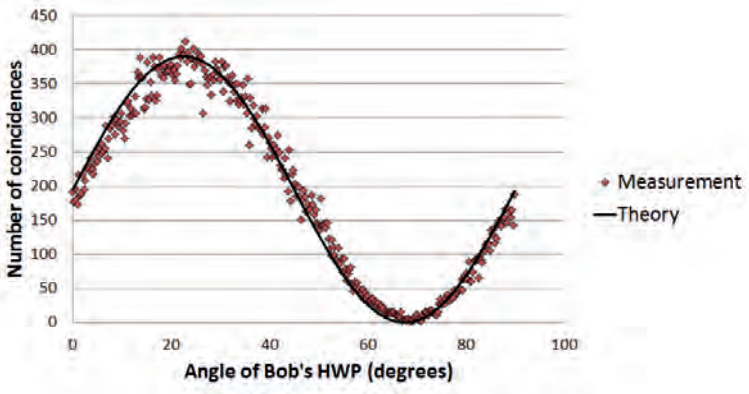

Figure 6.2: The measured and theoretical values of the number of coincidences $(+-)$ in a fixed scan where Alice is in the diagonal basis, with the compensating crystal in place.

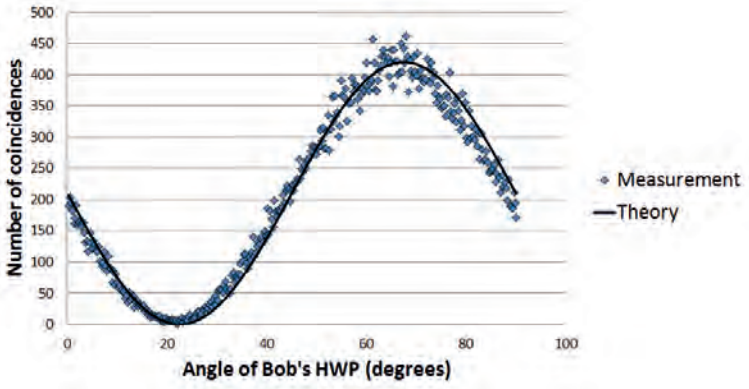

Figure 6.3: The measured and theoretical values of the number of coincidences $(++)$ in a fixed scan where Bob is in the diagonal basis, with the compensating crystal in place.

$$P_{\text{QM}}(--) \propto \sin^2(2\alpha - 2\beta) \tag{6.14}$$

Using equation (2.42) we arrive at

$$E = P_{++} + P_{--} - P_{+-} - P_{-+} \propto -\cos 4(\alpha - \beta) \tag{6.15}$$

If we look at a twin scan, where $\alpha = \beta = \theta$, we see that the cosine argument in the expression for the correlation will become zero, so we simply get

$$E = -1 \tag{6.16}$$

Thus, we see that the correlation in a twin scan (Alice's and Bob's HWP rotating simultaneously) is equal to -1 for all angles in the quantum mechanical case.

Calculation without the compensating crystal

If we assume that the CC is responsible for the entanglement, then without the CC, we are dealing with product states. Thus, our state before the NPBS becomes

$$|\Psi\rangle_0 = |H\rangle|V\rangle \tag{6.17}$$

The NPBS has the same effect on the states as before (equation (2.57)), and gives us

$$\begin{aligned} |\Psi\rangle_{\text{NPBS}} &= (|H\rangle_a + i|H\rangle_b)(|V\rangle_a - i|V\rangle_b) \\ &= |H\rangle_a|V\rangle_a - i|H\rangle_a|V\rangle_b + i|H\rangle_b|V\rangle_a + |H\rangle_b|V\rangle_b \end{aligned} \tag{6.18}$$

The effect of the HWPs is given by equation (6.6), and from this we get

$$\begin{aligned} |\Psi\rangle_{\text{HWP}} = &\cos 2\alpha \sin 2\alpha \, (|V\rangle_a|V\rangle_a - |H\rangle_a|H\rangle_a) \\ &+ \cos 2\beta \sin 2\beta \, (|V\rangle_b|V\rangle_b - |H\rangle_b|H\rangle_b) \\ &+ \cos^2 2\alpha |H\rangle_a|V\rangle_a - \sin^2 2\alpha |V\rangle_a|H\rangle_a \\ &+ \cos^2 2\beta |H\rangle_b|V\rangle_b - \sin^2 2\beta |V\rangle_b|H\rangle_b \\ &- i \left[\cos 2\alpha \sin 2\beta |H\rangle_a|H\rangle_b + \cos 2\alpha \cos 2\beta |H\rangle_a|V\rangle_b \right. \\ &- \sin 2\alpha \sin 2\beta |V\rangle_a|H\rangle_b + \sin 2\alpha \cos 2\alpha |V\rangle_a|V\rangle_b \\ &+ \cos 2\beta \sin 2\alpha |H\rangle_b|H\rangle_a - \cos 2\beta \cos 2\alpha |H\rangle_b|V\rangle_a \\ &\left. + \sin 2\beta \sin 2\alpha |V\rangle_b|H\rangle_a - \sin 2\beta \cos 2\beta |V\rangle_b|V\rangle_a \right] \end{aligned} \tag{6.19}$$

One should note that here, we have not used the fact that the ordering in a Hilbert space has no special meaning. This is because we no longer have a situation where we cannot tell the difference between the photons. Thus, the photons are separate (not to be considered as one bi-photon entity), which becomes an important factor when calculating the probabilities. For example, we can look at the doubles at Alice during a twin scan. In this case we consider only the states with combinations of $|H\rangle_a|V\rangle_a$ and $|V\rangle_a|H\rangle_a$. This gives us

$$P_{\text{non-entangled}}(\text{Doubles at Alice}) \propto |\cos^2 2\alpha|^2 + |-\sin^2 2\alpha|^2 = \cos^4 2\alpha + \sin^4 2\alpha \tag{6.20}$$

Had we assumed that $|H\rangle_a|V\rangle_a = |V\rangle_a|H\rangle_a$ then the probability would have become

$$P_{\text{non-entangled}}(\text{Doubles at Alice}) \propto \cos^2 4\alpha \tag{6.21}$$

If we now plot these two cases together with the measured values, we see that the first case gives good agreement while the second does not, as can be seen in figure 6.4.

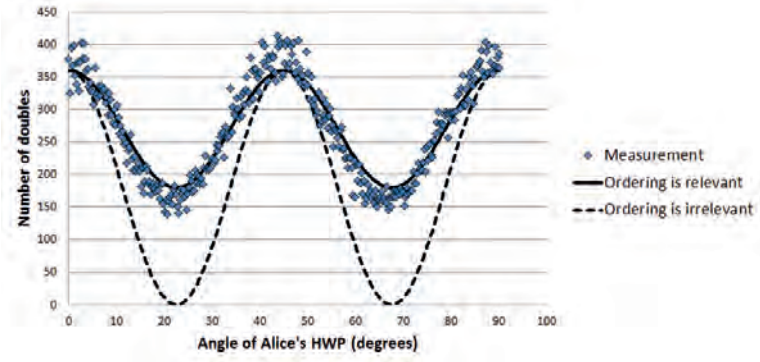

Figure 6.4: The measured and theoretical values of the number of doubles at Alice as a function of angle of Alice's HWP in the case of no compensating crystal. The theoretical plots include both the case when we assume that ordering is relevant ($|H\rangle_a|V\rangle_a \neq |V\rangle_a|H\rangle_a$) and ordering is irrelevant ($|H\rangle_a|V\rangle_a = |V\rangle_a|H\rangle_a$).

Let's pause here for a moment and remember what we said in the beginning about similarity of the mathematics in different theories leading to different physical interpretations. From a quantum point of view we say that no photon is being split at the beam splitter, while any light entering the beam splitter in the classical case will be split, no matter the intensity. However, if we look at the mathematics used, we see from equation (2.57) that this is actually similar to how we would write an expression for the light being split at the beam splitter. Now, of course, we do not claim that the single photon is being split here, but in a purely mathematical form there is a strong similarity between these two cases. The difference between the entangled case and the non-entangled case (which here is a product state and in many ways similar to a classical calculation with pulses) shows when calculating the probabilities. In the entangled case we get cross terms which we don't have in the non-entangled case. This is due to the fact that we cannot assume that $|H\rangle_a|V\rangle_a = |V\rangle_a|H\rangle_a$ for the product state. This means that we square the sum of probability amplitudes in the entangled case, while we sum the squares in the non-entangled case. So if we just look at the mathematics in these calculations, we could have ignored the assumption of no difference between $|H\rangle_a|V\rangle_a$ and $|V\rangle_a|H\rangle_a$. This would then have given us two expressions for the probabilities, which we would have solved in the entangled case by squaring over the sum of probability amplitudes, and in the product state case summed the squares, a procedure which would have seemed more natural.

Similar to the procedure above, we can use equation (6.19) to calculate probabilities for other relations, such as the coincidences between the transmitted channel at Alice (+) and the reflected channel at Bob (−). Again, what we need to look for in this case, are combinations of the form $|H\rangle_a|V\rangle_b$ and $|V\rangle_b|H\rangle_a$. This gives us

$$\begin{aligned} P_{\text{non-entangled}}(+-) &\propto |-i\cos 2\alpha \cos 2\beta|^2 + |-i\sin 2\alpha \sin 2\beta|^2 \\ &= (\cos 2\alpha \cos 2\beta)^2 + (\sin 2\alpha \sin 2\beta)^2 \end{aligned} \tag{6.22}$$

Or we can look at the coincidences between the transmitted channel at Alice (+) and the transmitted channel at Bob (+), which gives us

$$\begin{aligned} P_{\text{non-entangled}}(++) &\propto |i\cos 2\alpha \sin 2\beta|^2 + |-i\sin 2\alpha \cos 2\beta|^2 \\ &= (\cos 2\alpha \sin 2\beta)^2 + (\sin 2\alpha \cos 2\beta)^2 \end{aligned} \tag{6.23}$$

Plotting both of these calculations together with the measured values in a fixed scan with Alice in the diagonal basis ($\alpha = \pi/8$) gives the result as shown in Figure 6.5, which agrees reasonably well with the measurements.

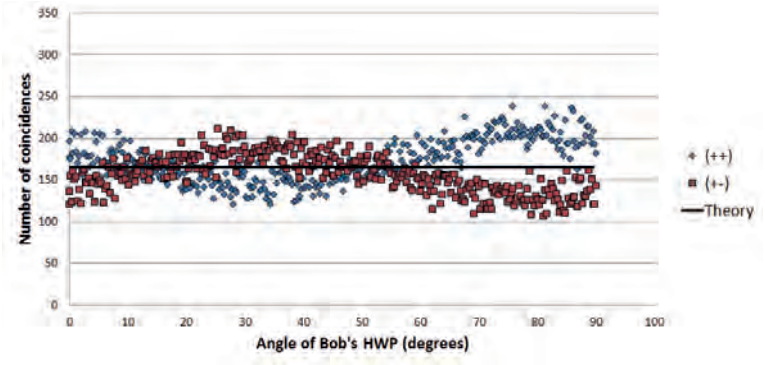

Figure 6.5: The measured and theoretical coincidences when Alice is in the diagonal basis, as a function of angle of Bob's HWP when no compensating crystal is present.

Measuring Bell's inequality

In section 2.4 we arrived at the following expression for the correlation coefficient (equation (2.43)) where θ was the angle between Alice's and Bob's HWPs

$$E_{QM}(a, b) = \cos 2\theta \tag{6.24}$$

The value for S could then be expressed as

$$S = E(a, b) - E(a, b') + E(a', b) + E(a', b') \tag{6.25}$$

where the different a's and b's are different settings of Alice's and Bob's HWPs. In general, a, a', b, b' can be chosen to have any value, but let's assume for simplicity that the relative angle between the settings of the HWPs is such that

$$(a, b) = (a', b) = (a', b') = \theta \tag{6.26}$$

then from a purely geometrical point of view we must have

$$(a, b') = 3\theta \tag{6.27}$$

This then gives following expression for the CHSH inequality

$$S(\theta) = 3\cos(2\theta) - \cos(6\theta) \tag{6.28}$$

To find the extreme values for S we need to take the partial derivatives of the expression with respect to θ. This gives

$$\theta = \frac{\pi}{8} \text{ and } \theta = \frac{3\pi}{8} \tag{6.29}$$

Thus, maximum violation of Bell's inequality will occur for these angular settings. Figure 6.6 shows the relations between the directions of the polarizers.

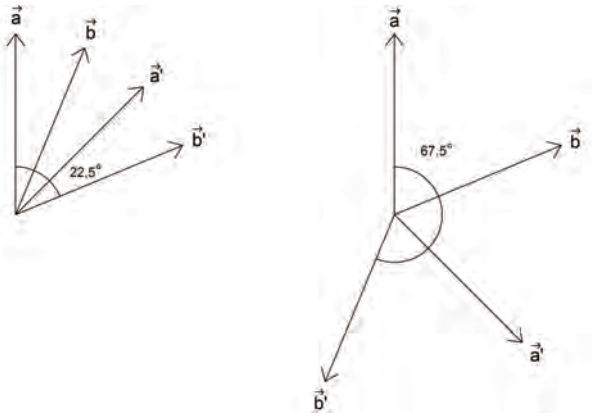

Figure 6.6: The orientations of the polarizers leading to the maximum values for the CHSH inequality.

Based on this result, two fixed scans with the SPDC source with the CC were performed: one scan in the zero basis ($\theta_{Bob} = 0$ and Alice rotating from 0 to $90°$) and one scan in the diagonal basis ($\theta_{Bob} = 22.5°$). Figure 6.7 shows the correlation in both the zero and diagonal bases. The visibility in these two scans is as high as 99.6 % in the zero basis and 98.5 % in the diagonal basis. One should note that we obtain these results without having to subtract so called accidental counts.

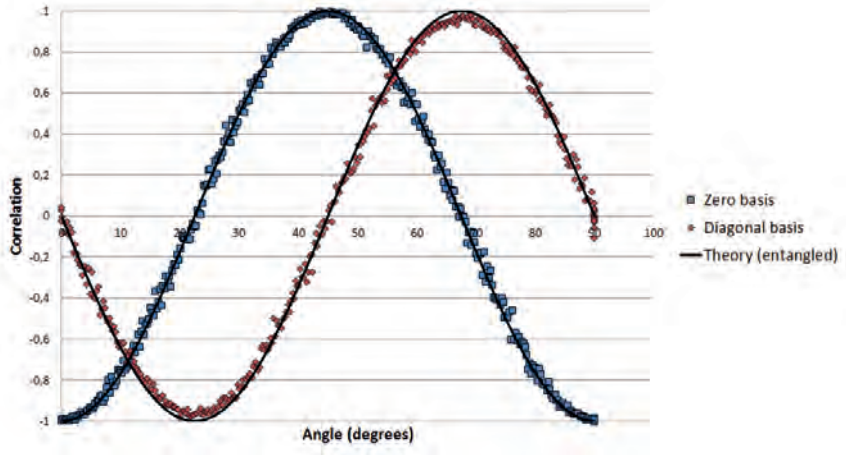

Figure 6.7: The correlation in a scan in the zero basis and in the diagonal basis, as Alice HWP is varied from 0 to $90°$.

From these graphs, the values for the correlation that we need in order to calculate S becomes

$$E(a_i, b_j) = E(0, \pi/16) = -0,70 \tag{6.30}$$
$$E(a_i, b_{j'}) = E(0, 3\pi/16) = 0,68 \tag{6.31}$$
$$E(a_{i'}, b_j) = E(\pi/8, \pi/16) = -0,65 \tag{6.32}$$
$$E(a_{i'}, b_{j'}) = E(\pi/8, 3\pi/16) = -0,75 \tag{6.33}$$

where we have used that a and b are the orientations of the polarizers, i.e. twice the angle of the HWP. Using these values we get the following value for S

$$S = -0,70 - 0,68 - 0,65 - 0,75 = -2,78 \tag{6.34}$$

This is fairly close to the ideal value of $-2\sqrt{2} \approx -2,84$ and is certainly different from -2. Thus the CHSH inequality is not satisfied, as expected.

A more accurate measurement done with the HWP set to the appropriate angles and measured for a duration of 10 seconds, which gave 10 000 measurement points (compared with the 2000 that Aspect and his colleges had), gave the following value for S:

$$S = -0,69 - 0,71 - 0,72 - 0,66 = -2,78 \tag{6.35}$$

which is the same value as above. This seems to indicate that the number of registrations we have in our plots is enough to obtain reliable statistics (that is, we do not gain anything more by using more counts per second).

6.2.2 Measurements without the compensating crystal

For the theoretical calculation when the compensating crystal was removed from the setup, we assumed a product state of the two photons. This led to the expression given by equation (6.19). Figure 6.8 shows the measured and theoretically calculated plots (using equation (6.19)) for (from top to bottom) singles, doubles, coincidences and the correlation in (from left to right) a fixed scan with Bob in the zero basis, a fixed scan with Alice in the diagonal basis and a twin scan. An interference filter with a spectral width of 1 nm and a coincidence window of 8 ns was used in all of these measurements.

6.2.3 Measurements with the compensating crystal

We have already seen some of the measurement plots from scans made with the CC in place in the preceding sections. Here we have collected the plots of the singles, doubles, coincidences and the correlation from all the different scans mentioned in the introductory part of this chapter, together with the theoretical calculated plot using equation (6.9). These are plotted in Figure 6.9. One should remember that in arriving at this equation we required the state of the photon-pair to be an entangled state, which explains the difference between these plots and the ones shown in Figure 6.8.

6.2.4 Singles

If we look at the plots in Figure 6.8 and 6.9, we see that all scans, both with and without the compensating crystal, have a constant rotational invariant number of singles. This was therefore the first task to achieve in our attempt to emulate the SPDC results with the pulsed source. As been discussed in section 4.2.5, a rotational invariance of the singles could be achieved in the pulsed case by introducing different variations in the piezoelectric mirror.

But let's stay with the results obtained with the crystal source for a moment. In the theoretical calculations above we were primarily concerned with the behaviour of the doubles, coincidences and the correlation, and we did not consider the singles at all. Is there anything we can learn from the behaviour of the singles? Why are singles are constant in the first place?

The answer lies in the fact that we are dealing with different directions of the polarization of the incoming light. The measured number of singles does not depend on the coincidence window and therefore does not depend on the timing of the photons in a single pair. Thus, there is no correlation between registrations. Since it is completely random which photon (H or V) that goes into either arm we will register a completely random mixture of H and V, which sums to a constant level for all angles. That is why the singles are constant in all scans. The singles does not require that the photons arrive in pairs, however, only that the polarization is averaging out during the acquisition time. The pairwise nature becomes visible through the measured relations among the doubles and coincidences.

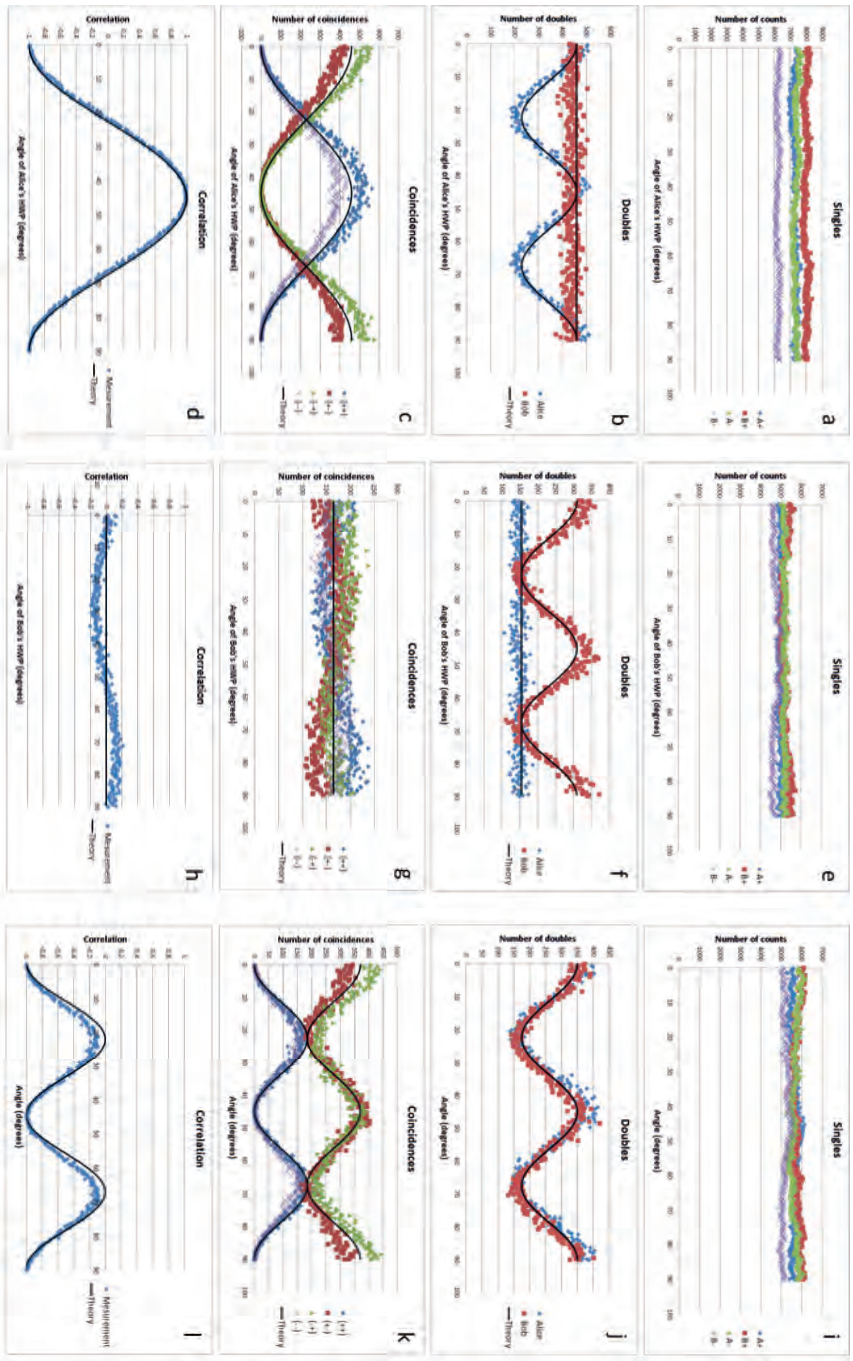

Figure 6.8: The measured and theoretically calculated singles, doubles, coincidences and the correlation in a fixed scan with Bob in the zero basis (left), a fixed scan with Alice in the diagonal basis (middle) and a twin scan (right) using a SPDC source ***without*** *compensating crystal.*

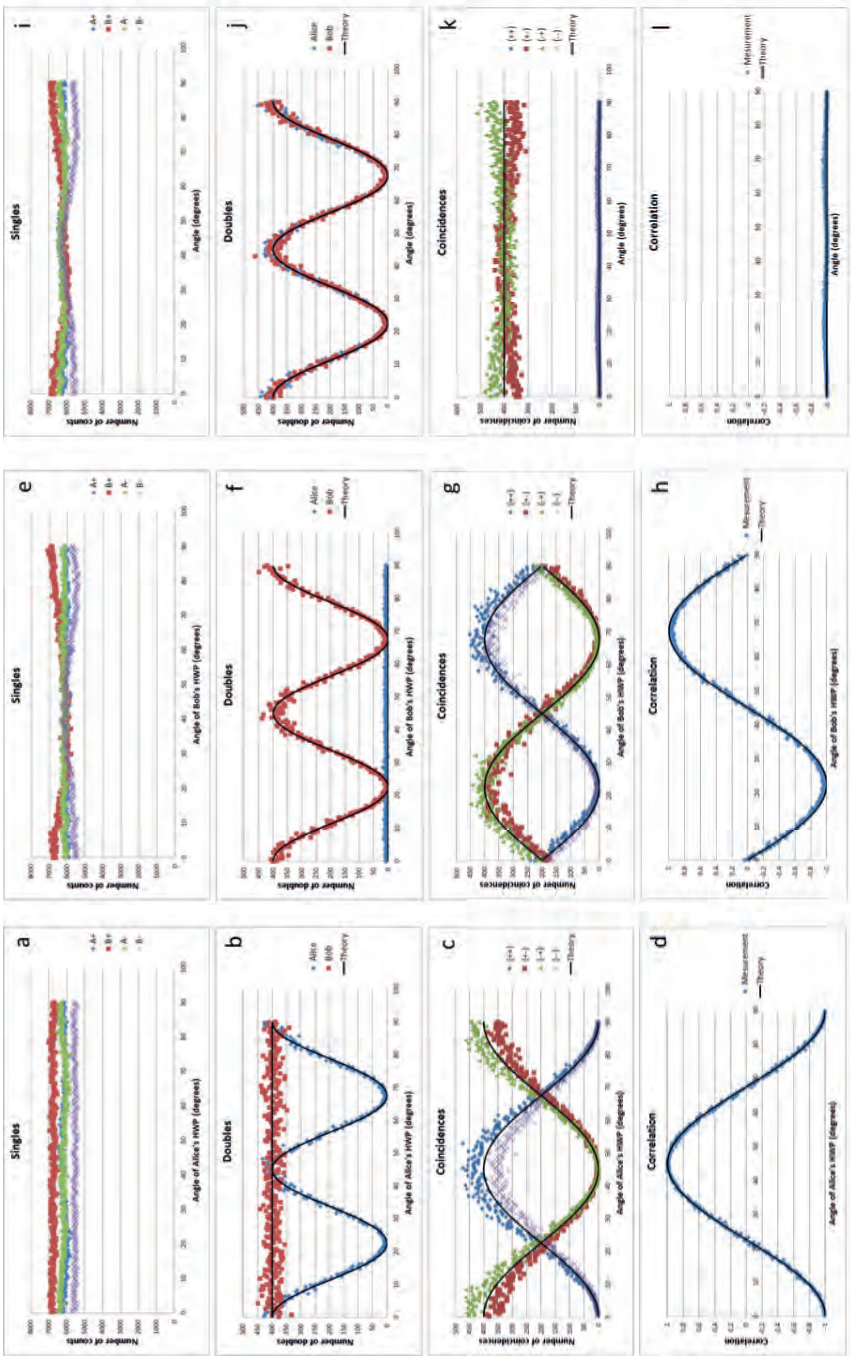

Figure 6.9: The measured and theoretically calculated singles, doubles, coincidences and the correlation in a fixed scan with Bob in the zero basis (left), a fixed scan with Alice in the diagonal basis (middle) and a twin scan (right) using a SPDC source ***with*** *compensating crystal.*

6.3 Pulsed source

As has been explained, with the pulsed source we wished to investigate whether it was possible to obtain similar results as we got with the SPDC source, by trying to emulate the SPDC process. For this, the photon pair became substituted with two highly attenuated parts of a pulse, generated by passing the pulse through a 50/50 beam splitter. To emulate the state of polarization for the photons, which are orthogonal to each other, the two linear polarized parts of the pulse were sent through half wave plates located in each arm; one set at 0° and the other at 45°. These two parts, with now orthogonal polarizations, were then combined into a pair.

Since the time between two pulses in the pulse train from the oscillator was around 12.5 ns, which translates into a distance of over 3 m travelled by the pulse before the next one arrived, and the pulses themselves had a spatial extension of only 300 μm, there was never any possibility for interaction or overlap between different pulses. It should therefore be clear that when we speak about interactions and overlaps we refer to interaction between the two parts coming from a single pulse being split in the Mach-Zehnder interferometer. Nevertheless, to highlight the difference we will use the word ”part” (as in ”part of a pulse”) when discussing the interaction, overlap and interference, and use the word ”pulse” when talking about a single pulse in the pulse train or the combined pulse leaving the Mach-Zehnder interferometer.

The pulsed source was set up with the following configuration: The external pump laser was set to 4 W output power, which was directed into the Ti:sapphire oscillator. The oscillator then generated a mode-locked pulse train containing 80 million, approximately 50 fs long, pulses per second. The number of pulses per second was reduced by a factor 10 by running the Pockels cell at 100 kHz and allow 80 pulses to pass per trigger pulse. This modified pulse train then passed through four absorbing NFD's, having a combined attenuation of the order of 10^7 (the pulse train was also attenuated before entering the Pockels cell, due to the dichroic mirror, by a factor of 10^2). Further attenuation was added from the 1 nm interference filter located before the Mach-Zehnder interferometer. The full attenuation could not be measured with the available equipment we had, but using the single photon counters we registered between 10 000 and 20 000 counts per second at this level, which was in line with the previous SPDC measurements and at the same time gave enough doubles and coincidences to display a behaviour which would give us reliable statistics.

The effect of the interference filter (and possibly other components in the analyzing setup) resulted in an increased pulse duration of 1 ps, as explained in the last chapter. The center wavelength, also due to the interference filter, was now 810 nm, just as in the case with our SPDC source.

The two combined parts were sent to the analyzing setup, which was equal to the setup used in the SPDC case, just with the interference filter moved outside. The coincidence window was set to 8 ns in these measurements, which was the same as in the SPDC case.

6.3.1 Non-overlapping pulses

When the CC is not in place in the SPDC setup, the quantum mechanical theory tells us that the timing of the photons is such that one always arrives before the other, although the time

difference may vary from pair to pair. How are we to emulate this situation with our pulsed source? Obviously, it means that one of the parts always have to be in front of the other. But what is not so obvious is how big this difference between the parts should be. In section 2.5.2 we calculated the maximum arrival time difference between the photons created in the ppKTP crystal, based on the assumption that they were created at a specific location inside the crystal and could be viewed as point particles, and found this time difference to be of the order of 1 ps. Based on this crude calculation we may use this value as a reference for the settings in the pulsed case.

However, there is also another factor that comes into play, and that is: how well does the length of the parts correspond with the ”length” of the photons in the SPDC case? Obviously, speaking about the spatial extension of a photon is not a trivial matter, but if we assume that we can imagine the photons as wave packets, we can use the fact that the time-bandwidth product dictates the minimum duration of a pulse based on its spectral bandwidth, thus giving us a minimum duration that this wave packet can have. Since a 1 nm filter was used in the SPDC measurements, and if we assume the photon to be something like a wave packet, this would translate into a minimum possible duration of around 1 ps (see table 3.1). This just happens to be the duration also of the parts in our pulsed setup.

Now, all of this argumentation is very simple and perhaps even naive, but let’s see where it brings us.

As a control, the retroreflector was set to a maximum distance of 4 mm (8 mm back and forth) leading to a time difference of around 17 ps between one part of the pulse and the next. Again, with the time between two pulses in the pulse train from the oscillator being 12.5 ns there where no possibility for interactions between individual pulses. This measurement was done both in terms of the argumentation about the length of the wave packets given above and the fact that a measurement of two non-overlapping separable parts with orthogonal polarizations would result in an invariance in the number of singles. Such an invariance was observed in all scans in the SPDC case.

Figure 6.10 shows the measured results from the same type of scans that were conducted with the SPDC source above, that is, a fixed scan with Bob in the zero basis, a fixed scan with Alice in the diagonal basis and a twin scan.

Although the results of these scans do not appear to be very interesting at first sight, one should notice that the doubles, coincidences and the correlation are completely independent of the angle of the HWPs. This is quite different from the SPDC cases, where we often have a clear dependence on the angle, as we have seen.

When we have two non-interacting parts with orthogonal, linear polarizations entering the analyzer setup, we will get completely opposite behaviour of the singles for these two cases. That is, if the angle dependence of A^+ and B^+ is that of sine squared for one of the parts, it will be that of cosine squared for the other. In Figure 6.11 we have measured the singles when first blocking the reflected arm in the Mach-Zehnder interferometer during a twin scan (top), and then doing the same scan again but this time with the transmitted arm blocked (middle). As can be seen, the number of registrations in the detectors are opposite of each other in the two cases. Since the acquisition is taken over 1 s and the parts arrive in non-overlapping pairs, on average the overall number of clicks in each detector will be near constant for the singles (bottom).

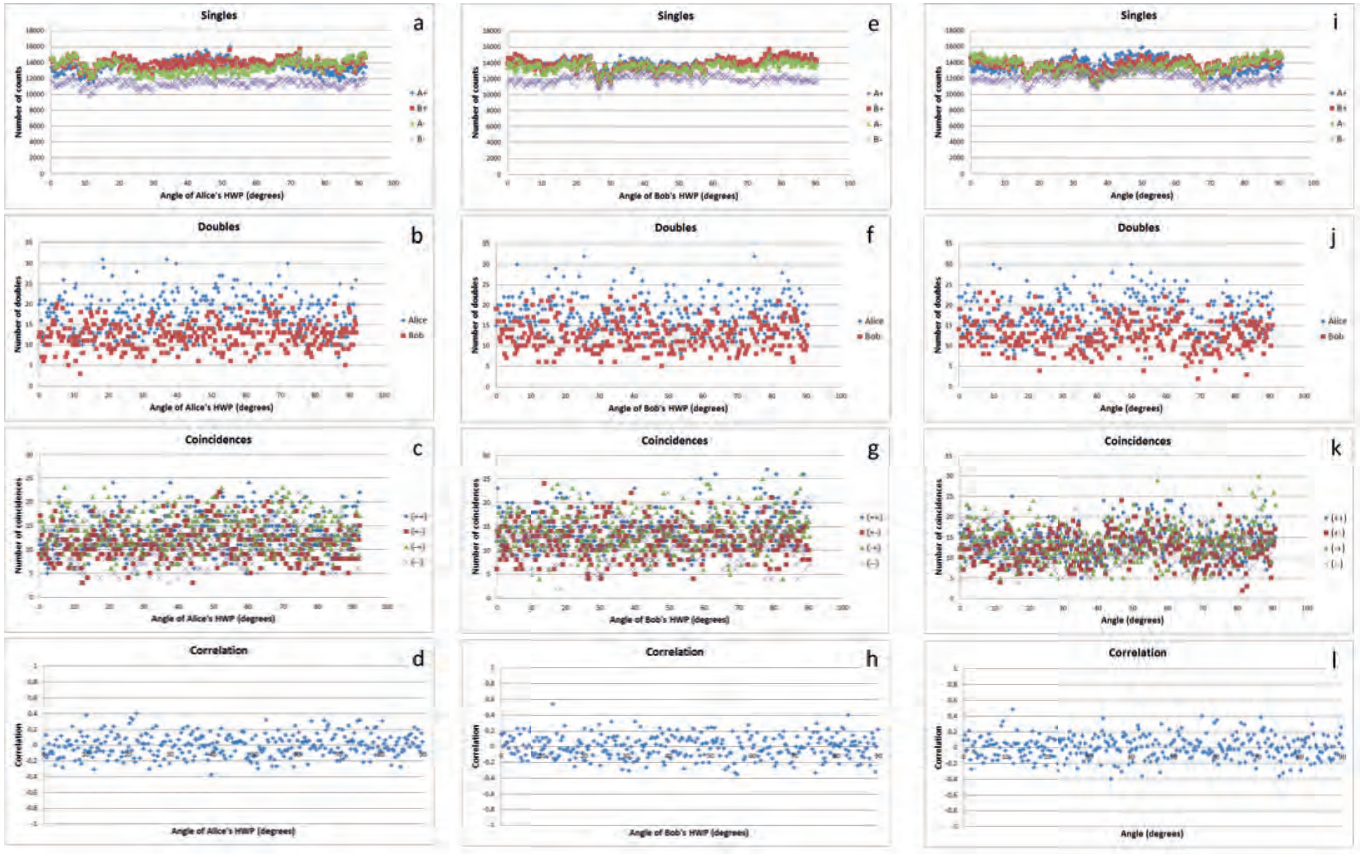

Figure 6.10: The measured and theoretically calculated singles, doubles, coincidences and the correlation in a fixed scan with Bob in the zero basis (left), a fixed scan with Alice in the diagonal basis (middle) and a twin scan (right) using a a pulsed source with orthogonally polarized, ***non-overlapping*** *parts of a pulse.*

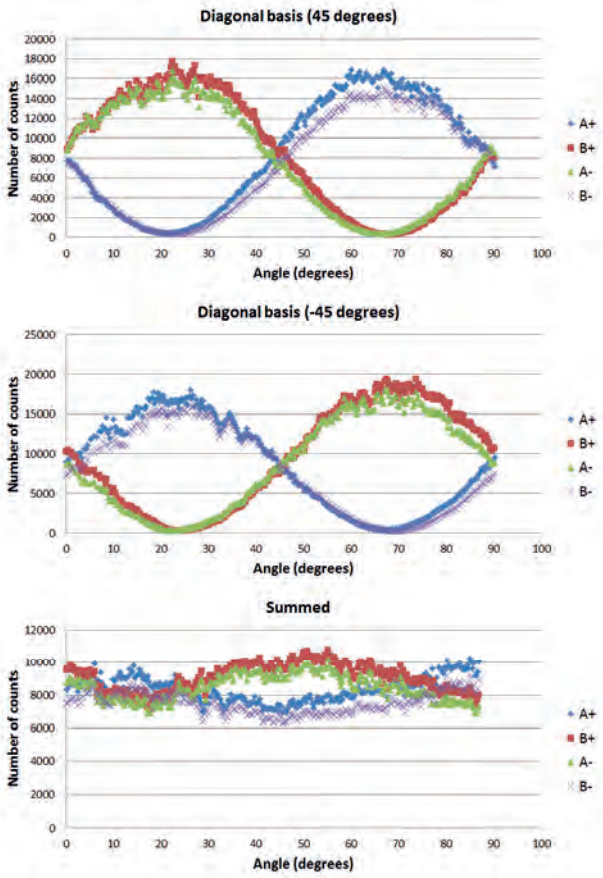

Figure 6.11: The measured number of singles when only the transmitted arm in the Mach-Zehnder is open (top) and when only the reflected arm is open (middle), as well as the averaged sum of the two (bottom). We see that the summation leads to a near rotational invariance in the number of singles.

But if we measure the doubles in scans made only with horizontal or vertical polarized pulses, we will find that the angle dependence is identical in these two cases (both going as cosine squared two times the angle), instead of being opposite of each other. This means that if we were to sum these two plots in order to get the average, as we did with the singles, we will not get a constant, rotational invariant behaviour for the doubles. We would get something which was angle dependent, in conflict with the results presented in Figure 6.10. So how can we arrive at the correct results? Obviously, there is an additional factor determining the doubles and coincidences, and that's the coincidence window. Whereas the singles are just measured

as the number of counts at each detector over one second, the doubles and coincidences are related to simultaneous detections within the coincidence window. The acquisition program works by comparing the registration times of two neighbouring detections and calculates the difference between these times. If the time difference is within the chosen coincidence window, it becomes registered as a double or a coincidence. Thus, the width of the coincidence window determines the number of doubles and coincidences that we get. What complicates matters is that the registered arrival times are not related to the real arrival events in a simple way, since, as has been explained, delays in the electronics and through the semiconductor in the detection process also delays the detection of the trigger event. These delays may vary from registration to registration.

A speculative description of the relations involved in the detection process, in order understand the effect of changing the size of the coincidence window, can be as follows: When the Pockels cell is open, the pulse train is allowed to pass through, in theory, unaffected in its linear polarization except for a rotation of 90°. When the Pockels cell is closed, the polarization of the light that still gets through becomes heavily distorted, due to the orthogonal polarizers which together with the Pockels cell make up the pulse picker.

What we are measuring in the double and coincidences counts are the simultaneous effects of registrations within the coincidence window, i.e. the correlated detections in two detectors. The patters that we see as a function of angle of the HWPs are a result of correlations in the polarization of the light we are measuring.

When the parts are overlapping, the superposed polarization will determine the correlations among the detections. That is, if the total polarization is linear and, say, horizontal and Alice HWP is at 0°, we should in theory register a detection in one of Alice's detectors but not the other. If we do not have this overlap or a total polarization which is randomized, the correlation between the detections will be less visible.

Now, the detectors are single photon detectors and as such any level of light may cause a triggering, even the light slipping through when the pulse picker is closed. Since the duration of the pulses is so short compared to the time between them, there is a non-negligible probability for registrations from contributions outside of the pulses. This would suggest that the measured doubles and coincidences loose their correlation when the distance between the pulses or the coincidence window is large. In simple terms: if there is a strict linear polarization for the light inside the pulse, but a random polarization for the light outside the pulse, then it matters "which light" triggers the single photon detectors. When the coincidence window is increased, the probability for a detector to click due to light outside the pulse increases as well.

As in the example with the horizontal, linear polarization above, we should only have a click in one detector if the polarization is kept strictly linear. If random polarized light also can contribute, we no longer obtain results corresponding to a strict polarization relationship, and thus the patters in our graphs disappear. Figure 6.12 is an figuratively attempt to illustrate the concept.

But why shouldn't the light between the pulses have a well defined polarization? From the interference process leading to mode-locking it would seem natural to think that the phase of the entire pulse train is well defined. However, we've seen that there are fluctuations in the amplitudes of the pulse train. We also know that the KLM process is optimized for the high

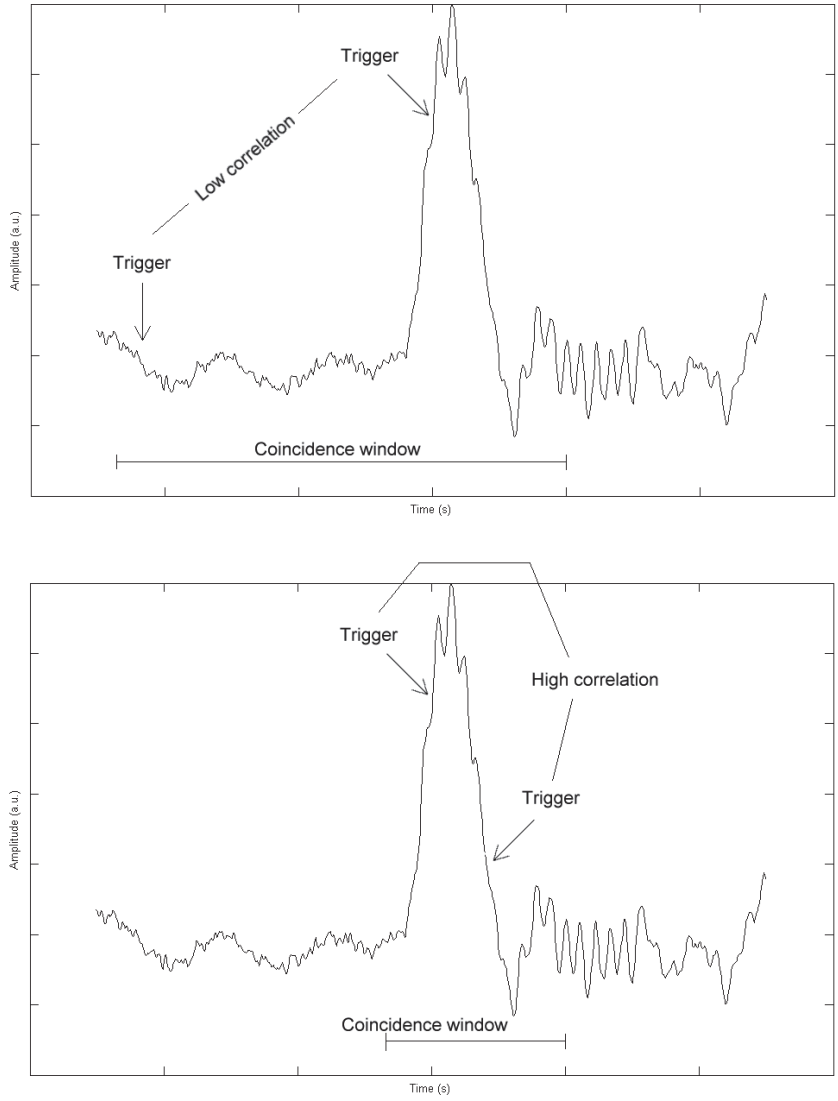

Figure 6.12: The behaviour of doubles and coincidences is dependent on the phase relations of the interfering parts of the pulse (the plot shows a pulse (measured with an ordinary photo detector) from the pulse train after it has exited the pulse picker, but before its been split in by the beam splitter in the Mach-Zehnder interferometer). If the light that makes the single photon detector click comes from two parts with little phase relation (top), the resulting behaviour will be random, while if the two parts have a strict phase relation (bottom), the behaviour will be more pronounced.

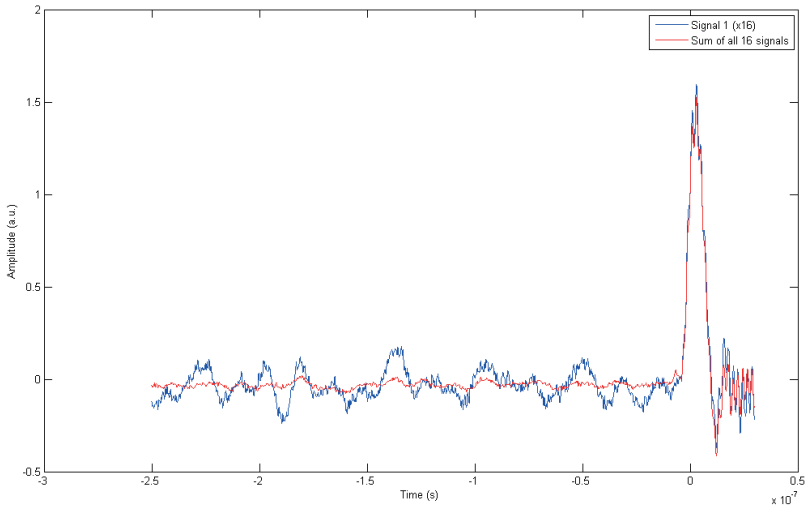

Figure 6.13: The sum of 16 signals (red) compared to a single signal multiplied by a factor 16 (blue). The amplitude to the left of the pulse is clearly not increasing linearly with the number of summed signals, and is mostly due to noise.

energy part of the field inside the cavity, and not the low energy parts. Thus, it may seem likely that the well-behaved oscillatory behaviour of the field is mainly to be found within the pulse, while the light between the pulses has a more random phase and is dominated by noise. A hint of this being the actual case can be seen when we do N similar measurements with an ordinary photo detector of the output signal from a single pulse, sum the amplitudes of of all of these, and compare the result with a single measurement having its amplitude multiplied by N. If the intensity of the summed signals increases with a factor N, the measurement would be mostly due to the signal in the pulse, but if the intensity only increases with a factor $\sqrt{N}$, the intensity would be mostly due to noise.

The summed measurement results from 16 individual measurements on a pulse is shown in Figure 6.13 (red line). Also plotted is the amplitude of a single pulse multiplied by 16 (blue line). As can be seen, the main pulse at t $= 0$ has an amplitude which is equal to 16 times the single measurement. On the other hand, the signal before the pulse only increases with a factor 4.

So from this plot it would appear that the signal between the pulses is primarily due to noise.[4]

[4]Another option is that it is a result of the limitations in the detector itself. For example, the intensity may be too low for the detector to respond, in which case the signal would result from noise as well.

6.3.2 Overlapping pulses without phase variation

We saw in the previous section that with a very large distance between the parts we could get a rotational invariance in the number of singles, but nothing else would suggest that we were approaching the results obtained with the SPDC setup. Would we get a better result if the distance between the parts were reduced? Here we let the parts overlap while keeping the piezoelectric mirror stationary. In this way the temporal relation, or phase relation, between the two parts was kept constant.

However, with this setting, the effect of instability in the interferometer became much more important than in the scan above, where the pulses were not overlapping. This was of course a consequence of the interference of the two parts. The polarizations were still orthogonal to each other, but for any other setting of the angle of the HWP at Alice and Bob than 0° and 90°, we would see interference effects between the two parts. Thus, the stability of the Mach-Zehnder interferometer became important in terms of variations in the phase relation, which in the end determined the outcome of the measurements. So we had to allow the Mach-Zehnder interferometer to reach a temperature equilibrium before making any measurements[5].

Theoretical predictions

In the general case, with two equal, overlapping classical pulses with orthogonal, linear polarizations we can use the superposition principle to find the total polarization and then use Malus' law to calculate the intensities at the detectors. Let's assume that the phase relation between the two parts is fixed so that the total polarization becomes diagonal, linearly polarized. If the phase relation was not fixed, the total polarization could be anything from linear to circular (left and right handed), as shown in Figure 6.14.

Let's assume that the two superposed parts add to a total linear diagonal polarization. The superposed parts enters the beam splitter in the analyzing setup (see Figure 4.6) where they split equally in the transmitted and reflected arm. In the transmitted arm the superposed diagonal polarization continues through Alice's HWP and into the PBS, which is located just after the HWP. Malus' law dictates the intensity at the detectors, and we assume that the intensity is proportional with the probability for detection in these. Thus, we get

$$p(A^+) \propto \cos^2(2\theta_A + \pi/4) \tag{6.36}$$

$$p(A^-) \propto \sin^2(2\theta_A + \pi/4) \tag{6.37}$$

where θ_A is the angle of Alice HWP and the phase factor $\pi/4$ comes from the fact that the incoming polarization is diagonal.

In the reflected arm there is a phase shift of $\pi/2$ for the light with polarization in the vertical direction due to the reflection in the beam splitter. This means that the total diagonal polarization exiting the reflected arm of the non-polarizing beam splitter will be orthogonal to the diagonal

[5]Even so, there were still slow variations in the phase relation, so that a slight adjustment of the optimal overlap position had to be made between every scan.

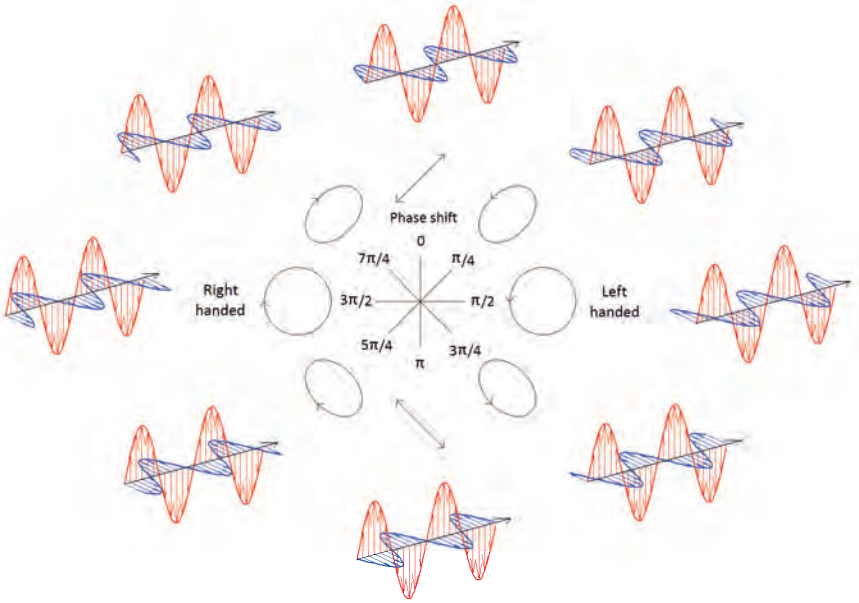

Figure 6.14: The superposed polarization for different phase relations between the two parts of the split pulse (we only consider the electric fields in this figure, pictured in blue and red for the two parts). The phase relation is shown in the middle, on the outside of this is the resulting superposed polarization and outside this again an illustration of the two overlapping linear polarizations and their phase relation.

polarization in the transmitted arm. The phase factor can then be written $-\pi/4$, and the probability for detection at Bob's detectors become

$$p(B^+) \propto \cos^2(2\theta_B - \pi/4) = \sin^2(2\theta_B + \pi/4) \tag{6.38}$$
$$p(B^-) \propto \sin^2(2\theta_B - \pi/4) = \cos^2(2\theta_B + \pi/4) \tag{6.39}$$

We can now calculate the probabilities for doubles and coincidences, which becomes

$$p(\text{Doubles at Alice}) =\propto p(A^+)p(A^-) = \cos^2(2\theta_A + \pi/4)\sin^2(2\theta_A + \pi/4) \tag{6.40}$$
$$p(\text{Doubles at Bob}) =\propto p(B^+)p(B^-) = \sin^2(2\theta_B + \pi/4)\cos^2(2\theta_B + \pi/4) \tag{6.41}$$

and

$$p(++) =\propto p(A^+)p(B^+) = \cos^2(2\theta_A + \pi/4)\sin^2(2\theta_B + \pi/4) \tag{6.42}$$
$$p(+-) =\propto p(A^+)p(B^-) = \cos^2(2\theta_A + \pi/4)\cos^2(2\theta_B + \pi/4) \tag{6.43}$$
$$p(-+) =\propto p(A^-)p(B^+) = \sin^2(2\theta_A + \pi/4)\sin^2(2\theta_B + \pi/4) \tag{6.44}$$
$$p(--) =\propto p(A^-)p(B^-) = \sin^2(2\theta_A + \pi/4)\cos^2(2\theta_B + \pi/4) \tag{6.45}$$

Plotting these theoretical calculations together with the measured ones, shows a relatively good agreement, as shown in Figure 6.15.

One graph that does not appear to fit very well with the theory is Figure 6.15 b. This can be explaind by looking at the behaviour of the singles (6.15 a). If the phase relation had been fixed and perfectly overlapping, the number of registrations at A^+ would have reached zero at 22.5° and A^- would have reached zero at 67.5°. We do not reach these levels, which means that the superposed polarization is not linear, but more elliptical. The ellipticity prevents the doubles from reaching zero, and therefore the overlap between measurement and theory is less good here.

6.3.3 Overlapping pulses with phase variation

But the above measurements does not seem to entirely agree with the results obtained with the SPDC source. We do start to see some similarity in the doubles, and the correlations are starting to approach the SPDC case without the CC (Figures 6.8 d, h and l), just with switched roles of the fixed scans (Figures 6.15 d and h compared to 6.8 d and h) and what looks like a phase shift of $\pi/4$ in the correlation in the twin scan (6.15 l and 6.8 l). But there are also other differences. Most obvious is the angular dependence in the singles in the pulsed case (Figures 6.15 a, e, i) which we do not have in the SPDC case. Could we improve the plots by adding a variation in the timing (a phase variation) between the two parts, and thus approach the situation as described in the SPDC case?

The biggest challenge would be to define the variation of the piezoelectric mirror. We have previously argued (section 4.2.5) that if the phase relation was completely random from pair to pair, the average output would be a random polarization and therefore not give anything of interest in the classical case. We continued to argue that in order to get rotational invariance in the singles (as in the SPDC case), but at the same also be able have doubles and coincidences

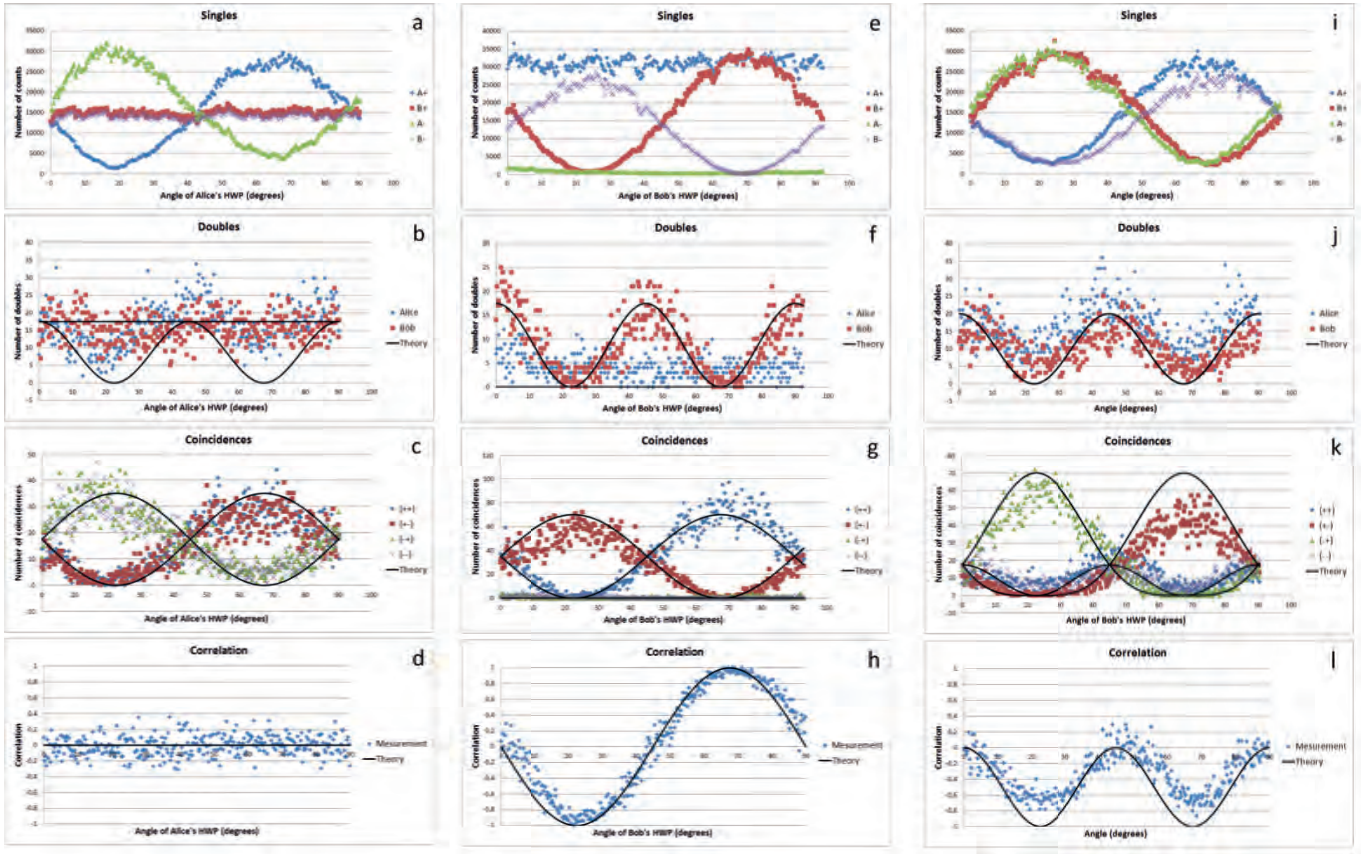

Figure 6.15: The measured and theoretically calculated singles, doubles, coincidences and the correlation in a fixed scan with Bob in the zero basis (left), a fixed scan with Alice in the diagonal basis (middle) and a twin scan (right) using a a pulsed source with orthogonally polarized, ***overlapping parts of a pulse with a fixed phase relation****.*

which are not always constant, we said that we could use two linear polarizations which were orthogonal to each other, such as diagonal and off-diagonal. In order to be able to achieve this in our experimental setup, we would need a very strict control of the phase relation. Unfortunately, we do not have such strict control, both due to the instabilities in the interferometer and due to the noise and other uncertainty factors in the signals to the piezoelectric transducer. The best setting for the variation that we achieve, was therefore a periodically varying control signal with a amplitude setting such that we move between total linear polarizations in orthogonal directions. With this setting we could do our measurements.

Theoretical predictions

The addition of a varying phase relation complicates things also in terms of the theoretical predictions. However, if we assume that we are only alternating between the two orthogonal linear polarizations (and only these two), we can simplify matters quite a bit and at the same time get an indication of how the plots would have looked like in the ideal case.

The calculations become very similar to the ones we had above, but instead of doing a calculation for only one diagonal polarization, we do it for two: the diagonal and the off-diagonal. We then sum these two calculated intensity contributions at the detectors and calculates the probabilities for doubles and coincidences based on these values. A Matlab program where this has been done is give in the appendix. The results obtained, both measured and theoretical, are plotted in Figure 6.16.

In comparison with the measurement results from the SPDC source without the compensating crystal (Figure 6.8), the results obtained in Figure 6.16 do show some familiarity. The singles are rotational invariant as in the SPDC case, but as before, there appears to be a phase shift of $\pi/4$ between the measured coincidences in the pulsed and SPDC case, and the roles of the fixed scans also seem to have switched. Also, the coincidences does not reach the zero level in the pulsed case (compare figures 6.16 k and 6.8 k). We see, however, that the ideal theoretical case do reach the zero level, so we may assume that contributions from other polarizations than the two linear diagonal ones are responsible for this in the pulsed case.

We should especially note the behaviour of the correlation in a twin scan (Figure 6.16 l). This plot has a clear angle dependence, as in the SPDC case without the CC (Figure 6.8 l). In the case of SPDC with the CC we see no such angle dependence (Figure 6.9 l) and we have also calculated this to be the case (equation (6.16)) by using an entangled state. Thus, the constant correlation in a twin scan would seem to indicate the presence of entanglement.

6.3.4 Overlapping pulses with phase variation – second attempt

From the theory of SPDC with the CC we've said that the fact that we cannot distinguish the photons in the pair by looking at their arrival time, led to a inclusion of cross terms in the probability calculations, which in turn resulted in a different plot than the case when we could distinguish the photons. The condition of indistinguishability has real effects on the output, but at the same time it is not dependent on the way we measure, because our registration and counting acquisition cannot distinguish between the arrival time difference in the case with and without the CC.

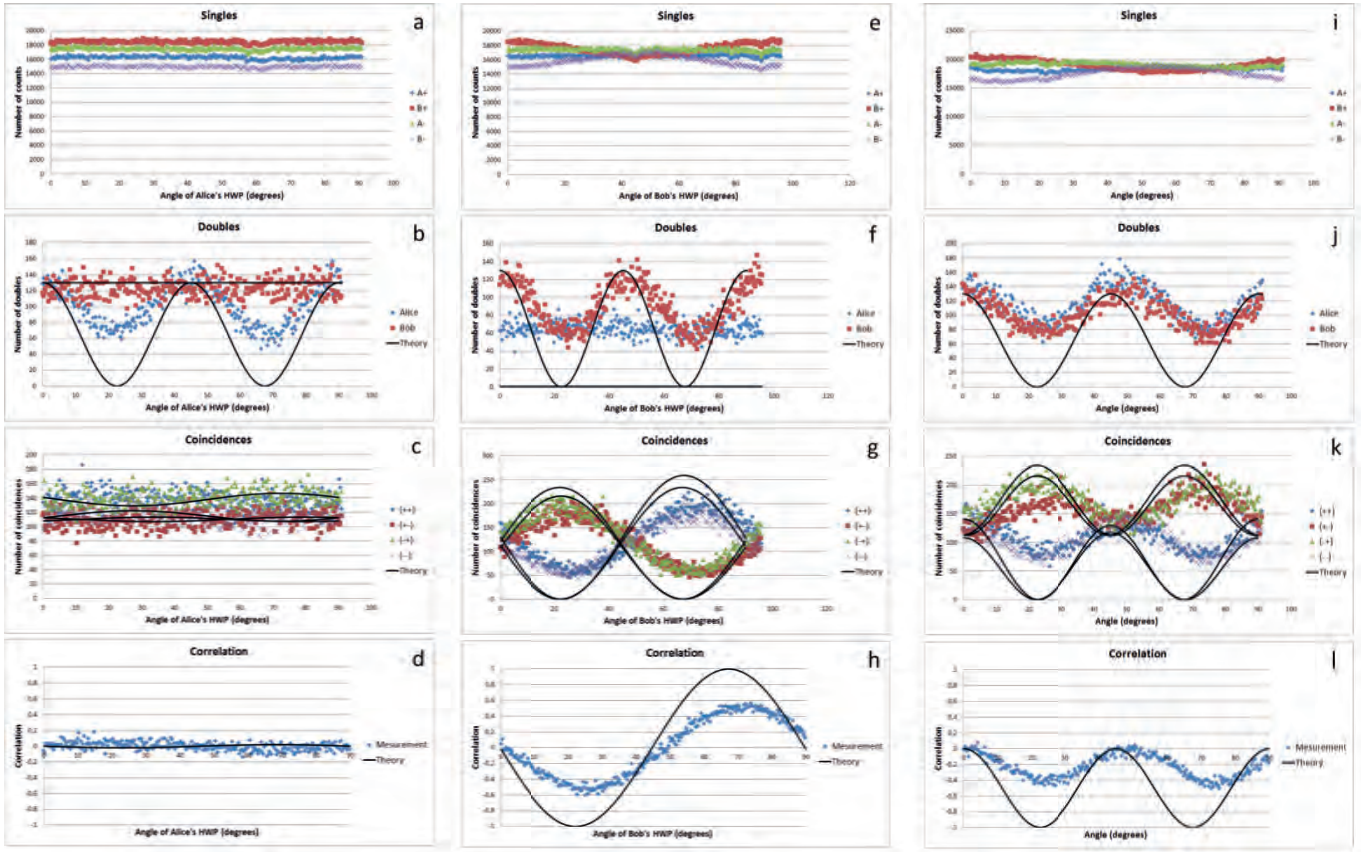

Figure 6.16: Measurement of singles, doubles, coincidences and the correlation in a fixed scan with Bob in the zero basis (left), a fixed scan with Alice in the diagonal basis (middle) and a twin scan (right) using a a pulsed source with orthogonally polarized, overlapping pulse pairs ***with a varying phase relation****. The theoretical plots for the ideal case of strict variation are included as well (a slight deviation in the amplitudes of the coincidences was added to better show the behaviour).*

It does not have that kind of precision. So how do we emulate this effect with the pulsed setup?

The way the setup has been used so far has been with an approximate overlap position (not stable in time) and some variation around this. This was very crude and the measurement results would at best look somewhat similar the SPDC case without the CC. Since one of our main objectives was to attempt to emulate the situation with CC using our pulsed setup, we needed to a much better control of the phase relations as well as higher stability in the Mach-Zehnder interferometer, because we would need to vary between two strict polarizations around a fixed overlap position.

We therefore replaced the piezoelectric mirror and its control with a newly developed mirror with three piezoelectric controllable axes[6]. The biggest advantage with this mirror compared to the bulky mirror that we've used so far, was the possibility for much stricter control of its movement. Thus, in principle, we would obtain a situation where we moved between diagonal and off-diagonal polarization around a fixed overlap position. Figure 6.17 shows the mirror and control electronics mounted in a custom made holder.

Unfortunately, the mirror also had a few disadvantages: it is very fragile, both mechanically and in term of electro statics. This made the handling and setup process a delicate one. Another unexpected issue arose from the small size of the mirror. This meant that it became much more temperature dependent than the bulk mirror, again leading to challenges during alignment.

The major factor for why this setup did not work as hoped, however, had less to do with the mirror and more to do with the stability of the whole interferometer. As we saw for example in Figure 4.14 we have rapid oscillations in the interferometric pattern as the retroreflector is moved. This shows that even small differences in the path length can cause large variations in the outputs, thus we need strict mechanical and thermal stability in order to make sure that we are at the exact overlap position. If we are trying to emulate a situation where we have indistinguishability *in principle*, it would obviously mean that variations and positions have to be kept very precise, if we wish to see similarities in the results.

But it is obviously not only as simple as getting stability in the setup, as we can see by looking at the theoretical plots in Figure 6.16. The theoretical prediction is a simulation of the ideal case, where we have no stability issues or problems with overlap positions, and we can see that the results does not portray the SPDC case with the CC. So is there another factor, not included in the theoretical model, that can be adjusted in order to get similar results as the entangled case?

The coincidence window

So far, we have made all measurements with the same coincidence window as in the SPDC case – 8 ns – and in the theoretical calculations it has not been included at all. We tried to argue for how the role of the coincidence window may be of importance for the outcome of the measurements in section 6.3.1. The importance of the size of the coincidence window can be further strengthened by looking at the behaviour of the coincidences in a twin scan at different coincidence window sizes, as shown in Figure 6.18.

As the coincidence window is reduced, the number of counts naturally also becomes reduced,

[6]We are very grateful to SINTEF for letting us borrow their mirror in order to make these measurements.

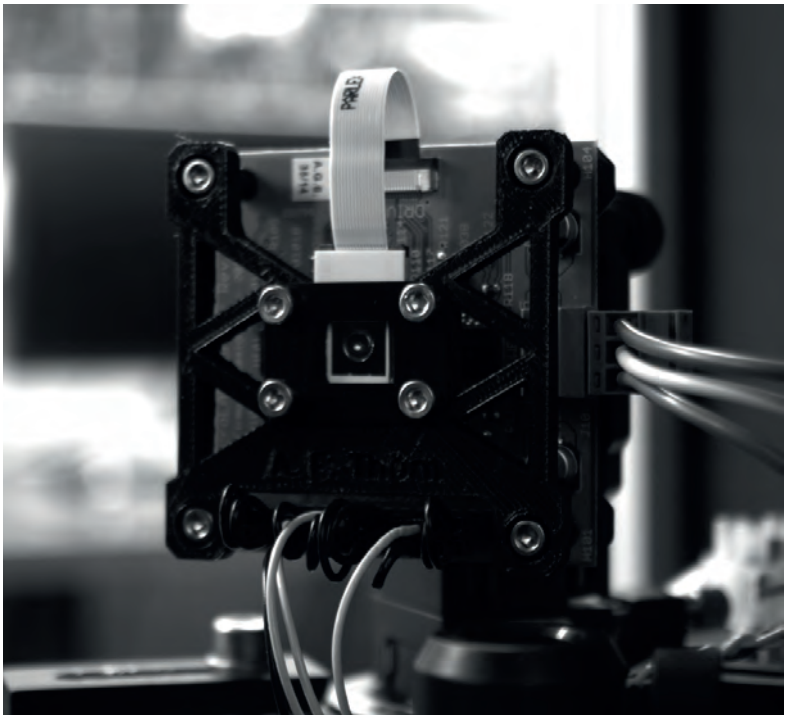

Figure 6.17: A precision three-axis piezoelectric mirror from SINTEF. The custom made holder was designed to work in our setup and printed on a 3D printed. The bright dot in the middle of the mirror is the un-attenuated pulse train used during the alignment process. The control electronics can be seen behind the mirror.

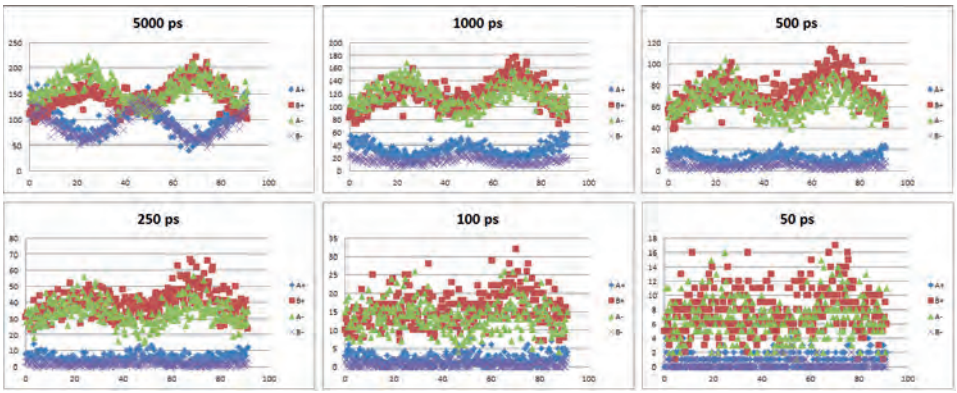

Figure 6.18: The behaviour of the coincidences in a twin scan for different widths of the coincidence window. As the coincidence window is reduced we approach the results from the SPDC case, until the number of registrations becomes too low and noise becomes dominant.

leading to greater fluctuations in the plots. At the same time, however, the behavioural pattern becomes more pronounced. So there is a balance between having enough counts so that fluctuations and noise does not smear out the pattern we wish to study and at the same time have a narrow coincidence window.

We now reduced the coincidence window to 300 ps. With this setting, a twin scan was again performed with the pulsed source with varying phase relation and compared with the results obtained with the SPDC source with compensating crystal.

The singles are not affected by the width of the coincidence window and remain rotational invariant, just as in the SPDC case.

A plot of the number of doubles for both the pulsed and SPDC case is shown in Figure 6.19.

Although the plots are not exactly the same, there is a tendency of similarity between them.[7] We do not reach zero doubles in the pulsed case, which comes from the fact that the phase relations are not strictly varying between two linear diagonal polarizations, but also has contributions from elliptical and circular polarization, as was explained earlier.

More important is the behaviour of the coincidences, which now became relatively similar in their behaviour to the SPDC case, with N^{++} and N^{--} being close to zero and N^{+-} and N^{-+} being equal and less pronounced in their angle dependence (see Figure 6.20).

As a result of this behaviour, the correlation in the pulsed case also became similar to the correlation in the quantum case, as is shown in Figure 6.21.

From these plots, and specifically the correlation, we see that, although the correlation is not as near to being constant -1 as the quantum case, the dependence on the angle is much

[7]The behaviour of the doubles alone is not showing us anything new at this stage, as the behaviour is the same as in the SPDC case without CC and the pulsed case with 8 ns coincidence window, but the plot is included here for the sake of completeness – an concept which we will discuss in the next chapter.

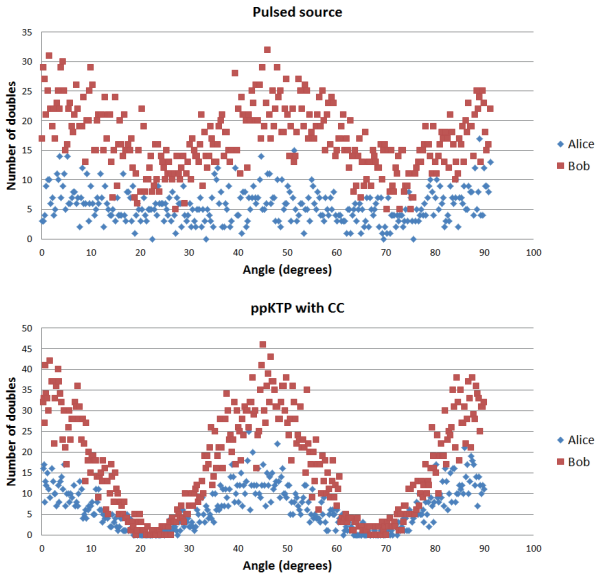

Figure 6.19: The behaviour of the doubles measured in a twin scan using the pulsed and the SPDC source, with a coincidence window of 300 ps.

less pronounced than in the classical case, where the correlation would vary between 0 and -1 (as seen in Figure 6.16 l). Thus, it would seem that the measured results from the pulsed source is closer to being quantum mechanical than classical, and it would therefore, from our earlier argumentation about the rotational invariance of the correlation at -1 being a result of entanglement, be reasonable to ask if we now have generated some entanglement between the polarizations in the light from the pulsed source.

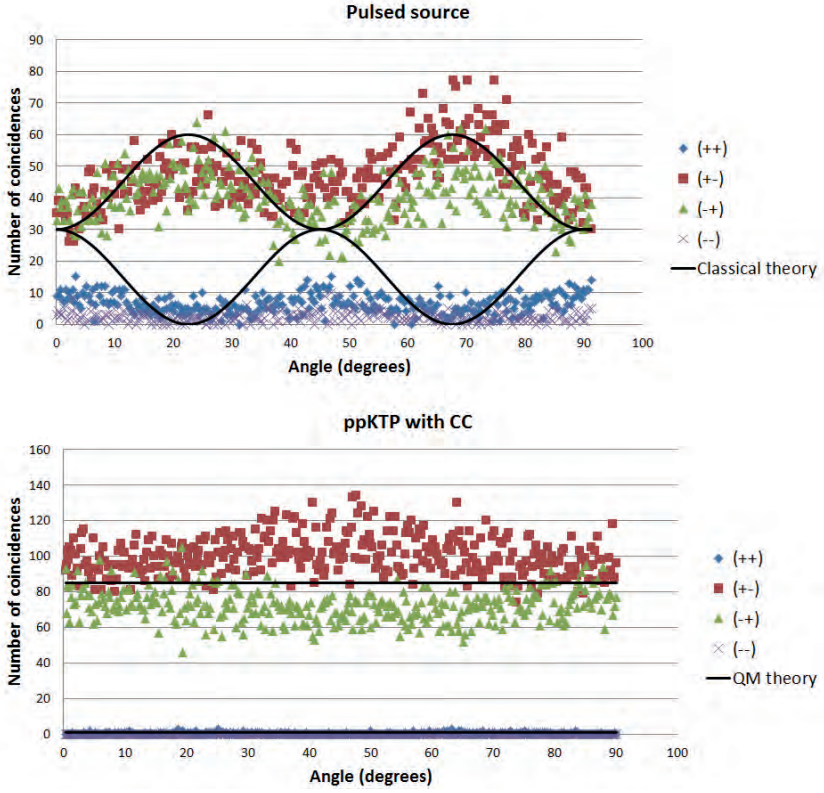

Figure 6.20: The measured coincidences in a twin scan using the pulsed and the SPDC source, with a coincidence window of 300 ps. The upper part of the figure could be compared with Figure 6.16 k.

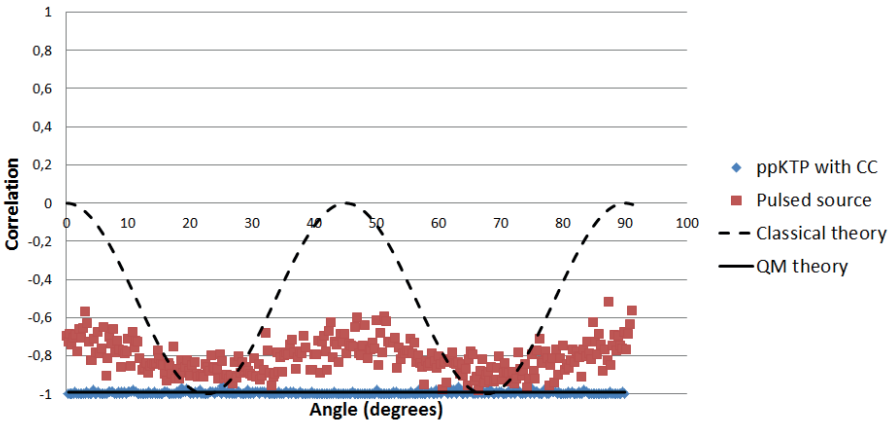

Figure 6.21: The correlation measured in a twin scan using the pulsed and the SPDC source, with a coincidence window of 300 ps. Figure 6.16 l can be used as comparison for the pulsed case.

Chapter 7

Conclusions

From the foregoing measured results with the narrow coincidence window, is it possible to say that we have generated something similar to quantum light by combining and manipulating the characteristics of classical pulses? That is, have we managed to emulate the SPDC process using a classical pulsed source? The plain and simple answer is: no. And the reason why is because we have not looked at the full picture of the measurement results, nor the physical conditions we have when obtaining these results.

7.1 The complete picture

In order to be able to compare the results using the pulsed source with the results obtained with the SPDC source, we have to compare all aspects of it if our conclusions are going to be valid. This includes the relative behaviour of the doubles compared to the coincidences, the phases and the behaviour in all fixed scans.

In the last section of the presentation of the measurements we looked specifically at a comparison between the pulsed source and the SPDC source in a twin scan (Figure 6.21). This was because we said that the -1 correlation in a twin scan was a characteristic signature of an entangled state. While this remains true, we should also look at the behaviour in the fixed scans to see if the measurements also here agree with the results when using the SPDC source with the compensating crystal. We have already seen that it does so to some degree in the case of a fixed scan in the diagonal basis (compare Figures 6.16 e-h and 6.9 e-h), even in the case of a coincidence window of 8 ns. However, a fixed scan in the 0 basis with a 8 ns coincidence window showed no correlation at all (Figure 6.16 d), whereas we had a clear angle dependence with the SPDC source (6.9 d). What about a coincidence window of 300 ps, which above gave us good results for the twin scan? Will a measurement in a fixed scan in the zero basis portray the quantum mechanical behaviour?

The result is plotted in Figure 7.1. The coincidences and the correlation measured with the pulsed source is shown on the left and the SPDC case with CC on the right. As can be seen, there is a huge difference in the behaviour; while the SPDC case is dependent on the angle, the pulsed remains rotational invariant as before. Thus, the much narrower coincidence window does not

help us getting closer to a result similar to the entangled case.

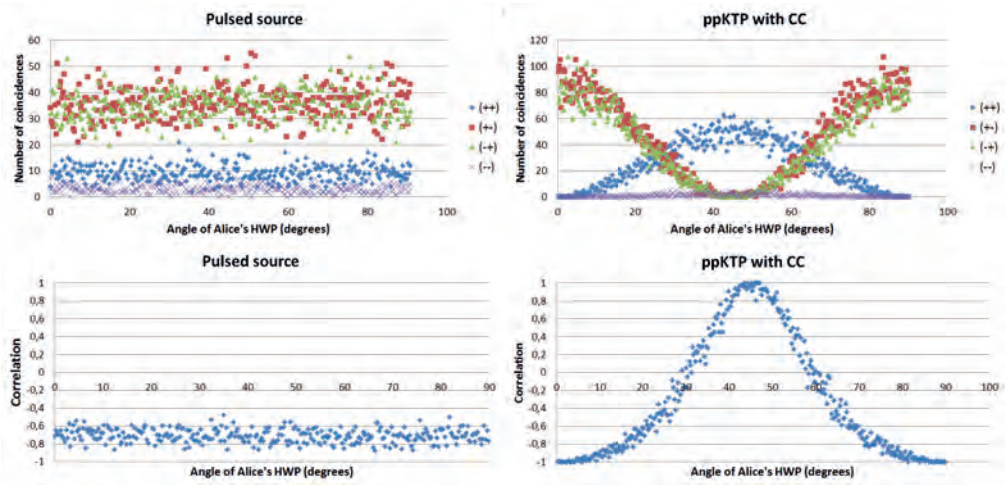

Figure 7.1: The measured coincidences and the correlation in a fixed scan with Bob in the 0 basis when using the pulsed source (left) and SPDC (right) when the coincidence window is 300 ps.

We saw in section 6.2.1 that we could measure a maximum violation of Bell's inequality using two fixed scans; one taken in the zero basis and the other in the diagonal basis. From the common interpretation of Bell's inequality it should not come as a surprise that a measurement of the inequality should give us a definite answer to whether we are working with an entangled state or not, i.e. if we've actually managed to create what we defined as quantum light or if our light is classical. With reference to Figure 6.7 and the correlations obtained in the fixed scans above, we can immediately see that we do not break Bell's inequality with our pulsed source in these measurements.[1]

Nevertheless, we do get a correlation in the twin scan which seems to have a similarity to non-classical behaviour. How can this be?

The fact that we get a behaviour of the coincidences in a twin scan which resembles the result obtained from SPDC with CC when the coincidence window is reduced, does not seem to be related to which specific scan we are performing. We can see this by looking at Figure 7.2, which shows the behaviour of the coincidences for different coincidence windows in a fixed scan with Bob in the zero basis.

From this figure we see that the behaviour is similar to the one we had in Figure 6.18. This is not what we would expect from a fixed scan if we where approaching the entangled case. In

[1]Remember that the S parameter in the calculation of the CHSH inequality is the sum of the correlation at four different angle settings of Alice's and Bob's HWP ($S = E(a,b) - E(a,b') + E(a',b) + E(a',b')$). For violation of Bell's inequality $S > 2$. If the sum of two of the correlation values are always equal to zero, the sum of the other two can never be larger than 2, thus, Bell's inequality cannot be violated.

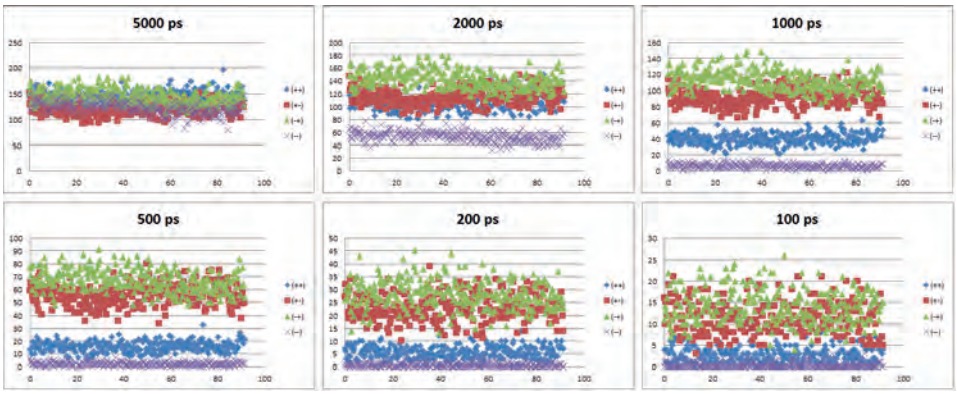

Figure 7.2: The behaviour of the coincidences in a fixed scan with Bob in the zero basis for different widths of the coincidence window.

that case, we should have seen a behaviour which was dependent on the angle (see Figure 6.9 d). Instead we see a lowering of the $(++)$ and $(--)$ counts only, just as in the case with the twin scan.

But what does a reduction in the coincidence window really mean? It means that the measured time difference between two registrations at different detectors has to be smaller in order to register as a coincidence. This would suggest that the $(++)$ and $(--)$ counts are in general more often a result of triggering that's happening further from each other in time than the $(+-)$ and $(-+)$ counts. The coincidence window is never larger than 8 ns and would therefore only register the events which were coming from a single pulse from the pulse train. So it would seem to be more likely to generate $(+-)$ and $(-+)$ counts from the same part of the pulse, while $(++)$ and $(--)$ counts seem to be generated mostly from contributions which are dependent on the energy between the pulses (with reference to Figure 6.12). As the coincidence window is reduced, fewer registration coming from this in-between-energy will be included in the coincidence count.

But why should the $(+-)$ and $(-+)$ counts be more tied to the pulses than the $(++)$ and $(--)$? Is it so that the phase shift in the NPBS and the definite direction of polarisation within the pulse are responsible for this correlation between the counts? For a twin scan, that could be a possible reason, since the phase shift at the NPBS makes the probability for registering an A^+ equal to the probability for registering a B^-, and similar for A^- and B^+. That is, if the number of A^+ counts is high, then so is the number of B^- counts, leading to a high number of $(+-)$ counts. But if A^+ is high, B^+ will be low, leading to a low number of $(++)$ counts.

But for a fixed scan this is not so easily argued for, since if Alice's HWP is at 0° and Bob's is at 45°, then the situation would be directly opposite to what we just said (i.e. the probability for registering an A^+ equal to the probability for registering a B^+). Thus, at the moment, no satisfactory explanation can be given.

If we allow ourself to speculate, we may look at the work by Michielsen et al. [1, 2] and

de Raedt et al. [3], where the role of the coincidence window has been discussed. Their main conclusions is that the ability to break Bell's inequality depends on our choice of the value for the coincidence window. It is the filtering of the detection events introduced by the coincidence window which generates the correlation dependencies among the detection events. Removing this time-tagging, and Bell's inequality cannot be broken. In addition, they also show that experiments such as our own (based on our data, in fact), does not exclude that the data can be described by a state which does depend on the setting of *both* HWPs. Or in other words; a situation that is not necessarily local. Unfortunately, the processes responsible for generating the same results "have not been identified yet" [1].

While we've seen from the theoretical derivation that the timing of the events is essential for the generation of the entangled state and thus in a way agrees with the conclusion of Michielsen and de Raedt, it is the role of the coincidence window which is most interesting in respect to the behaviour we have observed. In very simplified terms the idea of Michielsen's and de Raedt's model (which they applied to a neutron interferometer experiment, but can be applied to photons as well) is that the particles involved in the interference, acts as messengers which leaves messages or traces behind as they move through the components in the setup. These can be detected and acted upon by the next particle that comes along, thus leading to correlation effects. It is a sort of memory effect or adaptive learning in the components.

The relation between the width of the coincidence window and the ability to break Bell's inequality can be seen quite clearly in our own measurements when using SPDC with the compensating crystal. If we look at the fixed scan with Bob in the zero basis and increase the coincidence window, then the behaviour in all measurements (doubles, coincidences and the correlation) become equal to the pulsed case with varying phase relation. A comparison is shown in Figure 7.3. This plot shows that there may be more to the coincidence window than first assumed, since by increasing it, the SPDC approaches the pulsed case, and if we reduce it in the pulsed case, it approach the SPDC case (to some extent at least). We may also note that we have to increase the coincidence window substantially (by a factor 10 000) in order to observe the effect in the SPDC case. It is possible that we need to reduce the coincidence window much more than we have done in order to observe the effect in a fixed scan with the pulsed source. But reducing it more than by a factor 100 will result in too few counts and too much noise to see any patterns.

In any case, the picture of the physical process, when changing the coincidence window in the photon case, is that when the window is large, we include the possibility of measuring the correlation between photons which does not necessarily comes from the same pair. In that way we loose the strict pairing of the orthogonal polarizations which leads to the results we see in Figure 7.3. So the fact that Bell's inequality is no longer broken, does not seem all that surprising.

In the pulsed case, we may already have less strict pairing of the orthogonal polarizations due to the contributions from the energy between the pulses. In that way, a better correlation would be expected when the coincidence window is reduced.

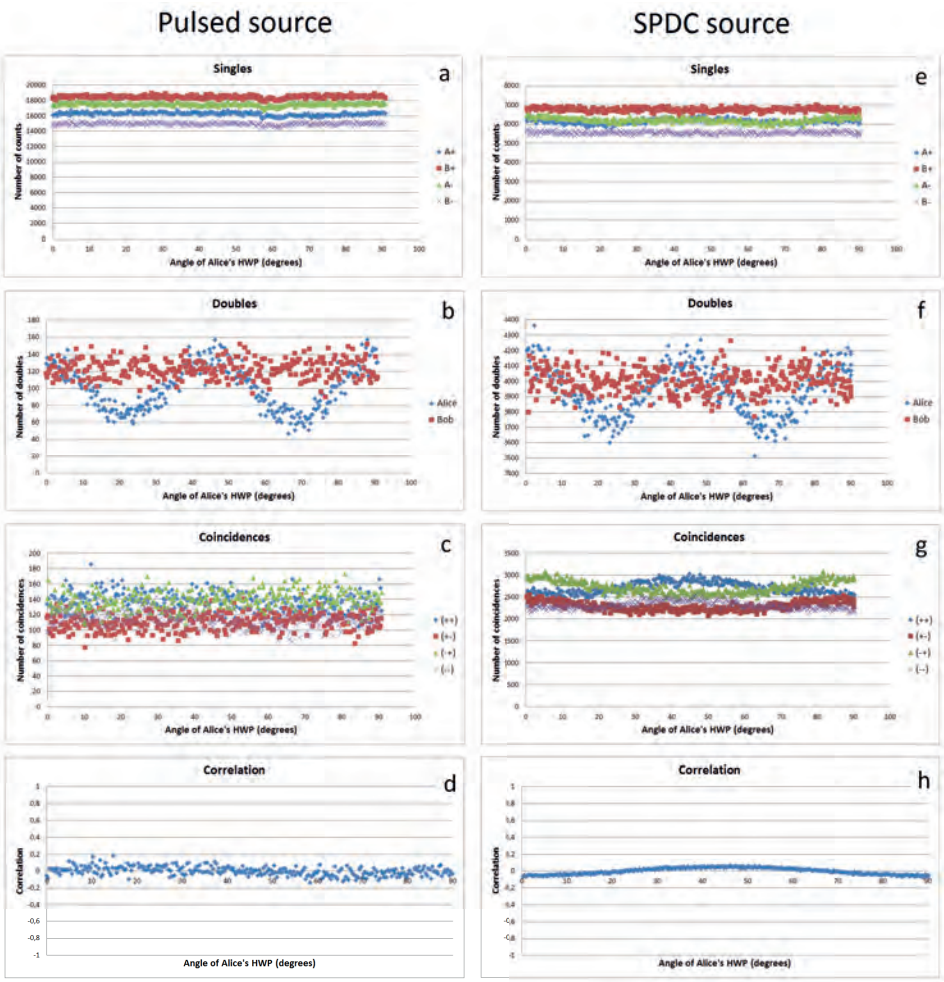

Figure 7.3: A fixed scan with Bob in the zero basis measured with the pulsed source with a coincidence window of 8 ns (left) and the SPDC source with CC and a coincidence window of 80 μs (right).

7.2 Absence of the complete picture in general

The need for the complete picture may seem like an obvious requirement, but it is not always taken into account. In Paper B (see chapter 8) the Hong-Ou-Mandel effect is discussed from the point of view of interpretations and their validity. In this paper we discuss a number of experiments and theoretical derivations which would suggest that the so called Hong-Ou-Mandel dip does not necessarily have to be an indication of a quantum nature of light. In fact, it has even been claimed to be possible to generate the dip using thermal sources [4] or other sources of classical light [5–9].

In an experiment performed by Chen et al. [4] in 2011, they used a pulsed Ti:sapphire laser with pulse durations of the order of 150 fs and a rotating ground glass diffuser to produce pseudo-thermal light. This light was used as a source in the Hong-Ou-Mandel interferometer. The light exiting the rotating diffuser entered a beam splitter, and was, in each arm, coupled to polarization maintaining fibers mounted on translational stages. In this way, the spatial coherence could be changed at will. By positioning half wave plates between the exit tip of the fibers and the beam splitter in the Hong-Ou-Mandel interferometer, and changing the position of the entrance tip of one of the fibers in the longitudinal direction, they were able to measure a dip in the coincidence count. The visibility was claimed to be as high as 93.2 ± 5.1 %.

In the photon picture, the Hong-Ou-Mandel dip is characterized by the change in the number of coincidences when two correlated photons enters each of the input ports of a beam splitter. However, we also have the possibility of contributions to the coincidences when both photons comes from the same input arm. The coincidence counts generated in these cases are defined as background counts, and are removed from the measurements by measuring the coincidences with one of the input arms is blocked. This is done in separately conducted measurements. Such an approach, although common, is far from legitimate when measuring Bell's inequality. By subtracting counts in this manner, effects similar to the detection loophole in a Bell measurement are introduced in the analysis. The detection loophole, or fair sampling assumption, states that if the detection efficiency is less than 100 % (which is always the case in a real experiment), the limits of the CHSH inequality will change. Thus, if the subtracting procedure was valid, one would in fact be able to "violate" Bell inequalities with classical fields.

It is therefore somewhat presumptuous to claim, as Chen at al. does in their article, that they have generated Bell states (i.e. entangled states) with their pseudo-thermal light. The visibility without the subtracted background in their experiment is more of the order of 15 %. Thus, again, we see that not including the complete picture in terms of all measurement and their relations, can lead to incorrect conclusions about the nature of light.

With reference to our own measurement in the case of a twin scan; it's what we don't measure that gives us the complete picture, because the fixed scans will show a behaviour of the correlation which will not lead to a violation of Bell's inequality. So, again, the complete picture is required if one is to make any statements about the measurements. Observations of single quantum-like signatures in certain measurements do not tell the whole truth about the nature of the light we're observing.

The experiments by Chen et al. have been discussed from a semi-classical point of view by Shapiro [10, 11]. It is shown in these articles that the results obtained by Chen, which shows

similarities with Bell-state interference measurements, also can be obtained when using a semi-classical photodetection theory and looking at the photocurrent cross-correlation. Furthermore, it is shown that in the semi-classical theory, these effects will be visible also at higher intensities, due to the fact that the interference pattern originates from intensity-fluctuation correlations between the fields at the two outputs of the beam splitter. This is in many ways similar to the results of Hanbury Brown and Twiss (HBT) [12]. Shapiro also shows that the substraction of the background is different from the post-selection of correlations generated in SPDC. This, he claims, is because the classical self-intensity correlations are subtracted on an average level in separate measurement rather than being performed on a pair-to-pair basis.

An important difference between our experiments and the ones performed by Chen et al. in terms of the source, is that we are using the coherent laser light directly, whereas Chen added means to make their light (quasi-)thermal. This is important if we wish to relate to the effects observed in a HBT measurement, because it is the fluctuations in the intensity, resulting from the spatial coherence, which gives rise to the correlation effects observed in these measurements. In our setup we wished to maintain the coherence and introduced varying phase relations instead, in order to relate to the familiar process of first order interference. We did, however, try several measurements with a rotating diffuser similar to the setup by Chen et al. placed at different positions both outside and inside the Mach-Zehnder interferometer. No improvement in the results could be observed.

7.3 A closer comparison between the pulsed and SPDC results

Looking at the singles in the SPDC case, we've seen that these are rotational invariant in all scans. In order to achieve this with the pulsed source, we added a variation of the phase relation between the two parts of the pulse in the Mach-Zehnder interferometer. In the theoretical simulation of this, we alternated between two orthogonal directions of linear polarization, which averaged to a constant number of singles for all angles. We did not have such strict phase control in our measurements, so a certain degree of randomness in the polarization limited the visibility in the plots.

In the ideal case we have also seen that the behaviour of the doubles will reach zero at 22.5° and 67.5° in a twin scan, which again is in agreement with the entangled case (SPDC with CC).

But even with the strict variation in the phase relation that we have in the simulated results, the coincidences does not portray the behaviour of SPDC with the CC (the entangled state), and therefore neither does the correlation.

On the other hand, the coincidences and the correlation will have an angle dependent behaviour in a twin scan which is more similar to the case of SPDC without the compensating crystal, as shown in Figure 7.4. The plots on the left hand side of this figure (a, c, e, g) are mathematically simulated plots of the behaviour of the singles, doubles, coincidences and the correlation for the pulsed source. We see that these resembles the results obtained with the SPDC source without the CC (right side of Figure 7.4).

An interesting difference to note in these plots is what appear to be a phase difference of $\pi/4$ between the measurements and theoretical plots in the coincidences (and the correlation). One

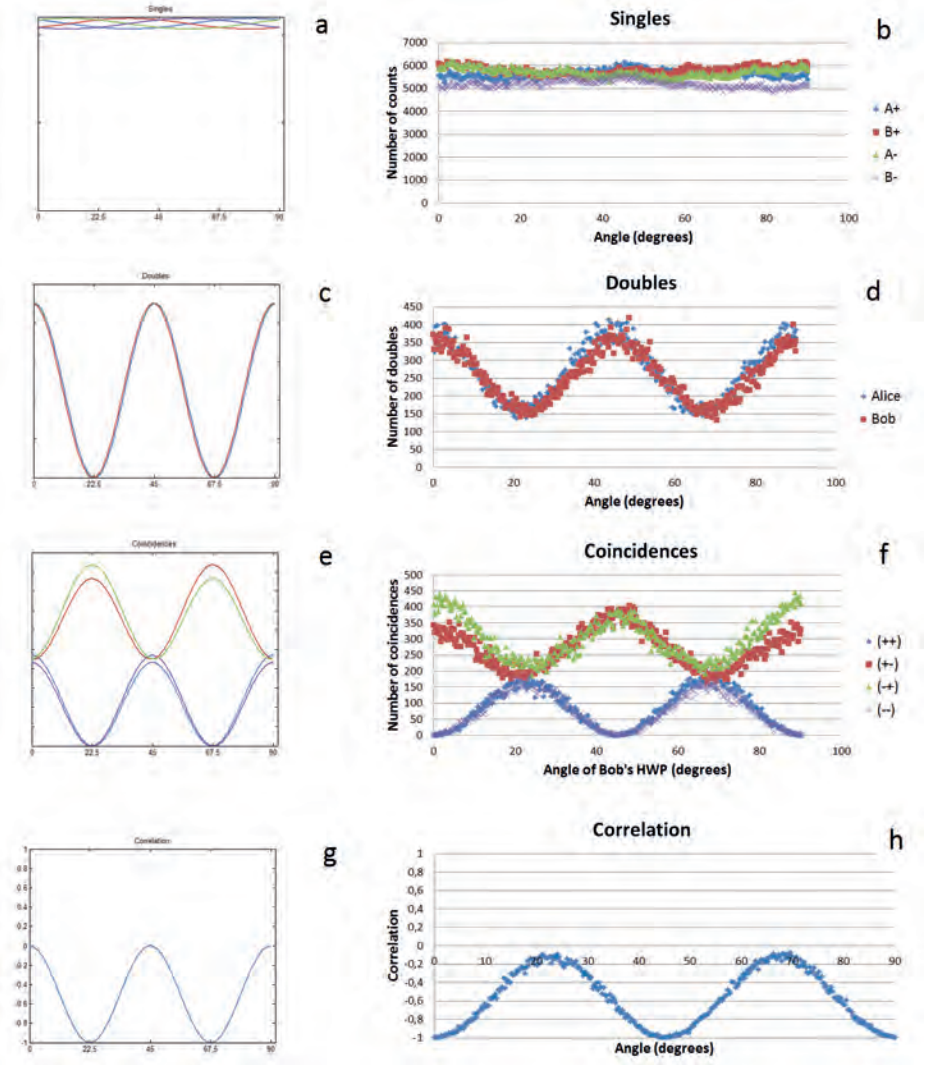

Figure 7.4: A mathematical simulation (left) of the pulsed source for generation of singles, doubles, coincidences and the correlation in a twin scan when the phase relation is strictly varying between 0 and π. The case of SPDC without the CC (right) is included for comparison. The Matlab code for the calculation can be found in the appendix.

might think that this was a result of the setting of the HWP before the analyzing setup (see Figure 4.6) being different in the two cases, since it rotates both polarizations before entering the NPBS and thus adds an overall phase shift. However, the setting of this HWP cannot help us. In fact, there is no setting on the HWP which would give us a behaviour which would correspond with *all* the measured results from the SPDC case without the CC, as long as we are using classical light.[2]

We can see this from the following argumentation. In the SPDC case we can explain the observed results from the quantum mechanical theory given in the last chapter by assuming that the photon and its characteristics are indivisible. Thus, no photon is being split at the NPBS in the analyzing setup. Instead, the photons are either going into one arm each or both goes into the same arm, while retaining their polarization characteristics. The doubles counts are resulting from the cases when both photons goes into the same arm, while the coincidences arises from the photons going into each of the arms. It is important to note however, that if both photons are going into a single arm, the probability for detection is dependent on the sum of the amplitudes of the polarizations and their relative directions. In this way, the calculation can be made as if the polarization of the photons summed to a total diagonal linear polarization. In this picture, the total polarization would be diagonal when both photons are going into a single arm, but purely vertical and horizontal when each of them goes into separate arms. In this way, when the angle of the HWPs are at zero degrees, both Alice's and Bob's doubles are at their maximum values (as seen in Figure 7.4 c), while the number of $(++)$ and $(--)$ coincidences in the SPDC case are zero, and $(+-)$ and $(-+)$ are at their maximum value (Figure 7.4 e).

In the classical case we do not have this situation, because the superposed light will be split by the beam splitter and both parts will contribute to the doubles and coincidences simultaneously. The polarization will therefore remain diagonal both for the doubles and the coincidences. So we get an equal number of counts for the coincidences when the HWPs are set at 0°, as seen in Figure 7.4 f. Thus, there is no case where the horizontal or vertical polarization becomes separated from the superposed light at the beam splitter and only goes into one of the arms.

Again, we can shift the behaviour of the coincidences and the correlation to match the SPDC behaviour using the HWP before the NPBS, but only at the cost of getting the same phase shift in the doubles. Thus, should we choose to only look at a specific scan or characteristic of the measurements (which is sometimes done), it may appear that we can obtain characteristics which we do not necessarily have. So we have to include the complete picture, that is, the behaviour of the singles, doubles, coincidences and the correlation and the relations between them. If we had not included the behaviour of the doubles, we could easily adjusted the plots to match the SPDC case without the CC. By including the behaviour of the doubles we see that there is a deeper underlying physical difference than just a simple global phase shift.

7.3.1 Fixed scans

The photon's retainment of their polarization is also the reason for why we get opposite outcomes for the correlation in the pulsed case compared to the SPDC case without the CC in the

[2]Meaning here; light which always splits (amplitude and polarization) at the NPBS.

fixed scans. In order to understand this we again have to look at the state of polarization of the incoming light. In the mathematical simulation of the pulsed source, the light is diagonally linear polarized and it retains this diagonality when measuring both doubles and coincidence counts. In the SPDC case however, the polarization can be viewed as diagonal only in the case of the doubles, since in this case both photons are going into the same arm. In the coincidence measurements, the polarizations is horizonal and vertical, respectively, in either arm.

As an example, let's conduct a scan with, say, Alice in the zero basis and look specifically at the behaviour of the coincidences. Let us also keep ourselves to the ideal case of total diagonal and off-diagonal polarization in the pulsed case, as we have done before in the mathematical simulations. With Alice in the zero basis, the polarization of the light hitting the PBS after Alice's HWP will always remain diagonal or off-diagonal. Thus, the number of counts at A^+ and A^- will always be the same. The behaviour of the coincidences are therefore only determined by the measurements at the detectors at Bob, B^+ and B^-. The counts here depend on the setting of Bob's HWP and on the incoming polarization. The diagonal polarization will give results which are opposite to the off-diagonal polarization, as illustrated to the upper left in Figure 7.5. The expected correlation, as given by

$$E = \frac{N^{++} - N^{+-} - N^{-+} + N^{--}}{N^{++} + N^{+-} + N^{-+} + N^{--}} \tag{7.1}$$

then becomes 0 for all angles of Bob's HWP.

In the case of SPDC without the CC on the other hand, the polarization of the light hitting the PBS after Alice HWP would be found to be either horizontal or vertical if measured here, because only a single photon enters each arm in the coincidence counts. This gives a maximum number of counts in A^+ and B^- and zero in A^- and B^+ when the vertically polarized photon is transmitted through the NPBS and the horizontally polarized is reflected. When the situation is reversed (H is transmitted and V is reflected), the number of registrations will also be reversed (A+ and B- is zero and A^- and B^+ is maximum). As Bob's HWP is rotated, the probability for registrations at B^+ and B^- will change according to Malus' law, and we will obtain the behaviour of the coincidences and the correlation as shown to the lower left in Figure 7.5.

For a fixed scan with Alice in the diagonal basis, the pulsed case will, if we assume the same ideal case as above, give a polarization after Alice's HWP which is horizontal or vertical, because the incoming diagonal polarization is now rotated 45° due to the HWP being set to 22.5°. The behaviour at Bob will, however, be the same as before. The coincidences for the two polarizations (diagonal and off-diagonal) will then follow the curves as seen to upper right in Figure 7.5 which results in an angle dependence in the correlation.

In the SPDC case, the polarization of the single photon will also be rotated, but with purely horizontal or vertical polarization before the HWP, the polarization hitting Alice PBS would be measured as diagonal after passing through Alice's HWP. So, on average, the number of counts at A^+ and A^- will always be equal. Again, the situation at Bob remains the same as before. But because we now have a non-zero probability for detections at both of Alice's detectors, all the coincidences will be dependent on the angle of Bob's HWP. However, the behaviour of the coincidences will be opposite of each other (similar to what we had in the pulsed case in the zero

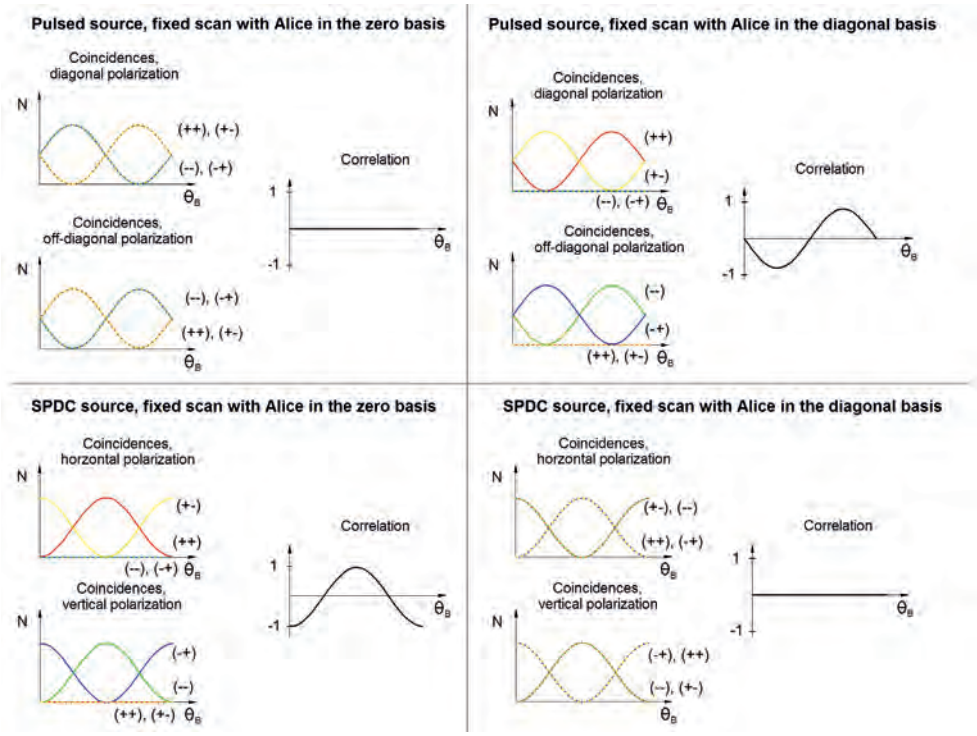

Figure 7.5: A schematic illustration showing the origin of the difference in the behaviour of the correlation when generated by the pulsed source (two upper figures) and the SPDC source (the two lower figures), in a fixed scan with Alice in the zero basis (left) and the diagonal basis (right). The coincidences are colour coded as follows: (++) in red, (–) in green, (+-) in yellow and (-+) in blue. The difference can be traced back to the indivisibility of the photon and the retainment of its polarization.

basis), so the averaged sum becomes constant, as shown to the lower right in Figure 7.5. This results in a correlation which is zero.

Thus, we see that as a consequence of the photon's retainment of their polarization we get opposite behaviour of the coincidences in the SPDC case compared with the pulsed case in the fixed scans. And this is also what we see in the measurements (compare Figure 6.8 c and g with Figure 6.16 c and g).

7.3.2 Pulsed source in the photon picture

The number of pulses being registered by the detectors in the pulsed case were between 10 000 and 20 000 per second, while our modified pulse train contained 8 million pulses per second. One might therefore conclude that we have much less than one photon per pulse and therefore operates below single photon level. Another observation that would strengthen this claim is the low number of observed triple counts. Since the combined pulse from the Mach-Zehnder interferometer would have the possibility to split at all beam splitters (also the PBS when the HWPs are at any other angle than $n\pi/8$, were $n = 1, 2, 3, \dots$) if the intensity is above single photon level, it would be natural to see a relatively high number of triples. However, we have only measured an insignificant number of these in any of our scans.

While it is not completely unrealistic to assume that we are working at a single photon level, other effects which may reduce the number of counts should be taken into consideration as well. This includes scattering and absorption of the light as it passes through or is being reflected by the many optical components in the setup, the possibility of a non-optimal spot size and/or location of the focal spot at the detectors, the dead time of the detectors and, more importantly, the fact that with such short pulses, a pulse hitting the detector will generate only a single click no matter the intensity. A higher intensity makes it more probable for the detector to click, but the output is still the same (one click or no click).

Another consideration to take into account when it comes to triples is the probability for detecting three "simultaneous" registrations when contributions other than from the pulses are non-negligible (that is, when contributions from the energy between the pulses in the pulse train cannot be ignored). If we look at the ratio of singles over doubles (Figures 6.8 and 6.16), we see that in the SPDC case it is approximately $200/6000 \approx 3\%$, while in the pulsed case it is only $100/16000 \approx 0.6\%$. This difference could be attributed to registrations which are not related to the pulses (but the energy in between them) and which does not contribute to the double counts. With less strict polarization relations among the registrations, which are happening in a less timely ordered fashion, registering doubles within the coincidence window (at a given rate of registered singles) becomes less probable, and registering triples even less probable.

Let's make a calculation of the rate of photons per pulse based on the numbers that we have available. We know that we are sending $8 \cdot 10^6$ pulses into the interferometer per second. Let's call this number N_p. These pulses were heavily attenuated, leading to n number of photons per pulse. The total number of registered singles per second, N_s, is what we measure with our single photon counters. The relation between the number of photons per pulse, n, and the total number

of singles per second, N_s, can be expressed as

$$\eta n N_p = N_s \tag{7.2}$$

if we assume that every detection corresponds to only one photon. η is the detection efficiency, which here also should include the effects of scattering and absorption as the pluses travels through the optical setup, as well as imperfect alignments and focusing. In the ideal case of no other reduction in the efficiency than from the detectors, the detection efficiency would be around 60 %. Let's use this value for η as an upper limit. Inserting this and a value for $N_s = 4 \cdot 16 \cdot 10^3$, gives a value of n of the order of

$$n = \frac{N_s}{\eta N_p} = \frac{4 \cdot 16 \cdot 10^3}{0.6 \cdot 8 \cdot 10^6} \approx 0.1 \tag{7.3}$$

which is indeed less than one. Again, this assumes that each registration is a result of only a single photon.

If we try to describe the puled case in a photon picture, we obviously need to have at least two photons from the Mach-Zehnder interferometer within the coincidence window, to be able to register doubles and coincidences. If we assume that the above argumentation is right, and we actually do have less than one photon per part in the interferometer, getting two photons in the combined outgoing pulse will not be very likely, and getting more than two will be very unlikely. But if we in fact do have only two incoming photons, why don't we then get a behaviour in the coincidences which has the same behaviour as in the SPDC case? And why do we get a $\pi/4$ phase shift?

We can imagine at least three reasons for this:

1. There are contributions from parts which does not have orthogonal polarizations (as was discussed in the last chapter).

2. We have contributions to the coincidences which arises from two photons in the same arm in the interferometer (HH or VV) and therefore does not portray the expected behaviour as when we only have H and V.

3. We actually do have more than just one photon in each arm.

We cannot easily check the first reason, but if true, it would explain the difference in the behaviour of the coincidences compared to the SPDC case (the $\pi/4$ phase shift), since we then can have relations among the coincidences which are not related to the strict orthogonal relation of polarizations.

The second reason can in fact be calculated, that is, we can assume that the incoming photon-pair is $|HH\rangle$ or $|VV\rangle$ and calculate the probability for the coincidences following the same procedure as in section 6.2.1. Doing so does not, however, lead to predictions which does not agree with our measurements with the pulsed source.

For the third reason, that is, we assume that each of the parts in the interferometer are consisting of several photons, the pulse exiting the interferometer can be viewed as a mixture of several

photons with two orthogonal directions of linear polarization. In this picture, it is possible to have a splitting at the NPBS similar to what as discussed above, were both polarizations (both H and V) are exiting the NPBS. This could then result in the measured behaviour similar to the classical case, since we never get only one polarization in each of the arms of the NPBS. However, as was discussed above, it is not very likely that we have a high number of photons per part in the interferometer, simply by looking at the ratio between singles and doubles.

Can we then conclude that the combined pulses we have used in our experiments do in fact consist of less than a single photon? It is plausible, but yet somewhat odd that we don't get more similar results with the SPDC case. Either the registrations involving a strictly polarized and one close-to unpolarized part of light dominates the coincidence counts, or we cannot say that the strong attenuation of the light implies that we are working with single photons. In other words: that there is a difference between the photon from the crystal[3] and a photon from the pulsed source. The most likely scenario is probably the first of these, since this actually is a different physical effect which is not assumed to be present in the SPDC case.

At the end of section 2.2 we said that a Fock state could not be identified with classical fields even if the number of photons in this state would go to infinity, and in the footnote we asked whether this also was true in the opposite case (i.e. that we cannot go to a Fock state by reducing the intensity of the beam to single photon level). If we assume that we have attenuated the pulses to such a low level of intensity, the results that we have measured could seem to indicate that this statement is true. Thus, we should expect fluctuations in the photon number, and this is perhaps also the reason why we can have such a low average number of photons in each pulse and still observe doubles and coincidences.

7.4 Processes

From the foregoing discussions about the phase relation and interference effects due to the overlap of the two parts of a pulse, we have seen that it is possible to adjust these so that we obtain results which are somewhat similar to the SPDC case *without* the compensating crystal. The lack of strict control of the phase relation resulted in less pronounced behaviour when measured (such as the doubles and coincidences not going all the way down to zero). We can overcome this, as the theoretical simulation has shown, by using a stricter control of the phase relation.

Thus, we can tie some familiar classical effects to the results obtained with the SPDC without the CC, even though the indivisibility of the photon (or its polarization characteristics) has to be included in order to reach equal results. And indeed, it would seem probable, from the theoretical discussion in the last section, that if the polarization relations among the contributing light could be more strictly maintained, by increasing the stability in the amplitude of the pulse train and reducing the energy between the pulses, results more direct in line with the SPDC case without CC could be obtained.

In this way, the only real difference between the theory of the two cases (pulsed and SPDC without CC) would seem to be the requirement of the existence of a indivisible, smallest unit

[3]Remember that we are not requiring the photon to be entangled at this stage.

of light which retains its polarization when separated from a pair or group (i.e. the existence of a photon). All effects seen in the measurements would then follow from considerations of interference, phase shifts and the use of Malus' law applied to a large ensemble of detections. How the photon itself should be understood, however, is less clear.

If we now look at the case of SPDC *with* the compensating crystal, the situation is less clear in terms of responsible processes, but it is interesting to note that the measurement results with the pulsed source in a fixed scan in the diagonal basis, are, at least in the theoretical case, identical to the results from the SPDC case. A comparison is shown in Figure 7.6.

Although we have already concluded that this similarity does not mean that we have an entangled state in the pulsed case, it could be interesting to try to relate the results to familiar processes and try to apply these. In the pulsed case we are only considering the superposed polarization throughout the optical setup. The entangled photon pair seems to behave in a similar manner, i.e. as a superposition of the two polarizations. This is in some respects in line with the understanding of the concept of entanglement (there is no specified polarization of either photon before the measurement). Thus, even if we know that only a single photon enters each of the arms, we cannot tell which one and therefore the polarization remains as a possible superposition of the two orthogonal polarizations (H and V). This is similar to what we have said about the difference between the SPDC source with and without the CC. In the case of no CC we could treat the photons as individual entities and their registrations as separate events. This led to a calculation of the probability which could be calculated as a sum of squared amplitudes. When we had the CC in place, we had to square the sum of amplitudes, which would be in line with the idea of a superposed polarization.

This analogy is not working in the other scans however. The fixed scan in the zero basis is identical to the SPDC case without the CC (except for the doubles not reaching zero, compare figures 6.8 a-d and 6.9 a-d). In the SPDC without the CC we used a picture of localized photons with defined polarizations throughout the setup to obtain the correct behaviour. Thus, when the fixed HWP is set at 0° the picture is dominated by specified states of polarization (H and V), and when the HWP is set at 22.5° the picture gets dominated by undefined states of polarization (superposition of H and V). Thus, it would almost seem that depending on the setting of the fixed HWP before the PBS, i.e. into which basis we project, the behaviour of the coincidences varies between a specifically defined horizontal or vertical direction to a superposition of these two.

One could imagine that a twin scan then would be a mixture between these two situations, dominated by defined horizontal and vertical polarizations at 0°, 45° and 90°, and by superposed polarizations at 22.5° and 67.5°. However, such an approach does not give the correct predictions for all angles. Thus, using a picture of interference and superposition does not work.

We are somewhat limited in our capabilities to compare the entangled case with our measurements with the pulsed source, due to the lack of photon-pairs with strict orthogonal polarizations. It would seem clear from the discussion above that this requirement is necessary for obtaining similar results.

There is, however, also at least one parameter which we have not included in the setup, and that is the possible difference in frequency of the two parts in the Mach-Zehnder interferometer. It was disregarded due to the narrow width of the interference filter, but it is possible that it may have some effect not accounted for.

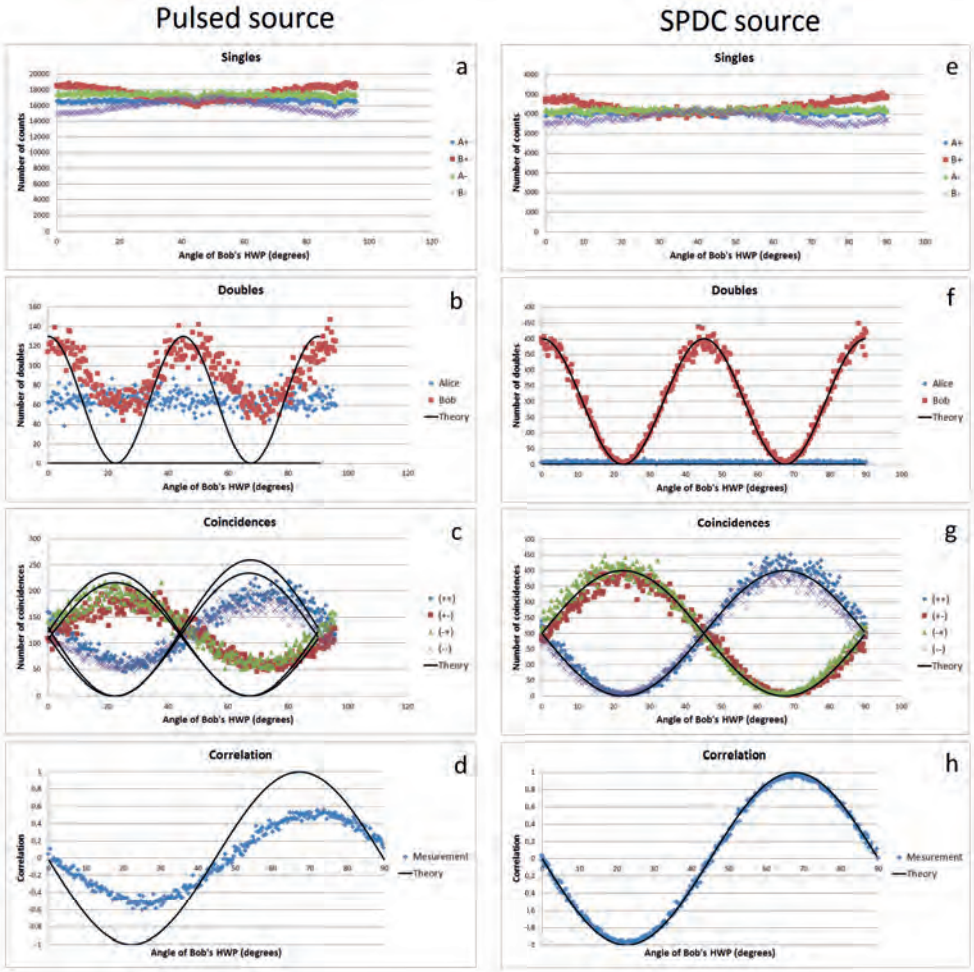

Figure 7.6: The measured results from a fixed scan with Alice in the diagonal basis with the pulsed source (left) and the SPDC source with CC (right). The theoretical plots (using the program found in the appendix for the pulsed source and the quantum mechanical calculation (equation (6.9)*) for the SPDC source) are included.*

7.5 Omitted parameters

In Paper A (see chapter 8) we are discussing the effects that a change in the temperature of the nonlinear crystal has on the measured outcomes. It turns out that the measured behaviour at certain temperatures of the crystal can only be explained if the constituents are considered to be fermions. This conclusion is obtained from the symmetry postulate, which states that a particular species of particles only can be of one symmetry type. For bosons, this requires the states to be symmetric, while for fermions they have to be anti-symmetric.

Now, the problem is of course that photons are bosons, so we shouldn't be able to observe the fermionic behaviour in our experiments. The fact that we still do so, would suggest that some other degree of freedom, not considered in our calculations, could be responsible. This degree of freedom has to be anti-symmetric so that the total quantum state can revoke its symmetry.

In a forthcoming publication we will show that the missing degree of freedom is tied to the difference in the frequency of the photons. Because even with very narrow bandwidth of 1 nm that we have in the interference filter we cannot assume that we only have a single frequency for every photon pair, when the temperature of the crystal is changed. What we must have, and this is one parameter which has not been considered in the pulsed source setup, is a variation in the frequencies which are located symmetrically around half of the pump frequency, as was mentioned in section 2.3.1. Thus, SPDC dictates that the sum of the frequencies of the two generated photons should equal the pump frequency

$$\omega_p = \omega_s + \omega_i \tag{7.4}$$

but ω_s does not necessarily have to be equal to ω_i.

But in what way does the exclusion of this possibility affect the outcomes from the pulsed source? This remains an open question since the effect wasn't included in the optical setup. However, if we allow ourselves to speculate we realize that we will no longer have a relationship between the polarizations which adds to a total linear diagonal polarization, not even in the theoretical case. If the polarizations were parallel we would see a beating effect when the frequencies are different. With orthogonal polarizations the superposed polarization will vary throughout the length of the combined pulse from the interferometer. This is exemplified in Figure 7.7, which shows the change in the total polarization when the frequencies of the two fields are the same (top), when the frequencies are differing by a ratio of 0.98 (middle) and when the ratio between the frequencies is 0.8 (bottom). The figure clearly shows how the polarization can change along the overlap.

We know that the polarization is an important parameter in the pulsed case (as we have argued for many times now) and it is therefore not entirely improbable that the effect of including different frequencies of the two parts would generate effects not seen so far in our setup. How these effects would affect the outcomes remains to be investigated.

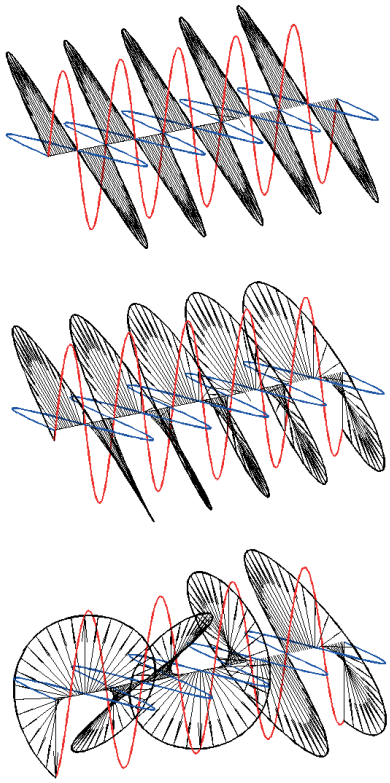

Figure 7.7: The change in the superposed polarization (here illustrated as black arrows) for two fields (red and blue) with linearly orthogonal polarizations and a frequency ratio of 1 (top), 0.98 (middle) and 0.8 (bottom). The clear deviation from a linear, diagonal polarization is seen for the cases when the frequencies are different.

7.6 Summary

We have in this thesis attempted to emulate the process of spontaneous parametric down-conversion in a non-linear ppKTP crystal by using weak pulses from an ultrafast Ti:sapphire laser. Especially, we compared with results based on entangled photon pairs and tried to relate these to familiar physical processes.

Our starting point was to achieve control over the parameters which from the quantum mechanical theory were said to the essential for the generation of entangled pairs, and relate these to our pulsed source. The most important effect was the relative timing of the photons at the detectors, and their polarization relation. We introduced these through a modified Mach-Zehnder

interferometer coupled to our ultrafast laser. In the pulsed case the timing was replaced by a control of the phase relation between the two parts, while the polarization was set by using half wave plates. The task of adjusting all the parameters to their optimal settings was not as simple as first assumed, and revealed complex and interconnected relations among the parameters.

But after substantial testing and characterisation of both the optical components and the pulses, we began conducting measurements both with the ppKTP crystal and the ultrafast laser as the source. For the crystal source we conducted measurements both with and without entangled photon-pairs. These were used as references in out attempts to obtain similar results with the pulsed source.

We could observe a number of similarities between the plots, especially when using unentangled photon pairs, but there were also differences. These differences were investigated and we found that it was actually possible to achieve results similar to the entangled case when using a very narrow coincidence window. Further investigation showed however that this effect could not be attributed to the state of entanglement, and we saw that Bell's inequality was not violated.

But we also saw differences which could not be removed by changing the settings of the parameters in the pulsed setup. It seemed that the behaviour of the polarization had to comply with the picture of indivisible entities of light to be able to give similar results as with the crystal source in *all* measurements. This led to an emphasising of the importance of including the full picture in the analysis in order to make valid conclusions.

It would also appear, although on a more speculative plane, that some differences might appear as a consequence of a less strict relationship between the polarizations of the light that is involved in the registrations. This could be a result of unwanted energy between the pulses in our pulse train, but would require a more thorough investigation before any definite conclusion can be drawn.

So what makes entangled photos entangled? In an overall conclusion we can say that certain features in the measurements made with the crystal source can be emulated with the pulsed source, but a full agreement in all measurements cannot. This is especially true in the entangled case, were the connection to general processes in *all* measurement scans could not be found. However, there were large uncertainties, instabilities and unknowns in the pulsed case, which both made it difficult to relate measurement results to real physical effects and to describe the detailed behaviour of the source. One of these unknowns which is of particular importance, is the question of the intensity level in the pulses, and the effect this would have on the results. Increased stability and improved control of the pulsed source should give a more definite answer.

References

[1] K. Michielsen and H. de Raedt, *Proc. of SPIE* **8832** 88321M-1 (2013)

[2] K. Michielsen, F. Jin and H. de Raedt, *Proc. of SPIE* **8832** 88321L-2 (2013)

[3] H. de Raedt, F. Jin and K. Michielsen, *Proc. of SPIE* **8832** 88321N-1 (2013)

[4] H. Chen, T. Peng, S. Karmakar and Y. Shih, *New J. Phys.* 13, 083018 **(2011)**

[5] H. Chen, T. Peng, and Y. Shih, *Phys. Rev. A* 88, 023808 **(2013)**

[6] R. Kaltenbaek, J. Lavoie, D. N. Biggerstaff, and K. J. Resch, *Nature Physics* **4**, 864 (2008)

[7] R. Kaltenbaek, J. Lavoie, and K. J. Resch, *Phys. Rev. Lett.* **102**, 243601 (2009)

[8] Y. Bromberg, Y. Lahini, R. Morandotti, and Y. Silberberg, *Phys. Rev. Lett.* **102**, 253904 (2009)

[9] V Torres-Company, H Lajunen, and A T Friberg, *New J. Phys.* **11**, 063041 (2009)

[10] J. H. Shapiro, *New J. Phys.* **14**, 058003 (2012)

[11] J. H. Shapiro and E. Lantz, *Phys. Rev. A* **85** 057801 (2012)

[12] R. Hanbury Brown and R.Q. Twiss, *Nature* **177**, 27 (1956)

Part V

Papers

Chapter 8

Published papers

Paper A: Observation of bosonic coalescence and fermionic anti-coalescence with indistinguishable photons

This first paper, published in the Proceedings of SPIE (*Proc. SPIE*, **8832**, 88321K-1 (2013)), discusses the measurement results obtained when the ppKTP crystal is not at the optimal temperature, and how these results should be understood then. It would appear that the photons no longer fulfills the symmetry requirement set by their bosonic nature at all temperatures, but can actually vary continuously between bosonic to fermionic behaviour as the temperature of the crystal is changed.

Paper B: What does the Hong-Ou-Mandel experiment really tell us about the nature of light?

The second paper, published in Quantum Matter (*Quantum Matter* **4**, 213-228 (2015)), is a review article about the Hong-Ou-Mandel effect, how it has been used and interpreted, and how the understanding of it has developed, from the time of its publication in 1986 until today. It also focuses on the connection with quantum optics and its role as a undisputable proof of the quantum nature of light.

Paper C: Observing quantum signatures of light from a classical source

The third paper, which is still in preparation, deals with the conclusions that can be made based on experimental results, and when these are valid. It shows that a measurement result, which in theory would only be possible in the quantum mechanical regime, also can be seen with classical light.

Part VI

Appendix

Appendix A

Programming codes

A.1 Matlab code for the autocorrelation function

Here follows the Matlab code for reading the data file containing the measurement of the autocorrelation function, and plotting it together with the theoretical calculated pulse (either Gaussian or sech^2).

```
clear all;
figure('Position',[100,50,1600,1000]);
fs = 1e15;                  % Conversion factor (s to fs)
w = 808;                    % Center wavelength of the interfering light in
                            % nm
S = 1e6;                    % Sample rate on the oscilloscope
lambda = w*10^(-9);         % The wavelength of the interfering light in m
c = 3e8;                    % Speed of light
omega = 2*pi*c/lambda;      % Angular frequency
x = -200e-15:1e-16:200e-15; % The distance or time travelled by the scanning
                            % pulse (the stationary pulse is fixed at x = 0)
t1 = -1:1e-4:1;             % Time range (should ideally go from -infinity
                            % to infinity)
E0 = 1;                     % Amplitude factor for the electric field
P0 = 1;                     % Amplitude factor for the Gaussian function

load M:\pc\Dokumenter\Experiment\Autocorrelation\ImprovedRatio\
ImprovedPeakToBackgroundRatio4.txt;
x1 = ImprovedPeakToBackgroundRatio4(:,1);
y1 = ImprovedPeakToBackgroundRatio4(:,2);

M = max(y1);        % Finding the maximum value of the amplitude
if min(y1)<0
    m = -min(y1);
    c = (M-m)/2;    % FWHM
else
    m = min(y1);    % Finding the minimum value of the amplitude
    c = (M+m)/2;    % FWHM
end
```

```
i = find(y1 > c);   % The index vector where the amplitude is larger
                    %  than the FWHM
i1 = i(1);          % The earliest value of the amplitude where amplitude is
                    % larger than the FWHM
i2 = i(size(i));    % The latest value of the amplitude where amplitude is
                    % larger than the FWHM

j = 0;
while i1+j<=i2(1)
    t(j+1)=x1(i1+j);   % A vector of the time values between the first and
                         last peak above FWHM
    a1(j+1)=y1(i1+j);  % A vector of the amplitudes between the first and
                         last peak above FWHM
    j = j + 1;
end
pks = findpeaks(a1);   % The number of peaks in this range
T = size(pks)*(w/1000000000)/300000000;  % The real time measured in this
                                         % range
avg = mean(y1(1:250000));                % Finding the background level and
                                         % uses it to scale the amplitude
plot((x1-mean(x1))*fs*S*(T/size(t)),(y1-m)/(avg-m),'k');

Time = (x1(i2)-x1(i1))*fs*S*(T/size(t));        % The FWHW duration time
annotation('textbox',[.65 .55 .1 .1],'String',['Measured FWHM pulse duration:
 ', num2str(Time(1),4), ' fs.'],'FontSize',14,'BackgroundColor',[1 1 1]);

hold;

% Gaussian pulse
%factor = 1.13;
%tau = Time(1)*10^(-15)*factor;   % The FWHM Gaussian pulse length
%annotation('textbox', [.65 .5 .1 .1],'String', ['Theoretical FWHM pulse
 duration: ', num2str(tau*10^(15),4), ' fs.'],'FontSize',14,'BackgroundColor',
 [1 1 1]);

%j = 0;
%while j < length(x)             % Calculates the intensity for every point
specified by x (i.e. as the scanning pulse moves across the stationary pulse)
%    j = j + 1;
%    n = 0;
%    A = 0;
%    while n < length(t1)        % "Integration" from t = -1 to 1 (~ -infinity
                                   to infinity)
%        n = n + 1;
%        P1 = E0*cos(-omega*t1(n))*P0*exp(-4*log(2)*(t1(n)/tau)^2);  % The
stationary pulse
%        P2 = E0*cos(-omega*(t1(n)+x(j)))*P0*exp(-4*log(2)*((t1(n)+x(j))
             /tau)^2);
% The scanning pulse
%        A = A + (abs((P1+P2)^2))^(3/2); % Not ^2 because we need to divide
```

```
                                        % by the square root of the
                                        % intensity itself
%    end
%    F1(j) =  A;       % The FRAC intensity when the scanning pulse is at
                         position x(j)
%end

%plot(x*10^(15),F1,'r');

% sech^2 pulse
factor = 0.648;
tau = Time(1)*10^(-15)*factor;  % The FWHM sech^2 pulse length
annotation('textbox', [.65 .5 .1 .1],'String', ['Theoretical FWHM pulse
 duration: ',num2str(tau*10^(15),4),' fs.'],'FontSize',14,'BackgroundColor',
 [1 1 1]);

j = 0;
while j < length(x)        % Calculates the intensity for every point
specified by x (i.e. as the scanning pulse moves across the stationary pulse)
    j = j + 1;
    n = 0;
    A = 0;
    while n < length(t1)   % "Integration" from t = -1 to 1
                           % (-infinity to infinity)
        n = n + 1;
        P1 = E0*cos(-omega*t1(n))*P0*(sech(t1(n)/tau))^2;
        P2 = E0*cos(-omega*(t1(n)+x(j)))*P0*(sech((t1(n)+x(j))/tau))^2;
        A = A + (abs((P1+P2)^2))^(3/2);
    end
    F2(j) =  A;            % The FRAC intensity when the scanning pulse is
                             at position x(j)
end

plot(x*10^(15),F2,'r');

grid(gca,'minor');
set(gca,'FontSize',14,'GridLineStyle', '-','Xgrid', 'on');
%set(gca,'YTickLabel',[]);
legend('Interferometric autocorrelation','Theoretical calculation');
xlabel('Time delay (fs)');
ylabel('Amplitude (arbitrary units)');
```

A.2 Matlab code for generating data files to be used in post-processing

The following program reads the raw data files generated from the Hydraharp during the measuerment process and compares the registered times with a theoretical pulse train as we would expect be generated from the Pockels cell had it had a 100 % extinction ratio. In order to find the

staring point, the measured time sequence is converted into a histogram with appropriate widths and is checked against the theoretical sequence in small steps covering the time period between two theoretical pulses. One a maximum value is found, the time displacement can be used as a given starting point for the analysis. A new displacement has to be found for every acquisition time (every second) due to the Hydraharp timing process. Only the raw data that can be found within the theoretical pulse train is saved in a new data file. These files can later be used in a post-processing analysis, similar to the one used during the measurements.

```
% This program takes raw data files from the HydraHarp and matches it to an
% assumed comb which would represent the theoretical output from the
% Pockels cell. By finding the overlap, a removal of the data points
% which are not due to the pulses can be done. The data can then be
% represented and analyzed in a familiar manner.

PulseWidth = 25000;
PCFreq = 100000;
M = 8000000;
sc = 1e12/M;
scale = 100/99.7510;
FileLocation = 'G:\Data2014\Testrun\December\04.12.2014\
TwinScanCheckAt3,6610mm\';
maxindex = 0;

filePattern = fullfile(FileLocation, '*.dat');
datFiles = dir(filePattern);

Name = sprintf('%sPostProcessed', FileLocation);
A = exist(Name,'dir');
if A == 0
    mkdir(FileLocation,'PostProcessed');
end

for k = 1:length(datFiles)/10
    tic;
    disp(sprintf('Processing file: Data%d-0.dat', k))
    baseFileName = sprintf('Data%d-0.dat', k);
    fullFileName = fullfile(FileLocation, baseFileName);
    Name = fopen(fullFileName);
    [D] = fscanf(Name, '%d %ld', [2 inf]);
    D = D';
    D1 = D(:,1);
    D2 = D(:,2);
    N = length(D2);
    fclose(Name);

    signal = zeros(M,1);
    for i = 1:N
        m = round(D2(i)/sc)+1;
        if m~=0 && m<=M
            signal(m) = signal(m) + 1;
```

```
    end;
end;

Ncomb = M + M/PCFreq + 1;
comb = zeros(Ncomb,1);
for i = 1:PCFreq-1
    h = round(M/PCFreq*scale*(i-1))+1;
    comb(h) = 1;
end;

shift = zeros(M/PCFreq,1);
scomb = zeros(M,1);
for i = 1:M/PCFreq
    for j = 1:M
        scomb(j) = comb(j+i);
    end;
    shift(i) = sum(signal.*scomb);
end;

maxindex = find(shift == max(shift));

if length(maxindex)~=1
    disp('The scale variable needs adjustment or the stated frequency
    of the Pockels cell is not the same as used in the measurement.')
    break;
else
    scomb2 = zeros(M,1);
    for j = 1:M
        scomb2(j) = comb(j+maxindex);
    end

    pulseInterv1 = zeros(M,1);
    pulseInterv2 = zeros(M,1);
    cntr = 1;

    for i = 1:M
        if scomb2(i) == 1
            pulseInterv1(cntr) = round(1+(i*sc)) - PulseWidth/2;
            pulseInterv2(cntr) = pulseInterv1(cntr) + PulseWidth;
            cntr = cntr+1;
        end;
    end;

    for l = 0:2
        for n = l+1:3
            if n > 3
                break;
            end;
            disp(sprintf('Processing file: Data%d-%d%d.dat', k, l, n))
            baseFileName = sprintf('Data%d-%d%d.dat', k, l, n);
            fullFileName = fullfile(FileLocation, baseFileName);
```

```
                Name = fopen(fullFileName);
                [D] = fscanf(Name, '%d %ld', [2 inf]);
                D = D';
                D1 = D(:,1);
                D2 = D(:,2);
                N = length(D2);
                fclose(Name);

                NumberOfRegistrations = 1;
                NumberOfPulses = 1;
                j = 1;

                while j<N && NumberOfPulses<M
                    while D2(j)<pulseInterv1(NumberOfPulses)
                        j = j+1;
                        if (j>N)
                            j = N;
                            break;
                        end;
                    end;
                    while (D2(j)>=pulseInterv1(NumberOfPulses))&&(D2(j)<=
                    pulseInterv2(NumberOfPulses))&&(j<=N)
                        VAL(NumberOfRegistrations) = D2(j);
                        VAL2(NumberOfRegistrations) = D1(j);
                        NumberOfRegistrations = NumberOfRegistrations+1;
                        j = j+1;
                        if (j>N)
                            break;
                        end;
                    end;
                    NumberOfPulses = NumberOfPulses+1;
                end;
                NumberOfRegistrations = NumberOfRegistrations - 1;

                NewName = sprintf('%sPostProcessed\\%s', FileLocation,
                 baseFileName);
                fid = fopen(NewName,'wt');
                for i = 1:NumberOfRegistrations
                    fprintf(fid,'%d \t %ld \n',VAL2(i),VAL(i));
                end;
                fclose(fid);
            end;
        end;
    end;
    toc;
end;
```

A.3 Matlab code for modelling singles, doubles, coincidences and the correlation with classical pulses

This program calculates and displays the behaviour of the singles, doubles, coincidences and the correlation in a twin scan for two similar interacting pulses with orthogonal polarizations. It is simplified, because it does not include the effect of the coincidence window, but assumes that the pulses are arriving at the detectors simultaneously and that only such a process generates doubles and coincidences.

```
% This program simulates the processes that occurs during the measurment
% process using the pulsed source, and plots the singles, doubles,
% coincideneces and the correlation.

clear all;

lambda = 810e-9;            % Wavelength (assumes this to be constant
                            % although we have a 1 nm bandwidth)
c = 3e8;                    % Speed of light
hbar = 6.63e-34/(2*pi);
omega = 2*pi*c/lambda;      % Angular frequency
t = -1e-11:1e-15:1e-11;     % Time range that the pulses span
E1 = 2e-8;                  % Amplitude factor for the electric field
                            % for the transmitted pulse
E2 = 2e-8;                  % Amplitude factor for the electric field
                            % for the reflected pulse
P1 = 1;                     % Amplitude factor for the Gaussian function
                            % for the transmitted pulse
P2 = 1;                     % Amplitude factor for the Gaussian function
                            % for the reflected pulse
tau = 1e-12;                % The FWHM Gaussian pulse length (in s)
thetaA = 0:0.01:pi/2;
thetaB = 0:0.01:pi/2;
theta3 = 0;
tc = 8e-9;                  % Coincidence time
Ep = hbar*omega;
x = zeros(1,2);
x(1) = 0;
x(2) = lambda/(2*c);

IAH1 = zeros(1,length(thetaA));
IAV1 = zeros(1,length(thetaA));
IBH1 = zeros(1,length(thetaB));
IBV1 = zeros(1,length(thetaB));
IAH2 = zeros(1,length(thetaA));
IAV2 = zeros(1,length(thetaA));
IBH2 = zeros(1,length(thetaB));
IBV2 = zeros(1,length(thetaB));
DoublesAlice1 = zeros(1,length(thetaA));
DoublesBob1 = zeros(1,length(thetaB));
DoublesAlice2 = zeros(1,length(thetaA));
```

```
DoublesBob2 = zeros(1,length(thetaB));
PP1 = zeros(1,length(thetaA));
PM1 = zeros(1,length(thetaA));
MP1 = zeros(1,length(thetaA));
MM1 = zeros(1,length(thetaA));
PP2 = zeros(1,length(thetaA));
PM2 = zeros(1,length(thetaA));
MP2 = zeros(1,length(thetaA));
MM2 = zeros(1,length(thetaA));
Correlation1 = zeros(1,length(thetaA));
Correlation2 = zeros(1,length(thetaA));
Correlation = zeros(1,length(thetaA));

% Twin scan:
l = 0;
while l < length(thetaA)
    l = l + 1;
    m = 0;
    AHH1 = 0;
    AVV1 = 0;
    BHH1 = 0;
    BVV1 = 0;
    AHH2 = 0;
    AVV2 = 0;
    BHH2 = 0;
    BVV2 = 0;
    AD1 = 0;
    BD1 = 0;
    AD2 = 0;
    BD2 = 0;
    pp1 = 0;
    pm1 = 0;
    mp1 = 0;
    mm1 = 0;
    pp2 = 0;
    pm2 = 0;
    mp2 = 0;
    mm2 = 0;
    while m < length(x)
        m = m  + 1;
        n = 0;
        AH = 0;
        AV = 0;
        BH = 0;
        BV = 0;
        if m == 1
            while n < length(t)
                n = n + 1;
                if theta3+thetaA(l) < pi/4
                    AH1 = (E1*cos(-omega*(t(n)+x(m)))*P1*exp(-4*log(2)
                    *((t(n)+x(m))/tau)^2))*cos(theta3+2*thetaA(l));
```

```
            AH2 = (E2*cos(-omega*t(n))*P2*exp(-4*log(2)*(t(n)
            /tau)^2))*cos(theta3+pi/2-2*thetaA(l));
        else
            AH1 = (E1*cos(-omega*(t(n)+x(m)))*P1*exp(-4*log(2)
            *((t(n)+x(m))/tau)^2))*(-cos(theta3+pi-2*thetaA(l)));
            AH2 = (E2*cos(-omega*t(n))*P2*exp(-4*log(2)*(t(n)
            /tau)^2))*cos(theta3+pi/2-2*thetaA(l));
        end;
        AH = AH + AH1 + AH2;

        if theta3+thetaA(l) < pi/4
            AV1 = (E1*cos(-omega*(t(n)+x(m)))*P1*exp(-4*log(2)
            *((t(n)+x(m))/tau)^2))*(sin(theta3+2*thetaA(l)));
            AV2 = (E2*cos(-omega*t(n))*P2*exp(-4*log(2)*(t(n)
            /tau)^2))*(-sin(theta3+pi/2-2*thetaA(l)));
        else
            AV1 = (E1*cos(-omega*(t(n)+x(m)))*P1*exp(-4*log(2)
            *((t(n)+x(m))/tau)^2))*sin(theta3+pi-2*thetaA(l));
            AV2 = (E2*cos(-omega*t(n))*P2*exp(-4*log(2)*(t(n)
            /tau)^2))*(-sin(theta3+pi/2-2*thetaA(l)));
        end;
        AV = AV + AV1 + AV2;

        if theta3+thetaA(l) < pi/4
            BH1 = (E1*cos(-omega*(t(n)+x(m)))*P1*exp(-4*log(2)
            *((t(n)+x(m))/tau)^2))*(-cos(theta3+2*thetaA(l)));
            BH2 = (E2*cos(-omega*t(n))*P2*exp(-4*log(2)*(t(n)
            /tau)^2))*(cos(theta3+pi/2-2*thetaA(l)));
        else
            BH1 = (E1*cos(-omega*(t(n)+x(m)))*P1*exp(-4*log(2)
            *((t(n)+x(m))/tau)^2))*(cos(theta3+pi-2*thetaA(l)));
            BH2 = (E2*cos(-omega*t(n))*P2*exp(-4*log(2)*(t(n)
            /tau)^2))*(cos(theta3+2*thetaA(l)-pi/2));
        end;
        BH = BH + BH1 + BH2;

        if theta3+thetaA(l) < pi/4
            BV1 = (E1*cos(-omega*(t(n)+x(m)))*P1*exp(-4*log(2)
            *((t(n)+x(m))/tau)^2))*(-sin(theta3+2*thetaA(l)));
            BV2 = (E2*cos(-omega*t(n))*P2*exp(-4*log(2)*(t(n)
            /tau)^2))*(-sin(theta3+pi/2-2*thetaA(l)));
        else
            BV1 = (E1*cos(-omega*(t(n)+x(m)))*P1*exp(-4*log(2)
            *((t(n)+x(m))/tau)^2))*(-sin(theta3+pi-2*thetaA(l)));
            BV2 = (E2*cos(-omega*t(n))*P2*exp(-4*log(2)*(t(n)
            /tau)^2))*(sin(theta3+2*thetaA(l)-pi/2));
        end;
        BV = BV + BV1 + BV2;
    end;
    AHH1 = AHH1 + AH;
    AVV1 = AVV1 + AV;
```

```
    BHH1 = BHH1 + BH;
    BVV1 = BVV1 + BV;

    AD1 = AD1 + AH*AV;
    BD1 = BD1 + BH*BV;

    pp1 = pp1 + AH*BH;
    pm1 = pm1 + AH*BV;
    mp1 = mp1 + AV*BH;
    mm1 = mm1 + AV*BV;
else
    while n < length(t)
        n = n + 1;
        if theta3+thetaA(l) < pi/4
            AH1 = (E1*cos(-omega*(t(n)+x(m)))*P1*exp(-4*log(2)
            *((t(n)+x(m))/tau)^2))*cos(theta3+2*thetaA(l));
            AH2 = (E2*cos(-omega*t(n))*P2*exp(-4*log(2)*(t(n)
            /tau)^2))*cos(theta3+pi/2-2*thetaA(l));
        else
            AH1 = (E1*cos(-omega*(t(n)+x(m)))*P1*exp(-4*log(2)
            *((t(n)+x(m))/tau)^2))*(-cos(theta3+pi-2*thetaA(l)));
            AH2 = (E2*cos(-omega*t(n))*P2*exp(-4*log(2)*(t(n)
            /tau)^2))*cos(theta3+pi/2-2*thetaA(l));
        end;
        AH = AH + AH1 + AH2;

        if theta3+thetaA(l) < pi/4
            AV1 = (E1*cos(-omega*(t(n)+x(m)))*P1*exp(-4*log(2)
            *((t(n)+x(m))/tau)^2))*(sin(theta3+2*thetaA(l)));
            AV2 = (E2*cos(-omega*t(n))*P2*exp(-4*log(2)*(t(n)
            /tau)^2))*(-sin(theta3+pi/2-2*thetaA(l)));
        else
            AV1 = (E1*cos(-omega*(t(n)+x(m)))*P1*exp(-4*log(2)
            *((t(n)+x(m))/tau)^2))*sin(theta3+pi-2*thetaA(l));
            AV2 = (E2*cos(-omega*t(n))*P2*exp(-4*log(2)*(t(n)
            /tau)^2))*(-sin(theta3+pi/2-2*thetaA(l)));
        end;
        AV = AV + AV1 + AV2;

        if theta3+thetaA(l) < pi/4
            BH1 = (E1*cos(-omega*(t(n)+x(m)))*P1*exp(-4*log(2)
            *((t(n)+x(m))/tau)^2))*(-cos(theta3+2*thetaA(l)));
            BH2 = (E2*cos(-omega*t(n))*P2*exp(-4*log(2)*(t(n)
            /tau)^2))*(cos(theta3+pi/2-2*thetaA(l)));
        else
            BH1 = (E1*cos(-omega*(t(n)+x(m)))*P1*exp(-4*log(2)
            *((t(n)+x(m))/tau)^2))*(cos(theta3+pi-2*thetaA(l)));
            BH2 = (E2*cos(-omega*t(n))*P2*exp(-4*log(2)*(t(n)
            /tau)^2))*(cos(theta3+2*thetaA(l)-pi/2));
        end;
        BH = BH + BH1 + BH2;
```

```
            if theta3+thetaA(l) < pi/4
                BV1 = (E1*cos(-omega*(t(n)+x(m)))*P1*exp(-4*log(2)
                *((t(n)+x(m))/tau)^2))*(-sin(theta3+2*thetaA(l)));
                BV2 = (E2*cos(-omega*t(n))*P2*exp(-4*log(2)*(t(n)
                /tau)^2))*(-sin(theta3+pi/2-2*thetaA(l)));
            else
                BV1 = (E1*cos(-omega*(t(n)+x(m)))*P1*exp(-4*log(2)
                *((t(n)+x(m))/tau)^2))*(-sin(theta3+pi-2*thetaA(l)));
                BV2 = (E2*cos(-omega*t(n))*P2*exp(-4*log(2)*(t(n)
                /tau)^2))*(sin(theta3+2*thetaA(l)-pi/2));
            end;
            BV = BV + BV1 + BV2;
        end;
        AHH2 = AHH2 + AH;
        AVV2 = AVV2 + AV;
        BHH2 = BHH2 + BH;
        BVV2 = BVV2 + BV;

        AD2 = AD2 + AH*AV;
        BD2 = BD2 + BH*BV;

        pp2 = pp2 + AH*BH;
        pm2 = pm2 + AH*BV;
        mp2 = mp2 + AV*BH;
        mm2 = mm2 + AV*BV;

    end;
end;

IAH1(l) = abs(AHH1)^2;
IAV1(l) = abs(AVV1)^2;
IBH1(l) = abs(BHH1)^2;
IBV1(l) = abs(BVV1)^2;

IAH2(l) = abs(AHH2)^2;
IAV2(l) = abs(AVV2)^2;
IBH2(l) = abs(BHH2)^2;
IBV2(l) = abs(BVV2)^2;

DoublesAlice1(l) = IAH1(l)*IAV1(l);
DoublesBob1(l) = IBH1(l)*IBV1(l);

DoublesAlice2(l) = IAH2(l)*IAV2(l);
DoublesBob2(l) = IBH2(l)*IBV2(l);

PP1(l) = IAH1(l)*IBH1(l);
PM1(l) = IAH1(l)*IBV1(l);
MP1(l) = IAV1(l)*IBH1(l);
MM1(l) = IAV1(l)*IBV1(l);
```

```
    PP2(l) = IAH2(l)*IBH2(l);
    PM2(l) = IAH2(l)*IBV2(l);
    MP2(l) = IAV2(l)*IBH2(l);
    MM2(l) = IAV2(l)*IBV2(l);

    Correlation1(l) = (PP1(l)+MM1(l)-PM1(l)-MP1(l))/
    (PP1(l)+MM1(l)+PM1(l)+MP1(l));
    Correlation2(l) = (PP2(l)+MM2(l)-PM2(l)-MP2(l))/
    (PP2(l)+MM2(l)+PM2(l)+MP2(l));
    Correlation(l)=(PP1(l)+MM1(l)-PM1(l)-MP1(l)+PP2(l)+MM2(l)-PM2(l)
    -MP2(l))/(PP1(l)+MM1(l)+PM1(l)+MP1(l)+PP2(l)+MM2(l)+PM2(l)+MP2(l));
end;

figure;
plot(thetaA,IAH1+IAH2,'color', [0.3098,0.5059,0.7412],'LineWidth',2);
hold;
plot(thetaA,IAV1+IAV2,'color', [0.7529,0.2778,0.3020],'LineWidth',2);
plot(thetaA,IBH1+IBH2,'color', [0.6078,0.7333,0.3490],'LineWidth',2);
plot(thetaA,IBV1+IBV2,'color', [0.5020,0.3922,0.6353],'LineWidth',2);
title('Singles');
set(gca,'XTick',0:pi/8:pi/2)
set(gca,'YTickLabel','')
set(gca,'XTickLabel',{'0','22,5','45','67,5','90'})
limsy = get(gca,'YLim');
set(gca,'Ylim',[0 limsy(2)]);

figure;
plot(thetaA,DoublesAlice1+DoublesAlice2,'color', [0.3098,0.5059,0.7412],
'LineWidth',2);
hold;
plot(thetaA,DoublesBob1+DoublesBob2,'color', [0.7529,0.2778,0.3020],
'LineWidth',2);
title('Doubles');
set(gca,'XTick',0:pi/8:pi/2)
set(gca,'YTickLabel','')
set(gca,'XTickLabel',{'0','22,5','45','67,5','90'})

figure;
plot(thetaA,PP1+PP2,'color', [0.3098,0.5059,0.7412],'LineWidth',2);
hold;
plot(thetaA,MM1+MM2,'color', [0.5020,0.3922,0.6353],'LineWidth',2);
plot(thetaA,PM1+PM2,'color', [0.7529,0.2778,0.3020],'LineWidth',2);
plot(thetaA,MP1+MP2,'color', [0.6078,0.7333,0.3490],'LineWidth',2);
title('Coincidences');
set(gca,'XTick',0:pi/8:pi/2)
set(gca,'YTickLabel','')
set(gca,'XTickLabel',{'0','22,5','45','67,5','90'})

figure;
plot(thetaA,Correlation,'color', [0.3098,0.5059,0.7412],'LineWidth',2);
title('Correlation');
```

```
set(gca,'YLim',[-1 1])
set(gca,'XTick',0:pi/8:pi/2)
set(gca,'XTickLabel',{'0','22,5','45','67,5','90'})

% Fixed scan (Alice fixed)
l = 0;
thetaAlice = pi/8;
while l < length(thetaB)
    l = l + 1;
    m = 0;
    AHH1 = 0;
    AVV1 = 0;
    BHH1 = 0;
    BVV1 = 0;
    AHH2 = 0;
    AVV2 = 0;
    BHH2 = 0;
    BVV2 = 0;
    AD1 = 0;
    BD1 = 0;
    AD2 = 0;
    BD2 = 0;
    pp1 = 0;
    pm1 = 0;
    mp1 = 0;
    mm1 = 0;
    pp2 = 0;
    pm2 = 0;
    mp2 = 0;
    mm2 = 0;
    while m < length(x)
        m = m  + 1;
        n = 0;
        AH = 0;
        AV = 0;
        BH = 0;
        BV = 0;
        if m == 1
            while n < length(t)
                n = n + 1;
                if theta3+thetaAlice < pi/4
                    AH1 = (E1*cos(-omega*(t(n)+x(m)))*P1*exp(-4*log(2)
                    *((t(n)+x(m))/tau)^2))*cos(theta3+2*thetaAlice);
                    AH2 = (E2*cos(-omega*t(n))*P2*exp(-4*log(2)*(t(n)
                    /tau)^2))*cos(theta3+pi/2-2*thetaAlice);
                else
                    AH1 = (E1*cos(-omega*(t(n)+x(m)))*P1*exp(-4*log(2)
                    *((t(n)+x(m))/tau)^2))*(-cos(theta3+pi-2*thetaAlice));
                    AH2 = (E2*cos(-omega*t(n))*P2*exp(-4*log(2)*(t(n)
                    /tau)^2))*cos(theta3+pi/2-2*thetaAlice);
                end;
```

```
    AH = AH + AH1 + AH2;

    if theta3+thetaAlice < pi/4
        AV1 = (E1*cos(-omega*(t(n)+x(m)))*P1*exp(-4*log(2)
        *((t(n)+x(m))/tau)^2))*(sin(theta3+2*thetaAlice));
        AV2 = (E2*cos(-omega*t(n))*P2*exp(-4*log(2)*(t(n)
        /tau)^2))*(-sin(theta3+pi/2-2*thetaAlice));
    else
        AV1 = (E1*cos(-omega*(t(n)+x(m)))*P1*exp(-4*log(2)
        *((t(n)+x(m))/tau)^2))*sin(theta3+pi-2*thetaAlice);
        AV2 = (E2*cos(-omega*t(n))*P2*exp(-4*log(2)*(t(n)
        /tau)^2))*(-sin(theta3+pi/2-2*thetaAlice));
    end;
    AV = AV + AV1 + AV2;

    if theta3+thetaB(l) < pi/4
        BH1 = (E1*cos(-omega*(t(n)+x(m)))*P1*exp(-4*log(2)
        *((t(n)+x(m))/tau)^2))*(-cos(theta3+2*thetaB(l)));
        BH2 = (E2*cos(-omega*t(n))*P2*exp(-4*log(2)*(t(n)
        /tau)^2))*(cos(theta3+pi/2-2*thetaB(l)));
    else
        BH1 = (E1*cos(-omega*(t(n)+x(m)))*P1*exp(-4*log(2)
        *((t(n)+x(m))/tau)^2))*(cos(theta3+pi-2*thetaB(l)));
        BH2 = (E2*cos(-omega*t(n))*P2*exp(-4*log(2)*(t(n)
        /tau)^2))*(cos(theta3+2*thetaB(l)-pi/2));
    end;
    BH = BH + BH1 + BH2;

    if theta3+thetaB(l) < pi/4
        BV1 = (E1*cos(-omega*(t(n)+x(m)))*P1*exp(-4*log(2)
        *((t(n)+x(m))/tau)^2))*(-sin(theta3+2*thetaB(l)));
        BV2 = (E2*cos(-omega*t(n))*P2*exp(-4*log(2)*(t(n)
        /tau)^2))*(-sin(theta3+pi/2-2*thetaB(l)));
    else
        BV1 = (E1*cos(-omega*(t(n)+x(m)))*P1*exp(-4*log(2)
        *((t(n)+x(m))/tau)^2))*(-sin(theta3+pi-2*thetaB(l)));
        BV2 = (E2*cos(-omega*t(n))*P2*exp(-4*log(2)*(t(n)
        /tau)^2))*(sin(theta3+2*thetaB(l)-pi/2));
    end;
    BV = BV + BV1 + BV2;
end;
AHH1 = AHH1 + AH;
AVV1 = AVV1 + AV;
BHH1 = BHH1 + BH;
BVV1 = BVV1 + BV;

AD1 = AD1 + AH*AV;
BD1 = BD1 + BH*BV;

pp1 = pp1 + AH*BH;
pm1 = pm1 + AH*BV;
```

```
        mp1 = mp1 + AV*BH;
        mm1 = mm1 + AV*BV;
    else
        while n < length(t)
            n = n + 1;
            if theta3+thetaAlice < pi/4
                AH1 = (E1*cos(-omega*(t(n)+x(m)))*P1*exp(-4*log(2)
                *((t(n)+x(m))/tau)^2))*cos(theta3+2*thetaAlice);
                AH2 = (E2*cos(-omega*t(n))*P2*exp(-4*log(2)*(t(n)
                /tau)^2))*cos(theta3+pi/2-2*thetaAlice);
            else
                AH1 = (E1*cos(-omega*(t(n)+x(m)))*P1*exp(-4*log(2)
                *((t(n)+x(m))/tau)^2))*(-cos(theta3+pi-2*thetaAlice));
                AH2 = (BG+E2*cos(-omega*t(n))*P2*exp(-4*log(2)*(t(n)
                /tau)^2))*cos(theta3+pi/2-2*thetaAlice);
            end;
            AH = AH + AH1 + AH2;

            if theta3+thetaAlice < pi/4
                AV1 = (E1*cos(-omega*(t(n)+x(m)))*P1*exp(-4*log(2)
                *((t(n)+x(m))/tau)^2))*(sin(theta3+2*thetaAlice));
                AV2 = (E2*cos(-omega*t(n))*P2*exp(-4*log(2)*(t(n)
                /tau)^2))*(-sin(theta3+pi/2-2*thetaAlice));
            else
                AV1 = (E1*cos(-omega*(t(n)+x(m)))*P1*exp(-4*log(2)
                *((t(n)+x(m))/tau)^2))*sin(theta3+pi-2*thetaAlice);
                AV2 = (E2*cos(-omega*t(n))*P2*exp(-4*log(2)*(t(n)
                /tau)^2))*(-sin(theta3+pi/2-2*thetaAlice));
            end;
            AV = AV + AV1 + AV2;

            if theta3+thetaB(l) < pi/4
                BH1 = (E1*cos(-omega*(t(n)+x(m)))*P1*exp(-4*log(2)
                *((t(n)+x(m))/tau)^2))*(-cos(theta3+2*thetaB(l)));
                BH2 = (E2*cos(-omega*t(n))*P2*exp(-4*log(2)*(t(n)
                /tau)^2))*(cos(theta3+pi/2-2*thetaB(l)));
            else
                BH1 = (E1*cos(-omega*(t(n)+x(m)))*P1*exp(-4*log(2)
                *((t(n)+x(m))/tau)^2))*(cos(theta3+pi-2*thetaB(l)));
                BH2 = (E2*cos(-omega*t(n))*P2*exp(-4*log(2)*(t(n)
                /tau)^2))*(cos(theta3+2*thetaB(l)-pi/2));
            end;
            BH = BH + BH1 + BH2;

            if theta3+thetaB(l) < pi/4
                BV1 = (E1*cos(-omega*(t(n)+x(m)))*P1*exp(-4*log(2)
                *((t(n)+x(m))/tau)^2))*(-sin(theta3+2*thetaB(l)));
                BV2 = (E2*cos(-omega*t(n))*P2*exp(-4*log(2)*(t(n)
                /tau)^2))*(-sin(theta3+pi/2-2*thetaB(l)));
            else
                BV1 = (E1*cos(-omega*(t(n)+x(m)))*P1*exp(-4*log(2)
```

```
                *((t(n)+x(m))/tau)^2))*(-sin(theta3+pi-2*thetaB(l)));
                BV2 = (E2*cos(-omega*t(n))*P2*exp(-4*log(2)*(t(n)
                /tau)^2))*(sin(theta3+2*thetaB(l)-pi/2));
            end;
            BV = BV + BV1 + BV2;
        end;
        AHH2 = AHH2 + AH;
        AVV2 = AVV2 + AV;
        BHH2 = BHH2 + BH;
        BVV2 = BVV2 + BV;

        AD2 = AD2 + AH*AV;
        BD2 = BD2 + BH*BV;

        pp2 = pp2 + AH*BH;
        pm2 = pm2 + AH*BV;
        mp2 = mp2 + AV*BH;
        mm2 = mm2 + AV*BV;

    end;
end;

IAH1(l) = abs(AHH1)^2;
IAV1(l) = abs(AVV1)^2;
IBH1(l) = abs(BHH1)^2;
IBV1(l) = abs(BVV1)^2;

IAH2(l) = abs(AHH2)^2;
IAV2(l) = abs(AVV2)^2;
IBH2(l) = abs(BHH2)^2;
IBV2(l) = abs(BVV2)^2;

DoublesAlice1(l) = IAH1(l)*IAV1(l);
DoublesBob1(l) = IBH1(l)*IBV1(l);

DoublesAlice2(l) = IAH2(l)*IAV2(l);
DoublesBob2(l) = IBH2(l)*IBV2(l);

PP1(l) = IAH1(l)*IBH1(l);
PM1(l) = IAH1(l)*IBV1(l);
MP1(l) = IAV1(l)*IBH1(l);
MM1(l) = IAV1(l)*IBV1(l);

PP2(l) = IAH2(l)*IBH2(l);
PM2(l) = IAH2(l)*IBV2(l);
MP2(l) = IAV2(l)*IBH2(l);
MM2(l) = IAV2(l)*IBV2(l);

Correlation1(l) = (PP1(l)+MM1(l)-PM1(l)-MP1(l))/
(PP1(l)+MM1(l)+PM1(l)+MP1(l));
Correlation2(l) = (PP2(l)+MM2(l)-PM2(l)-MP2(l))/
```

```
    (PP2(l)+MM2(l)+PM2(l)+MP2(l));
    Correlation(l)=(PP1(l)+MM1(l)-PM1(l)-MP1(l)+PP2(l)+MM2(l)-PM2(l)
    -MP2(l))/(PP1(l)+MM1(l)+PM1(l)+MP1(l)+PP2(l)+MM2(l)+PM2(l)+MP2(l));
end;

figure;
plot(thetaB,IAH1+IAH2,'color', [0.3098,0.5059,0.7412],'LineWidth',2);
hold;
plot(thetaB,IAV1+IAV2,'color', [0.7529,0.2778,0.3020],'LineWidth',2);
plot(thetaB,IBH1+IBH2,'color', [0.6078,0.7333,0.3490],'LineWidth',2);
plot(thetaB,IBV1+IBV2,'color', [0.5020,0.3922,0.6353],'LineWidth',2);
title('Singles');
set(gca,'XTick',0:pi/8:pi/2)
set(gca,'YTickLabel','')
set(gca,'XTickLabel',{'0','22,5','45','67,5','90'})
limsy = get(gca,'YLim');
set(gca,'Ylim',[0 limsy(2)]);

figure;
plot(thetaB,DoublesAlice1+DoublesAlice2,'color', [0.3098,0.5059,0.7412],
'LineWidth',2);
hold;
plot(thetaB,DoublesBob1+DoublesBob2,'color', [0.7529,0.2778,0.3020],
'LineWidth',2);
title('Doubles');
set(gca,'XTick',0:pi/8:pi/2)
set(gca,'YTickLabel','')
set(gca,'XTickLabel',{'0','22,5','45','67,5','90'})

figure;
plot(thetaB,PP1+PP2,'color', [0.3098,0.5059,0.7412],'LineWidth',2);
hold;
plot(thetaB,MM1+MM2,'color', [0.5020,0.3922,0.6353],'LineWidth',2);
plot(thetaB,PM1+PM2,'color', [0.7529,0.2778,0.3020],'LineWidth',2);
plot(thetaB,MP1+MP2,'color', [0.6078,0.7333,0.3490],'LineWidth',2);
title('Coincidences');
set(gca,'XTick',0:pi/8:pi/2)
set(gca,'YTickLabel','')
set(gca,'XTickLabel',{'0','22,5','45','67,5','90'})

figure;
plot(thetaB,Correlation,'color', [0.3098,0.5059,0.7412],'LineWidth',2);
title('Correlation');
set(gca,'YLim',[-1 1])
set(gca,'XTick',0:pi/8:pi/2)
set(gca,'XTickLabel',{'0','22,5','45','67,5','90'})


%Fixed scan (Bob fixed)
l = 0;
thetaBob = 0;
```

```
while l < length(thetaB)
    l = l + 1;
    m = 0;
    AHH1 = 0;
    AVV1 = 0;
    BHH1 = 0;
    BVV1 = 0;
    AHH2 = 0;
    AVV2 = 0;
    BHH2 = 0;
    BVV2 = 0;
    AD1 = 0;
    BD1 = 0;
    AD2 = 0;
    BD2 = 0;
    pp1 = 0;
    pm1 = 0;
    mp1 = 0;
    mm1 = 0;
    pp2 = 0;
    pm2 = 0;
    mp2 = 0;
    mm2 = 0;
    while m < length(x)
        m = m  + 1;
        n = 0;
        AH = 0;
        AV = 0;
        BH = 0;
        BV = 0;
        if m == 1
            while n < length(t)
                n = n + 1;
                if theta3+thetaA(l) < pi/4
                    AH1 = (E1*cos(-omega*(t(n)+x(m)))*P1*exp(-4*log(2)
                    *((t(n)+x(m))/tau)^2))*cos(theta3+2*thetaA(l));
                    AH2 = (E2*cos(-omega*t(n))*P2*exp(-4*log(2)*(t(n)
                    /tau)^2))*cos(theta3+pi/2-2*thetaA(l));
                else
                    AH1 = (E1*cos(-omega*(t(n)+x(m)))*P1*exp(-4*log(2)
                    *((t(n)+x(m))/tau)^2))*(-cos(theta3+pi-2*thetaA(l)));
                    AH2 = (E2*cos(-omega*t(n))*P2*exp(-4*log(2)*(t(n)
                    /tau)^2))*cos(theta3+pi/2-2*thetaA(l));
                end;
                AH = AH + AH1 + AH2;

                if theta3+thetaA(l) < pi/4
                    AV1 = (E1*cos(-omega*(t(n)+x(m)))*P1*exp(-4*log(2)
                    *((t(n)+x(m))/tau)^2))*(sin(theta3+2*thetaA(l)));
                    AV2 = (E2*cos(-omega*t(n))*P2*exp(-4*log(2)*(t(n)
                    /tau)^2))*(-sin(theta3+pi/2-2*thetaA(l)));
```

```
            else
                AV1 = (E1*cos(-omega*(t(n)+x(m)))*P1*exp(-4*log(2)
                *((t(n)+x(m))/tau)^2))*sin(theta3+pi-2*thetaA(l));
                AV2 = (E2*cos(-omega*t(n))*P2*exp(-4*log(2)*(t(n)
                /tau)^2))*(-sin(theta3+pi/2-2*thetaA(l)));
            end;
            AV = AV + AV1 + AV2;

            if theta3+thetaBob < pi/4
                BH1 = (E1*cos(-omega*(t(n)+x(m)))*P1*exp(-4*log(2)
                *((t(n)+x(m))/tau)^2))*(-cos(theta3+2*thetaBob));
                BH2 = (E2*cos(-omega*t(n))*P2*exp(-4*log(2)*(t(n)
                /tau)^2))*(cos(theta3+pi/2-2*thetaBob));
            else
                BH1 = (E1*cos(-omega*(t(n)+x(m)))*P1*exp(-4*log(2)
                *((t(n)+x(m))/tau)^2))*(cos(theta3+pi-2*thetaBob));
                BH2 = (E2*cos(-omega*t(n))*P2*exp(-4*log(2)*(t(n)
                /tau)^2))*(cos(theta3+2*thetaBob-pi/2));
            end;
            BH = BH + BH1 + BH2;

            if theta3+thetaBob < pi/4
                BV1 = (E1*cos(-omega*(t(n)+x(m)))*P1*exp(-4*log(2)
                *((t(n)+x(m))/tau)^2))*(-sin(theta3+2*thetaBob));
                BV2 = (E2*cos(-omega*t(n))*P2*exp(-4*log(2)*(t(n)
                /tau)^2))*(-sin(theta3+pi/2-2*thetaBob));
            else
                BV1 = (E1*cos(-omega*(t(n)+x(m)))*P1*exp(-4*log(2)
                *((t(n)+x(m))/tau)^2))*(-sin(theta3+pi-2*thetaBob));
                BV2 = (E2*cos(-omega*t(n))*P2*exp(-4*log(2)*(t(n)
                tau)^2))*(sin(theta3+2*thetaBob-pi/2));
            end;
            BV = BV + BV1 + BV2;
        end;
        AHH1 = AHH1 + AH;
        AVV1 = AVV1 + AV;
        BHH1 = BHH1 + BH;
        BVV1 = BVV1 + BV;

        AD1 = AD1 + AH*AV;
        BD1 = BD1 + BH*BV;

        pp1 = pp1 + AH*BH;
        pm1 = pm1 + AH*BV;
        mp1 = mp1 + AV*BH;
        mm1 = mm1 + AV*BV;
    else
        while n < length(t)
            n = n + 1;
            if theta3+thetaA(l) < pi/4
                AH1 = (E1*cos(-omega*(t(n)+x(m)))*P1*exp(-4*log(2)
```

```
            *((t(n)+x(m))/tau)^2))*cos(theta3+2*thetaA(l));
            AH2 = (E2*cos(-omega*t(n))*P2*exp(-4*log(2)*(t(n)
            /tau)^2))*cos(theta3+pi/2-2*thetaA(l));
        else
            AH1 = (E1*cos(-omega*(t(n)+x(m)))*P1*exp(-4*log(2)
            *((t(n)+x(m))/tau)^2))*(-cos(theta3+pi-2*thetaA(l)));
            AH2 = (E2*cos(-omega*t(n))*P2*exp(-4*log(2)*(t(n)
            /tau)^2))*cos(theta3+pi/2-2*thetaA(l));
        end;
        AH = AH + AH1 + AH2;

        if theta3+thetaA(l) < pi/4
            AV1 = (E1*cos(-omega*(t(n)+x(m)))*P1*exp(-4*log(2)
            *((t(n)+x(m))/tau)^2))*(sin(theta3+2*thetaA(l)));
            AV2 = (E2*cos(-omega*t(n))*P2*exp(-4*log(2)*(t(n)
            /tau)^2))*(-sin(theta3+pi/2-2*thetaA(l)));
        else
            AV1 = (E1*cos(-omega*(t(n)+x(m)))*P1*exp(-4*log(2)
            *((t(n)+x(m))/tau)^2))*sin(theta3+pi-2*thetaA(l));
            AV2 = (E2*cos(-omega*t(n))*P2*exp(-4*log(2)*(t(n)
            /tau)^2))*(-sin(theta3+pi/2-2*thetaA(l)));
        end;
        AV = AV + AV1 + AV2;

        if theta3+thetaBob < pi/4
            BH1 = (E1*cos(-omega*(t(n)+x(m)))*P1*exp(-4*log(2)
            *((t(n)+x(m))/tau)^2))*(-cos(theta3+2*thetaBob));
            BH2 = (E2*cos(-omega*t(n))*P2*exp(-4*log(2)*(t(n)
            /tau)^2))*(cos(theta3+pi/2-2*thetaBob));
        else
            BH1 = (E1*cos(-omega*(t(n)+x(m)))*P1*exp(-4*log(2)
            *((t(n)+x(m))/tau)^2))*(cos(theta3+pi-2*thetaBob));
            BH2 = (E2*cos(-omega*t(n))*P2*exp(-4*log(2)*(t(n)
            /tau)^2))*(cos(theta3+2*thetaBob-pi/2));
        end;
        BH = BH + BH1 + BH2;

        if theta3+thetaBob < pi/4
            BV1 = (E1*cos(-omega*(t(n)+x(m)))*P1*exp(-4*log(2)
            *((t(n)+x(m))/tau)^2))*(-sin(theta3+2*thetaBob));
            BV2 = (BG+E2*cos(-omega*t(n))*P2*exp(-4*log(2)*(t(n)
            /tau)^2))*(-sin(theta3+pi/2-2*thetaBob));
        else
            BV1 = (E1*cos(-omega*(t(n)+x(m)))*P1*exp(-4*log(2)
            *((t(n)+x(m))/tau)^2))*(-sin(theta3+pi-2*thetaBob));
            BV2 = (E2*cos(-omega*t(n))*P2*exp(-4*log(2)*(t(n)
            /tau)^2))*(sin(theta3+2*thetaBob-pi/2));
        end;
        BV = BV + BV1 + BV2;
    end;
    AHH2 = AHH2 + AH;
```

```
            AVV2 = AVV2 + AV;
            BHH2 = BHH2 + BH;
            BVV2 = BVV2 + BV;

            AD2 = AD2 + AH*AV;
            BD2 = BD2 + BH*BV;

            pp2 = pp2 + AH*BH;
            pm2 = pm2 + AH*BV;
            mp2 = mp2 + AV*BH;
            mm2 = mm2 + AV*BV;

        end;
    end;

    IAH1(l) = abs(AHH1)^2;
    IAV1(l) = abs(AVV1)^2;
    IBH1(l) = abs(BHH1)^2;
    IBV1(l) = abs(BVV1)^2;

    IAH2(l) = abs(AHH2)^2;
    IAV2(l) = abs(AVV2)^2;
    IBH2(l) = abs(BHH2)^2;
    IBV2(l) = abs(BVV2)^2;

    DoublesAlice1(l) = IAH1(l)*IAV1(l);
    DoublesBob1(l) = IBH1(l)*IBV1(l);

    DoublesAlice2(l) = IAH2(l)*IAV2(l);
    DoublesBob2(l) = IBH2(l)*IBV2(l);

    PP1(l) = IAH1(l)*IBH1(l);
    PM1(l) = IAH1(l)*IBV1(l);
    MP1(l) = IAV1(l)*IBH1(l);
    MM1(l) = IAV1(l)*IBV1(l);

    PP2(l) = IAH2(l)*IBH2(l);
    PM2(l) = IAH2(l)*IBV2(l);
    MP2(l) = IAV2(l)*IBH2(l);
    MM2(l) = IAV2(l)*IBV2(l);

    Correlation1(l) = (PP1(l)+MM1(l)-PM1(l)-MP1(l))/
    (PP1(l)+MM1(l)+PM1(l)+MP1(l));
    Correlation2(l) = (PP2(l)+MM2(l)-PM2(l)-MP2(l))/
    (PP2(l)+MM2(l)+PM2(l)+MP2(l));
    Correlation(l)=(PP1(l)+MM1(l)-PM1(l)-MP1(l)+PP2(l)+MM2(l)-PM2(l)
    -MP2(l))/(PP1(l)+MM1(l)+PM1(l)+MP1(l)+PP2(l)+MM2(l)+PM2(l)+MP2(l));
end;

figure;
plot(thetaB,IAH1+IAH2,'color', [0.3098,0.5059,0.7412],'LineWidth',2);
```

```
hold;
plot(thetaB,IAV1+IAV2,'color', [0.7529,0.2778,0.3020],'LineWidth',2);
plot(thetaB,IBH1+IBH2,'color', [0.6078,0.7333,0.3490],'LineWidth',2);
plot(thetaB,IBV1+IBV2,'color', [0.5020,0.3922,0.6353],'LineWidth',2);
title('Singles');
set(gca,'XTick',0:pi/8:pi/2)
set(gca,'YTickLabel','')
set(gca,'XTickLabel',{'0','22,5','45','67,5','90'})
limsy = get(gca,'YLim');
set(gca,'Ylim',[0 limsy(2)]);

figure;
plot(thetaB,DoublesAlice1+DoublesAlice2,'color', [0.3098,0.5059,0.7412],
'LineWidth',2);
hold;
plot(thetaB,DoublesBob1+DoublesBob2,'color', [0.7529,0.2778,0.3020],
'LineWidth',2);
title('Doubles');
set(gca,'XTick',0:pi/8:pi/2)
set(gca,'YTickLabel','')
set(gca,'XTickLabel',{'0','22,5','45','67,5','90'})

figure;
plot(thetaB,PP1+PP2,'color', [0.3098,0.5059,0.7412],'LineWidth',2);
hold;
plot(thetaB,MM1+MM2,'color', [0.5020,0.3922,0.6353],'LineWidth',2);
plot(thetaB,PM1+PM2,'color', [0.7529,0.2778,0.3020],'LineWidth',2);
plot(thetaB,MP1+MP2,'color', [0.6078,0.7333,0.3490],'LineWidth',2);
title('Coincidences');
set(gca,'XTick',0:pi/8:pi/2)
set(gca,'YTickLabel','')
set(gca,'XTickLabel',{'0','22,5','45','67,5','90'})

figure;
plot(thetaB,Correlation,'color', [0.3098,0.5059,0.7412],'LineWidth',2);
title('Correlation');
set(gca,'YLim',[-1 1])
set(gca,'XTick',0:pi/8:pi/2)
set(gca,'XTickLabel',{'0','22,5','45','67,5','90'})
```